THREE ESSAYS ON ECONOMIC AND SOCIETAL IMPLICATIONS OF DECADAL CLIMATE VARIABILITY AND FISHERY MANAGEMENT

A Dissertation

by

PEI HUANG

Submitted to the Office of Graduate and Professional Studies of
Texas A&M University
in partial fulfillment of the requirements for the degree of

DOCTOR OF PHILOSOPHY

Chair of Committee,	Bruce A. McCarl
Co-Chair of Committee,	Richard T. Woodward
Committee Members,	W. Douglass Shaw
	Andrew L. Johnson
Head of Department,	C. Parr Rosson III

August 2015

Major Subject: Agricultural Economics

ABSTRACT

This dissertation analyzes the yield, economic and societal implications of decadal climate variability (DCV) information in the Missouri River basin and policy regulations on the Chesapeake Bay blue crab fishery. The analysis is conducted within three main essays. The first essay investigates the effects of DCV on crop yields of 8 major crops in the Missouri River Basin (MRB). The study uses hierarchical models within a Bayesian framework to examine heterogeneity in DCV effects across counties, which prevents extreme estimates for counties with a small number of observations. The results show that DCV does alter crop yields on a geographically specific basis and suggest that adaptation is possible by altering crop mix.

The second essay evaluates economic value and management adaptations associated with DCV information again in the Missouri River Basin. Three types of information cases are investigated: perfect, conditional, and naïve information. The study employs a stochastic programming model applied across all the counties in the MRB region. That model simulates crop mix, market activity, and welfare changes under different DCV information. The results show that the conditional DCV information generates a net benefit of $28.83 million annually, while the perfect information results in a gain of $82.29 million. We also find adaptations in terms of crop mix and irrigation extent that vary across DCV information.

In the third essay, an integrated bioeconomic model is built to evaluate alternative fishery policies for the Chesapeake Bay blue crab fishery. This model combines an

economic demand model with a biological individual-based simulation model and a biological stock assessment model. The model is used to investigate the marginal impacts of crab harvest size, sex, and season regulations in a Monte Carlo setting. We then summarize the results using regression methods, yielding estimates of the marginal effect of alterations in regulation features. The results indicate that a short and temporarily closed female fishing season and a long male fishing season increase sustainable yield and revenue. For size limits, we find increases in minimum limits for males, females, peelers and soft-shell crabs increase sustainable catch and revenue, while imposing a larger maximum limit on mature female crabs increases sustainable revenue.

DEDICATION

To my family

ACKNOWLEDGEMENTS

I thank my advisory committee chairs, Dr. McCarl and Dr. Woodward, for their support and encouragement throughout the course of this research. Working under their guidance is and will be invaluable asset for me. Their mentoring and dedication have greatly influenced my growth as a researcher and as a person. I thank my advisory committee members for their insights and guidance: Dr. Shaw and Dr. Johnson. I also thank other professors in the Department of Agricultural Economics, with whom I took class or had discussion for my research: Dr. Bessler, Dr. Dunn, Dr. Griffin, Dr. Leatham, Dr. Mjelde, and Dr. Wu. Researchers from other institutes also deserve thanks: Dr. Douglas Lipton and Dr. David Tomberlin from National Oceanic and Atmospheric Administration, and Dr. Michael Wilberg from University of Maryland Center for Environmental Science, who substantially helped me with the fishery project.

Thanks also reach my friends, colleagues, and the department staff for making my time at Texas A&M University an unforgettable experience. I also want to extend my gratitude to the funding supports for the past three years: the Tom Slick Graduate Research Fellowship at the College of Agriculture and Life Sciences at Texas A&M University; the Maryland Sea Grant under award R/FISH/EC-103 from the National Oceanic and Atmospheric Administration; the U.S. Department of Commerce, the U.S. Department of Agriculture-National Institute of Food and Agriculture under grant 2011-67003-30213 in the NSF-USDA-DOE Earth System Modelling Program; and the

NOAA-Climate Programs Office-Sectoral Applications Research Program under grant NA12OAR4310097.

Finally, and most importantly, I gratefully acknowledge the support, encouragement, and love from my family through the years of pursuing my PhD degree, without which I would not have completed this dissertation successfully. In particular, I thank my mother, who raised me, educated me, and unconditionally supports my study both in China and the U.S. over these years. I also thank my brother.

NOMENCLATURE

AMO	Atlantic Multidecadal Oscillation
CS	Consumers' Surplus
DCV	Decadal Climate Variability
DOE	Department of Energy
ENSO	El Niño Southern Oscillation
FASOM	Forestry and Agriculture Sector Model
IAIDS	Inverse Almost Ideal Demand System
MCMC	Markov Chain Monte Carlo
MDE	Marginal Direct Effect
MDNR	Maryland Department of Natural Resources
MRB	Humane Society of the United States
MIE	Marginal Indirect Effect
MTE	Marginal Total Effect
NAO	North Atlantic Oscillation
NOAA	National Oceanic and Atmospheric Administration
NSF	National Science Foundation
OLS	Ordinary Least Square
PDO	Pacific Decadal Oscillation
PS	Producers' Surplus
RSS	Residual Sum of Squares

SST	Sea Surface Temperature
TAG	Tropical Atlantic Gradient
U.S.	United States
USDA	U.S. Department of Agriculture
VOI	Value of Information
WPWP	West Pacific Warm Pool

TABLE OF CONTENTS

LIST OF FIGURES

Page

LIST OF TABLES

1 INTRODUCTION

In a broad sense, ecosystem production is affected by environmental and natural resource conditions plus policy and information. For instance, ecosystem support of crop growth is greatly influenced by climate conditions and is vulnerable to climate variability, which in turn impacts societal welfare through agricultural market fluctuations (Mendelsohn, Nordhaus, and Shaw 1994; Chen and McCarl 2000; Schlenker, Hanemann, and Fisher 2006). For ecosystem support of fish harvest, fisheries throughout the world have experienced overexploitation for decades (Botsford, Castilla, and Peterson 1997; Jackson et al. 2001; FAO 2009), mainly due to ambiguous property rights (Gordon 1954; Scott 1955; Clark 1973). Given vulnerability and scarcity, society can improve the general ecosystem production through the distribution of climate information related to crop growing or through means such as direct fishery regulations.

The broad objective of dissertation is to investigate the economic implications of societal policies regarding climate information provision to the agricultural sector and fishery harvest. This is done within three essays addressing two specific settings: cropping under information on decadal climate variability (DCV) in the Missouri River Basin and the Chesapeake Bay blue crab fishery under regulations.

The first two essays address the effects of DCV information on agriculture. DCV is a title for a set of natural sea surface temperature anomalies that alter continental climate patterns for an extended time period (Mehta 1998; Mantua and Hare 2002; Wang and Mehta 2008; McCabe et al. 2008). These DCV phenomena have been found to affect

agricultural productivity in crop simulation studies (Mehta, Rosenberg, and Mendoza 2012). The first essay herein reports on a statistical study of the crop yield effects of DCV phase combinations in the Missouri River Basin (MRB) using observed crop yield and climate data. Furthermore, given knowledge of future DCV phases and the associated crop yield effects, farmers may react by changing crop mix and irrigation patterns, which could enhance their income and production. The second essay in Section 3 reports on a study of the economic value of informing farmers about DCV phases and corresponding yield effects plus examines management adaptations associated with different DCV information.

The third essay in Section 4 examines policy regulations within the Chesapeake Bay blue crab fishery. The stocks of blue crab in the Chesapeake Bay have declined in recent decades, to a large extent, due to overexploitation (Lipcius and Stockhausen 2002; Aguilar et al. 2008; Miller et al. 2011). To reverse the decline, management agencies have implemented numerous regulations since 2001, including season closures and size limits. This essay examines the biological and economic outcomes associated with alternative regulations. The results summarize the marginal effects of altering such regulations.

2 ESTIMATING DECADAL CLIMATE VARIABILITY IMPACTS ON CROP YIELDS: A HIERARCHICAL BAYESIAN APPROACH

2.1 Introduction

Crop growth relies heavily on climate and many empirical studies have found significant climate effects on crop yields (Mendelsohn, Nordhaus, and Shaw 1994; Chen and McCarl 2000; Chen, McCarl, and Schimmelpfennig 2004; Schlenker, Hanemann, and Fisher 2006; McCarl, Villavicencio, and Wu 2008; Schlenker and Roberts 2009; Yu and Babcock 2010; Tack, Harri, and Coble 2012). These studies have addressed both climate change and the effects of short term ocean phenomena such as El Niño Southern Oscillation (ENSO). This essay studies the crop yield effects of decadal climate variability (DCV), which is a set of long term ocean phenomena.

Ocean-related climate variability involves natural phenomena occurring in various ocean regions that results in systematic alterations in climate patterns over land. The climate impacts of such phenomena include temperature, precipitation, drought, and other extreme events. The ENSO and the North Atlantic Oscillation (NAO) are well-known ocean phenomena, and their climatic and societal impacts have been widely studied (Adams et al. 1995; Solow et al. 1998; Torrence and Webster 1999; Chen et al. 2005; Kim and McCarl 2005).

In addition to the ENSO and NAO, another category of ocean-related climate variability is called decadal climate variability, which lasts a longer period of time (Mehta, Rosenberg, and Mendoza 2011). More and more evidence shows that climate

anomalies and variations are associated with such DCV phenomena (McCabe, Palecki, and Betancourt 2004; McCabe et al. 2008; Mehta, Rosenberg, and Mendoza 2011). Several DCV phenomena have been the subject of climate studies: the Pacific Decadal Oscillation (PDO) (Mantua et al. 1997; Mantua and Hare 2002), the Tropical Atlantic Gradient (TAG) (Mehta 1998; Rajagopalan, Kushnir, and Tourre 1998), and the West Pacific Warm Pool (WPWP) (Wang and Mehta 2008).

Since the DCV phenomena impact climate conditions, they may also impact agricultural productivity. Mehta, Rosenberg, and Mendoza (2011) reveal that the three DCV phenomena, PDO, TAG, and WPWP, significantly influence water yields in the Missouri River Basin (MRB). Their follow-up simulation study (2012) further suggests that crop yields in this area are widely impacted mainly due to precipitation variations; with the effects varying across locations.

In this section, we examine the effects of DCV phenomena on crop yields on a regionally specific basis using observed crop yield and climate data in county level. The DCV effects in this study are decomposed into two parts: indirect and direct effects. The former depicts the DCV effects on climate and in turn on crop yields. The later part describes the indirect effects that are unobserved or effects exerted on crops directly. Although unobserved indirect effects are incorporated in the later part, we use the term "direct effects" as they are directly estimated from the crop yield equation in our model.

The essential questions addressed in this section are: "Can we observe the effect of DCV phenomena on crop yields using historical data?" and "How does this effect vary across locations?" To do this, we will use the hierarchical linear mixed effects model

introduced by Laird and Ware (1982). Although DCV is a set of global ocean-related phenomena, their effects on climate and crop yields may display spatial heterogeneity. Under a specific state of DCV phase combination, climate conditions across locations may respond differently due to varying longitude, latitude, altitude, and topography; crop yields in turn may show disparity owing to location-varying climate conditions as well as capacity managing climate. Hence, the estimation model should capture heterogeneous DCV effects across locations.

A key assumption in the hierarchical linear mixed effects model involves the form of the probability distributions that are assumed to represent variation. Here, we will assume a flexible distribution that allows skewness to be estimated in the crop yield equation, since many studies show crop yield distributions can be asymmetric (Ramirez, Misra, and Field 2003; Sherrick et al. 2004; Hennessy 2009; Tack, Harri, and Coble 2012). In particular, we employ a skew-normal distribution as proposed by Sahu, Dey, and Branco (2003).

To estimate the model, we will use a Bayesian approach for the following reasons (Layton and Levine 2003; Leon-Gonzalez and Scarpa 2008; Balcombe, Chalak, and Fraser 2009; Balcombe, Burton, and Rigby 2011). First, the Bayesian approach allows us to obtain parameters that vary by county. Second, the Bayesian approach can yield good estimation results with small number of data observations. Third, Bayesian methods provide more information to make inferences. Finally, Bayesian estimates asymptotically converge to maximum likelihood estimates.

2.2 Background on DCV Phenomena and Phase Combinations

There are multiple ocean-related DCV phenomena that occur in various ocean locations. Those examined in this dissertation include: the Pacific Decadal Oscillation (PDO), the Tropical Atlantic Gradient (TAG), and the West Pacific Warm Pool (WPWP). Each phenomenon is classified as exhibiting either a positive (+) or a negative (−) phase as determined by sea surface temperatures (SST). Hence, there are 8 total possible combinations of the positive and negative phases across the three phenomena. Each DCV phenomenon will be discussed below.

2.2.1 Pacific Decadal Oscillation

The PDO is a pattern of climate variability defined by SST conditions in the North Pacific (Mantua et al. 1997; Mantua and Hare 2002). The duration of a PDO phrase could be as long as 20 to 30 years (Deser, Phillips, and Hurrell 2004; Lee, Yamashita, and Mishima 2012). Although the mechanisms causing PDO remain unknown, there is evidence that PDO variation has had substantial impacts on climate in North America and the Pacific Rim, coinciding with periods of prolonged dryness and wetness (Miller and Schneider 2000; Mantua and Hare 2002). This in turn can result in significant impacts on agricultural productivity.

2.2.2 Tropical Atlantic Gradient

The TAG is a phenomenon with a time scale of up to 12 or 13 years that is characterized by SST conditions in the tropical areas of the Atlantic Ocean

(Rajagopalan, Kushnir, and Tourre 1998). In addition to SST conditions, the spatial gradients of SST variability are also important in determining TAG climate effects (Knutson and Manabe 1995). TAG conditions have been found to be associated with significant anomalies in atmospheric conditions and surface climate, such as winds in the lower troposphere, intense hurricanes, severe drought in the Sahel in Africa, and abundant rainfall in a wide area of the U.S. (Good, Lowe, and Rowell 2009; Murphy et al. 2010). Evidence shows that climate fluctuations due to TAG exert major impacts on agricultural production in northeast Brazil, the Sahel, and some other regions (Rowell et al. 1995; Sutton and Hodson 2005).

2.2.3 West Pacific Warm Pool

The WPWP refers to ocean conditions in the region located in the western tropical Pacific, an area that contains some of the warmest water in the open oceans (Webster and Lukas 1992; Picaut et al. 1996). The water in this area has a SST consistently higher than 28℃, approximately two to five degrees warmer than that of other equatorial waters (Yan et al. 1992; Wang and Mehta 2008). The WPWP conditions alter water salinity and ocean-atmosphere heat flux (Lukas and Lindstrom 1991; Huang and Mehta 2004). Some studies have revealed interactions between the WPWP and other climate variability phenomena, such as the PDO, and the Atlantic Multidecadal Oscillation (AMO) (Clarke, Wang, and Van Gorder 2000; Solomon and Jin 2005). The WPWP influences atmospheric circulation globally and affects atmospheric freshwater (Picaut et al. 1996). Wang and Mehta (2008) indicate that there is close relationship between the

WPWP variability and persistent rainfall anomalies in the U.S., which impacts U.S. water resources and agriculture.

2.2.4 DCV Phase Combinations

The three DCV phenomena, each with two phases, together constitute 8 mutually exclusive joint phase combinations. In this fashion, each year is characterized by a DCV phase combination. For example, in 1977, the positive PDO, the negative TAG, and the negative WPWP make the year fit in the phase combination category: PDO+ TAG− WPWP−. Mehta, Rosenberg, and Mendoza (2011) stress that climate variations such as drought or flood events are jointly caused by combinations of multiple DCV phenomena instead of a single one.

The DCV phase combinations for the years from 1950 to 2010 are shown in Table 2-1. Considering the frequency of each DCV phase combination occurring in those years, we construct a frequency-based probability distribution. The results are also presented in Table 2-1. These probabilities will be used to calculate expected crop yields.

2.3 Background on the Missouri River Basin

The study area for the empirical work is the Missouri River Basin. The MRB is the largest river basin in the U.S., partially or fully covering the states of Colorado, Iowa, Kansas, Minnesota, Missouri, Montana, Nebraska, North Dakota, South Dakota, and Wyoming. The MRB is also one of the major crop and livestock producing regions in

Table 2-1: The years from 1950 to 2010 associated the DCV phase combinations and the frequency-based probability distribution

PDO	TAG	WPWP	Year	Probability
+	−	−	1977, 1984, 1985, 1986, 1993	0.082
−	+	−	1955, 1966, 1967, 2001	0.049
−	−	+	1959, 1963, 1968, 1973, 1999, 2000, 2009	0.115
+	+	−	1976, 1978, 1979, 1980, 1982, 1983, 1987, 1992, 1997, 2006	0.164
+	−	+	1988, 1995, 1996, 2002, 2003	0.082
−	+	+	1950, 1951, 1952, 1953, 1954, 1956, 1961, 1962, 1964, 2007, 1969, 1970, 1990, 2010	0.246
+	+	+	1957, 1958, 1960, 1981, 1998, 2004, 2005	0.115
−	−	−	1965, 1971, 1972, 1974, 1975, 1989, 1991, 1994, 2008	0.148

Source: Fernandez (2013).

the U.S., producing approximately 46% of the U.S. total wheat, 22% of the grain corn, and 34% of the cattle (Mehta, Rosenberg, and Mendoza 2012).

Agriculture in the MRB region is vulnerable to climate variation, since almost 90% of the crops are planted under dryland practices. The decadal SST variability in the Pacific and the Atlantic is associated with major droughts in the Great Plains (McCabe, Palecki, and Betancourt 2004; Nigam, Guan, and Ruiz-Barradas 2011). Specifically in the MRB, precipitation and surface air temperature variability have been found to be highly correlated with the PDO, TAG, and WPWP phases (Cayan et al. 1998; Mehta, Rosenberg, and Mendoza 2011). Hence, given the importance of agriculture and its vulnerability to DCV, it is worth attention to studying the physical impacts of DCV on major crops in the MRB region.

2.4 Model Specification and Implementation

The empirical goal of this paper is to estimate the effect of the DCV phenomena on agricultural crop yields in the MRB. We estimate the DCV effect on yield by county, which consists of both direct and indirect impacts. As we develop in the next sections, there are several sets of parameters in different equations that need to be estimated.

2.4.1 The Conceptual Model

First, the DCV phenomena have an impact on regional climate such as precipitation and temperature, which in turn affect crop yields. We categorize these effects as indirect effects. Moreover, DCV may impact or influence crop yields via other factors that are unobserved. For example, in addition to precipitation and temperature variability, DCV is correlated with winds, storm incidence, air circulation, and pest distributions. However, it is difficult to explicitly include data that represent many possible climate effects in the model herein. Thus, we will estimate such yield impacts with direct DCV variables to reflect many omitted climate and other effects and will call this the "direct effects", since they are directly estimated in a crop yield equation.

In particular, we will look at yields of the 8 major dryland crops grown in the MRB: barley, corn, alfalfa hay, oats, sorghum, soybeans, spring wheat, and winter wheat. We will use climate variables of monthly mean temperature, total precipitation, count of number of days with maximum temperature greater than or equal to 90 ℉, count of number of days with precipitation greater than or equal to one inch in the summer

growing season, and number of days with minimum temperature less than or equal to 0 ℉ over the winter growing season.

The standard approach for modeling both direct and indirect effects involves two levels of equations (Baron and Kenny 1986). We adapt that approach and apply it to studying direct and indirect DCV effects on crop yields. First, we will estimate the effects of DCV on several climate conditions (equation (2.1) below). Second, we will estimate the effects of DCV on crop yields both including direct DCV effects and the indirect effects factoring in the climate conditions (equation (2.2) below).

The general forms of the estimating equations are:

$$\mathbf{w}_k = g_k\left(\mathbf{D},\mathbf{T};\boldsymbol{\theta}^k\right)+\boldsymbol{\epsilon}^k, \quad k=1,\ldots,K, \tag{2.1}$$

$$\mathbf{y} = f\left(\mathbf{D},\mathbf{W},\mathbf{T};\boldsymbol{\theta}^Y\right)+\boldsymbol{\epsilon}^Y, \tag{2.2}$$

where $\mathbf{w}_k$ is the k^{th} climate variable in $\mathbf{W}$ such that $\mathbf{W}=\left(\mathbf{w}_1,\ldots,\mathbf{w}_k\right)$, $k=1,\ldots,K$. g_k is the function describing the mean of the k^{th} climate variable, in which $\mathbf{D}$ represents dummy variables identifying the DCV phase combinations and $\mathbf{T}$ is a time trend variable. f depicts the mean of crop yield, $\mathbf{y}$, which is a function of the DCV variables $\mathbf{D}$, the full set of climate variables $\mathbf{W}$, and the time trend variable $\mathbf{T}$. $\mathbf{D}$ appears in both the climate equation (2.1) and the crop yield equation (2.2), implying that the DCV phase combinations affect both climate and crop yields. $\boldsymbol{\epsilon}^k$ and $\boldsymbol{\epsilon}^Y$ are the error terms in the two sets of equations. $\boldsymbol{\theta}^k$ and $\boldsymbol{\theta}^Y$ are the parameters estimated in the models, respectively. The above system of equations is applied to different crops individually.

In the above yield equation (2.2), we assume the explanatory variables are exogenous such that $\mathbf{D}$, $\mathbf{W}$, and $\mathbf{T}$ are uncorrelated with the error term ϵ^{Y}. This assumption implies that farmers do not make cropping decisions (i.e., fertilizer use, crop mix, and pesticide use) that affect crop yields in response to DCV phases and associated climate conditions. This assumption is appropriate, to some extent, since DCV phenomena and their impacts on crops were not widely distributed to farmers during the period covered in the data set we use, and even nowadays the information regarding DCV impacts on crop yields is still limited.

We also assume that the error terms and parameters in the system of equations are pairwise uncorrelated, which is exploitable in solving a recursive system of simultaneous equations (Wooldridge 2010). This assumption allows the system to be estimated equation by equation. In the next sections, we describe the specific forms for the above equations (2.1) and (2.2), and the Bayesian procedures employed to each equation.

2.4.2 Climate Equation with Continuous Dependent Variables

2.4.2.1 Equation with Varying Coefficients

Suppose there are $j = 1, \ldots, m$ counties, and for each county, there is a sequence of n_j observations.[1] The dependent variable for climate $\mathbf{w}_k$ may take continuous or discrete values.[2] Thus, different functional forms are needed to represent the continuous and discrete climate variables.

[1] The sample size of each county is allowed to differ.

[2] The specific climate variables selected in this model are listed in the Data section.

For a continuous climate variable $\mathbf{w}^C$ in (2.1), where the variable index k is suppressed, we use a linear functional form to capture the effects of DCV on climate for each county j:

$$\mathbf{w}_j^C = \mathbf{X}^W \boldsymbol{\theta}_j^C + \boldsymbol{\epsilon}_j^C, \quad j = 1, \ldots, m, \tag{2.3}$$

where $\mathbf{X}^W$ is a $n_j \times q$ matrix of explanatory variables such that $\mathbf{X}^W = (\mathbf{D}, \mathbf{T})$, including DCV phase combination dummies $\mathbf{D}$, and a time trend and its squared term $\mathbf{T}$.[3] In the climate equation, which only includes the DCV dummies and time, the explanatory variables $\mathbf{X}^W$ are constant across counties.

There are some caveats associated with the coefficients in the model that is estimated over multiple locations. If $\mathbf{X}^W$ can fully explain the variation of dependent variables among the subjects, the estimated parameters $\boldsymbol{\theta}_j^C$ in (2.3) are constant across counties such that $\boldsymbol{\theta}_j^C = \boldsymbol{\theta}^C$ for all j, implying that explanatory variables have the same mean effects across all locations. In this case, we can pool the data across locations, and then estimate the equation with the pooled data. If the model specifications are proper, it results in consistent estimates with large degrees of freedom.

The model with pooled data, although a good starting point, is not suitable for this application, since the coefficients in the model are not allowed to vary across counties. In fact, there are likely to be numerous unobserved factors that might make the marginal effects of DCV on climate vary across counties. In this sense, it may be unreasonable to

[3] To avoid singularity problem, we select the phase combination PDO− TAG+ WPWP+ as the base case that is not included in the equation.

assume identical coefficients across all locations. Hence, pooling the data would generate uninformative results. This concern results in our use of the model (2.3) that allows the parameters $\boldsymbol{\theta}_j^C$ to vary across counties.

A common but simple method is to estimate (2.3) county by county. The individual estimation assumes that the coefficients are completely independent across counties, implying that the information in other counties does not contribute to the estimation in county j. This assumption also may be inappropriate for data with multiple counties used in the model because neighboring counties would be expected to have similar geographic characteristics and climate patterns. Thus, DCV effects may not be completely independent among counties. In addition, it is probable for counties with small sample size that unrepresentative data are sampled and extreme estimates are generated.

The pooled and individual estimations represent the two extreme cases for data with multiple subjects. The former assumes that information is completely transferable among subjects, while the later assumes that information is only valid within the subject. This is why we choose the hierarchal model. The hierarchical model following Laird and Ware (1982) describes within-county variation of observations in the first level and then allows between-county heterogeneity using a sampling model in the second level. This model is able to accommodate cross-county heterogeneity, while allowing data information to share across counties. The hierarchical model is implemented in a Bayesian framework such that the coefficients are estimated to be county-specific.

In a hierarchical model setting, the within-county variation is expressed in (2.3), where the error terms $\boldsymbol{\epsilon}_j^C$ are assumed to be independently drawn from a multivariate normal distribution:

$$\boldsymbol{\epsilon}_j^C \left| \boldsymbol{\Psi}_j^C \sim \text{ind. Multi-Normal}_{n_j} \left(\mathbf{0}, \boldsymbol{\Psi}_j^C \right), \right. \tag{2.4}$$

where $\boldsymbol{\Psi}_j^C$ is a $n_j \times n_j$ covariance matrix. For the remainder of Section 2, we assume $\boldsymbol{\Psi}_j^C$ takes the form $\sigma_C^2 \mathbf{I}_{n_j}$, indicating that the standard error matrices are the same across counties but with different dimensions. This is a common assumption in studies with longitudinal data (Arellano-Valle, Bolfarine, and Lachos 2007).

Along with the linear functional form (2.3), the within-county variation can be expressed with a form such that the left hand side variables are independent with multivariate normal distribution:

$$\mathbf{w}_j^C \left| \boldsymbol{\theta}_j^C, \mathbf{X}^W, \sigma_C^2 \sim \text{ind. Multi-Normal}_{n_j} \left(\mathbf{X}^W \boldsymbol{\theta}_j^C, \sigma_C^2 \mathbf{I}_{n_j} \right). \right. \tag{2.5}$$

The heterogeneity among coefficients $\boldsymbol{\theta}_1^C, \ldots, \boldsymbol{\theta}_m^C$ is described with a between-county sampling model. The coefficients are modeled as being independently and identically sampled from some distribution, which represents the sampling variability across counties. In the continuous climate equation, the sampling distribution for coefficients $\boldsymbol{\theta}_j^C$ is assumed to be multivariate normal:

$$\boldsymbol{\theta}_j^C \left| \boldsymbol{\beta}^C, \boldsymbol{\Sigma}^C \sim \text{i.i.d. Multi-Normal}_q \left(\boldsymbol{\beta}^C, \boldsymbol{\Sigma}^C \right), \right. \tag{2.6}$$

where the $q \times 1$ mean vector $\boldsymbol{\beta}^C$ and the $q \times q$ covariance matrix $\boldsymbol{\Sigma}^C$ are unknown parameters to be estimated in the following Bayesian approach.[4]

2.4.2.2 Estimation with Bayesian Approach

Equations (2.3), (2.5), and (2.6) together form a typical hierarchical model for continuous dependent variables, which is then estimated with a Bayesian procedure. In Bayesian approaches, a prior distribution is assumed for each unknown parameter, which is then updated to yield a posterior distribution after observing the data. In general, Bayesian approaches approximate the joint posterior distribution for all unknown parameters in a model, for example, $\boldsymbol{\theta}_1^C, \ldots, \boldsymbol{\theta}_m^C, \boldsymbol{\beta}^C, \sigma_C^2, \boldsymbol{\Sigma}^C$ in the previous specified normal hierarchical model. The following briefly discusses the Bayesian procedure for the normal hierarchical model, while the detailed procedure is discussed in Appendix A.1.

An essential part of Bayesian analysis is to assign prior distributions to all unknown parameters. The priors represent a researcher's initial beliefs about the problem. In most cases, however, we do not have enough information to assign "precise" priors to a large number of parameters, and then they should be selected to be as non-informative as possible, which will generate more objective results (Hoff 2009). We follow proper

[4] The conditional distribution for $\boldsymbol{\theta}_j^C \left| \boldsymbol{\beta}^C, \boldsymbol{\Sigma}^C \right.$ in (2.6) represents sampling variability across counties. Hoff (2009) states that this distribution should be referred as a sampling distribution instead of a prior distribution, although it has a posterior distribution dependent on observed data. The sampling distribution is conceptually distinct from prior distributions such as $\boldsymbol{\beta}^C$ and $\boldsymbol{\Sigma}^C$ that are fixed but unknown quantities. The resulting posterior distribution for $\boldsymbol{\theta}_j^C$ is county-specific, although the sampling distribution in (2.6) is the same for all counties. We use the same argument for the following hierarchical models with varying coefficients.

studies using both diffuse priors and the unit information prior (Zhang and Davidian 2001; Arellano-Valle, Bolfarine, and Lachos 2007; Jara, Quintana, and San Mart ń 2008). A diffuse prior assigns approximately equal probability to large areas of the parameter space by selecting specific parameters in the prior distributions. A unit information prior uses the small amount of information from the data such as taking ordinary least square (OLS) estimates for the distribution parameters (Kass and Wasserman 1995). In order to obtain proper posterior distributions with standard forms for calculation convenience, conjugate priors are selected such that the corresponding posterior distributions have the same forms with the priors.[5]

Although the joint posterior distribution for all unknown parameters is of interest, it is quite difficult to obtain the marginal posterior distribution for each parameter. As an alternative, the full conditional distributions for unknown parameters can be straightforwardly derived from the joint posterior distribution. The full conditional distributions consist of a distribution for each parameter conditional on all other parameters. Then, these full conditional distributions are sampled using the Gibbs sampler, a Markov Chain Monte Carlo (MCMC) algorithm, which iteratively generates a sequence of samples for all relevant parameters (Hoff 2009). Hence, the joint and marginal posterior distributions can be approximated with the MCMC samples.

We make inference for parameters by obtaining confidence intervals based on posterior samples. For example, a 95% quantile-based confidence interval is constructed

[5] The specific choices for the prior parameters in the normal hierarchical model are discussed in Appendix A.1.2.

from the 0.025 and 0.975 quantiles of the posterior MCMC samples. The confidence level is equal to the posterior probability that the "correct" parameter is contained in the confidence interval. As the selected confidence level goes up, the interval increases.

2.4.3 Climate Equation with Discrete Dependent Variables

In equation (2.1), some climate dependent variables take on discrete values, and the model presented in (2.3) is not suitable for such situations. The Poisson regression model is an appropriate choice for within-county variation if the dependent variable is countable (Hoff 2009). In this approach, we take the log-mean of the discrete variable $\mathbf{w}_j^D$ as the dependent variable in a regression setting, where the subscript k associated with the variable is suppressed:

$$\log\left(\mathrm{E}\left(\mathbf{w}_j^D \middle| \mathbf{X}^W\right)\right) = \mathbf{X}^W \boldsymbol{\theta}_j^D, \quad j = 1, \ldots, m, \tag{2.7}$$

where $\boldsymbol{\theta}_j^D$ are the $q \times 1$ estimated parameters in the discrete climate equation for all j; $\mathbf{X}^W$ is the explanatory variables as defined for the continuous climate equation, including both DCV variables and time trend variables. Equation (2.7) is equivalent to:

$$\mathrm{E}\left(\mathbf{w}_j^D \middle| \mathbf{X}^W\right) = \exp\left(\mathbf{X}^W \boldsymbol{\theta}_j^D\right), \tag{2.8}$$

denoting the expected mean of the discrete dependent variable. By assuming the Poisson distribution for w_{ij}^D for the i^{th} observation in county j, the within-county variation can be displayed in the following form:

(2.9) $$w_{ij}^{D} \left| \mathbf{x}_i^{W}, \boldsymbol{\theta}_j^{D} \right. \sim \text{ind. Poisson}\left(\exp\left(\left(\boldsymbol{\theta}_j^{D}\right)^{T} \mathbf{x}_i^{W}\right)\right).$$

Again, the between-county heterogeneity is modeled by assuming that $\boldsymbol{\theta}_j^{D}$ is sampled from a multivariate normal distribution:

(2.10) $$\boldsymbol{\theta}_j^{D} \left| \boldsymbol{\beta}^{D}, \boldsymbol{\Sigma}^{D} \right. \sim \text{i.i.d. Multi-Normal}_q\left(\boldsymbol{\beta}^{D}, \boldsymbol{\Sigma}^{D}\right),$$

where $\boldsymbol{\beta}^{D}$ and $\boldsymbol{\Sigma}^{D}$ are parameters associated with the multivariate normal distribution. The equations (2.7), (2.9), and (2.10) constitute the generalized hierarchical model for discrete dependent variables.

The parameters for this model are also estimated with a Bayesian approach, in which the joint posterior distribution for all unknown parameters $\boldsymbol{\theta}_1^{D},\ldots,\boldsymbol{\theta}_m^{D},\boldsymbol{\beta}^{D},\boldsymbol{\Sigma}^{D}$ is produced. The posterior distributions for coefficients $\boldsymbol{\theta}_1^{D},\ldots,\boldsymbol{\theta}_m^{D}$ are different across counties, since they are conditional on the county-specific data. The priors for unknown parameters $\boldsymbol{\beta}^{C},\boldsymbol{\Sigma}^{C}$ are specified as non-informative in the same manner as for the normal hierarchical model. However, for the discrete case, the MCMC sampling algorithm is different. The Gibbs sampler is not practical in this case, since the full conditional distributions for $\boldsymbol{\theta}_1^{D},\ldots,\boldsymbol{\theta}_m^{D}$ are not in standard forms. We use the Metropolis-Hastings algorithm to approximate the posterior distribution for such parameters (Hoff 2009). It is a general MCMC method, sampling a sequence of values using a proposal distribution and an acceptance criterion. The parameter is sampled from the proposal distribution; whether it is accepted is based on the selected acceptance ratio. The details of implementing the Bayesian algorithm for the generalized hierarchical model for discrete dependent variables are discussed in Appendix A.2.

2.4.4 Crop Yield Equation

For the crop yield equation (2.2), we use a linear regression of the form:

$$\mathbf{y}_j = \mathbf{X}_j^Y \boldsymbol{\theta}_j^Y + \boldsymbol{\epsilon}_j^Y, \quad j = 1, \ldots, m, \tag{2.11}$$

where $\mathbf{y}_j$ is a $n_j \times 1$ vector of crop yield observations for county j; $\mathbf{X}_j^Y$ is a group-specific $n_j \times p$ matrix corresponding to p explanatory variables for county j, where $\mathbf{X}_j^Y = \left(\mathbf{D}, \mathbf{W}_j, \mathbf{T}\right)$. As above, $\mathbf{D}$ represents DCV phase combination dummies, and $\mathbf{T}$ includes a time trend and its squared term to capture technology development associated with crop yields. $\mathbf{W}_j$ includes county-specific climate variables that were modeled in the climate equations and their squared terms. The quadratic terms for the climate variables are included, because the effects of climate on crop yields have been found to be nonlinear (Mendelsohn, Nordhaus, and Shaw 1994; Schlenker and Roberts 2009). $\boldsymbol{\epsilon}_j^Y$ is a $n_j \times 1$ vector of standard errors and $\boldsymbol{\theta}_j^Y$ is a $p \times 1$ vector of estimated parameters.

The yield equation is modeled to capture spatial heterogeneity and with common effects across counties. Previous studies have shown that climate and DCV have effects on crop yields that vary across counties (Izaurralde et al. 2003; Mehta, Rosenberg, and Mendoza 2012). On the other hand, the DCV effects in different counties should not be treated as completely independent since neighboring counties often have similar climate conditions and physical characteristics.

The within-county variation over time is also expressed in a fashion that the error term $\boldsymbol{\epsilon}_j^Y$ is assumed to be sampled from a distribution. In most studies, the multivariate normal assumption is used. To some extent, however, the standard multivariate normal

distribution lacks robustness against deviations from the normality assumption (Verbeke and Lesaffre 1997; Zhang and Davidian 2001; Rosa, Padovani, and Gianola 2003; Ghidey, Lesaffre, and Eilers 2004; Jara, Quintana, and San Mart ń 2008; Lachos, Dey, and Cancho 2009). Hence, the normality assumption may not be a good fit for the crop yield equation here, because crop yields usually display skewness in their distributions.

The skew-normal distribution is a flexible parametric family, which is able to accommodate the situation that the true distribution deviates from a normal one (Arellano-Valle, Bolfarine, and Lachos 2007). In this study, we assume the error term $\boldsymbol{\epsilon}_j^Y$ in (2.11) as sampled from a skew-normal distribution:

$$\boldsymbol{\epsilon}_j^Y \left| \boldsymbol{\Psi}_j^Y, \boldsymbol{\Delta}_j \right. \sim \text{ind. Skew-Normal}_{n_j}\left(\mathbf{0}, \boldsymbol{\Psi}_j^Y, \boldsymbol{\Delta}_j\right), \tag{2.12}$$

where $\boldsymbol{\Psi}_j^Y$ is a $n_j \times n_j$ covariance matrix, and $\boldsymbol{\Delta}_j$ is a $n_j \times n_j$ diagonal skewness matrix. The probability density function of a skew-normal distribution and its linkage with a normal distribution are discussed in Appendix A.3. For the remainder of this section, we assume $\boldsymbol{\Psi}_j^Y = \sigma_Y^2 \mathbf{I}_{n_j}$ and $\boldsymbol{\Delta}_j = \delta \mathbf{I}_{n_j}$. The within-county variation can be expressed with a form such that crop yields are sampled from the following skew-normal distribution:

$$\mathbf{y}_j \left| \mathbf{X}_j^Y, \boldsymbol{\theta}_j^Y, \sigma_Y^2, \delta \right. \sim \text{ind. Skew-Normal}_{n_j}\left(\mathbf{X}_j^Y \boldsymbol{\theta}_j^Y, \sigma_Y^2 \mathbf{I}_{N_j}, \delta \mathbf{I}_{n_j}\right). \tag{2.13}$$

The between-county heterogeneity is modeled by allowing the parameters $\boldsymbol{\theta}_j^Y$ in (2.11) to be sampled from a skew-normal distribution as well:

$$\boldsymbol{\theta}_j^Y \left| \boldsymbol{\beta}^Y, \boldsymbol{\Sigma}^Y, \boldsymbol{\Pi} \right. \sim \text{i.i.d. Skew-Normal}_p\left(\boldsymbol{\beta}^Y, \boldsymbol{\Sigma}^Y, \boldsymbol{\Pi}\right), \tag{2.14}$$

where $\boldsymbol{\beta}^Y$ is a $p \times 1$ estimated mean vector; $\boldsymbol{\Sigma}^Y$ is a $p \times p$ estimated covariance matrix; $\boldsymbol{\Pi}$ is a $p \times p$ estimated diagonal skewness matrix such that $\boldsymbol{\Pi} = \text{diag}(\boldsymbol{\pi})$, where $\boldsymbol{\pi} = (\pi_1, \ldots, \pi_p)$. Equations (2.11), (2.13), and (2.14) constitute a skew normal hierarchical model. Although estimated parameters $\boldsymbol{\theta}_1^Y, \ldots, \boldsymbol{\theta}_m^Y$ are assumed to be sampled from a distribution as in (2.14), the posterior distributions for those are different across counties, which are conditional on county-specific data.

Again, the skew normal hierarchical model is estimated using a Bayesian framework. The procedure is similar to the normal hierarchical model but with more steps approximating the skewness parameters in the distribution. The priors are specified as non-informative, and the posterior distributions are approximated using Gibbs sampler. The details of implementing the Bayesian algorithm for the skew normal hierarchical model are presented in Appendix A.4.

2.5 Deriving and Simulating Results

2.5.1 Marginal Total Effects of DCV

As described above, we can calculate the county-specific marginal effects of DCV on crop yields using the estimated coefficients from the system of equations (2.3), (2.7), and (2.11). The county-specific marginal total effect (MTE) of DCV on crop yields is divided into two parts: the marginal direct effect (MDE) and the marginal indirect effect (MIE). Based on the general form of equations (2.1) and (2.2), the MDE for the l^{th} DCV

phase combination is then calculated by taking difference of the crop yield equation with respect to the l^{th} DCV variable:

$$\text{MDE}_l = \frac{\Delta f\left(\mathbf{D}, \mathbf{W}, \mathbf{T}; \boldsymbol{\theta}^Y\right)}{\Delta D_l}, \tag{2.15}$$

and the MIE is described as:

$$\text{MIE}_l = \sum_{k=1}^{K} \frac{\Delta g_k\left(\mathbf{D}, \mathbf{T}; \boldsymbol{\theta}^k\right)}{\Delta D_l} \times \frac{\partial f\left(\mathbf{D}, \mathbf{W}, \mathbf{T}; \boldsymbol{\theta}^Y\right)}{\partial \mathbf{w}_k}. \tag{2.16}$$

Since there are quadratic terms in the equations, the marginal effects are evaluated at the means of the explanatory variables. In practice, we exclude insignificant mean estimates at the 95% confidence level through making inferences with quantile-based intervals.

The marginal effects in equations (2.15) and (2.16) only represent relative numbers compared to the base DCV phase combination that we choose for the model. It is of interest to display the MTE for the whole set of DCV phase combinations. We change the baseline and make the MTE compare to the predicted mean yields. The adjusted MTE are calculated using the following steps, for each county $j = 1, \ldots, m$:

1. Calculate the MTE based on the estimated parameters according to (2.15) and (2.16).
2. Predict climate variables along with the mean of the MCMC samples for $\boldsymbol{\theta}_j^C$ and $\boldsymbol{\theta}_j^D$ under each DCV phase combination.

3. Incorporate the predicted DCV-specific climate values into (2.11), in conjunction with the estimated parameters $\boldsymbol{\theta}_j^Y$, to predict crop yield under each DCV phase combination.
4. Calculate the mean predicted yield as the weighted average of the predicted yields under different DCV phase combinations given the historical probabilities of DCV phase combinations presented in Table 2-1.
5. Calculate the difference between the yield in the base phase combination and the mean predicted yield calculated from the Step 4.
6. Adjust MTE estimates from Step 1 to a new baseline based on the results from Step 5.

2.5.2 Simulated Crop Yield Distribution

Results estimated from Section 2.5.1 provide insights into the county-specific mean effects of DCV phase combinations on crop yields. It is of interest to investigate how crop yield is distributed under the different DCV phase combinations. We use the system of hierarchical models to simulate crop yields under each DCV phase combination. The posterior distributions for coefficients $\boldsymbol{\theta}_j^C$, $\boldsymbol{\theta}_j^D$, and $\boldsymbol{\theta}_j^Y$ are applied to the simulation procedure. For each DCV phase combination, the simulation procedure involves the following steps:

1. For each county $j = 1,\ldots,m$, randomly draw parameters $\boldsymbol{\theta}_j^C$ and $\boldsymbol{\theta}_j^C$ from the corresponding posterior distributions;

2. Predict all climate variables conditional on the DCV phase combination, the parameters drawn in Step 1, and the predetermined time trend variable;[6]
3. For each county $j = 1, \ldots, m$, randomly draw a vector of parameters $\boldsymbol{\theta}_j^Y$ from their posterior distributions;
4. Using the state of DCV phase combination, time trend, and the drawn parameters, calculate the crop yield for each county.

We calculate the mean crop yields across county of each run to look at the predicted mean crop yield distribution.[7] Steps 1-4 are repeated for a large number of times, generating a sequence of crop yields. These simulated crop yields approximate the yield distribution under each DCV phase combination.

The steps for simulating expected crop yield distribution across DCV phase combinations is similar to the previous steps 1-4 but adding an additional step before Step 1 by randomly drawing a DCV phase combination from the historical probabilities as presented in Table 2-1. Then, the procedure is repeated for a large number of times to approximate the expected crop yield distribution.

2.6 Data

The data used in this section were obtained from multiple sources. The county-specific yield data were obtained from the U.S. Department of Agriculture Quickstats.

[6] In the climate and crop yield equations, the time trend variable is set to the level of 2015 for prediction.

[7] We can explore county-specific crop yield distribution without taking mean across counties for each run. For presentation simplicity, we present the mean crop yield distribution under each DCV phase combination in Section 2.7.

The yield data are longitudinal such that each county that has planted area of a specific crop has a sequence of annual observations. In general, the time span of the data is from 1950 to 2010. The climate data were obtained from the National Climatic Data Center, National Oceanic and Atmospheric Administration (NOAA). The climate data were selected as growing season observations which depended in timing on the crop. In particular, the 8 crops examined in this section were divided into two groups. The first group grows from April to September, including barley, corn, alfalfa hay, oats, sorghum, soybeans, and spring wheat. The corresponding climate variables for those crops are: monthly mean temperature, total precipitation, number of days with maximum temperature greater than or equal to 90 ℉, and number of days with precipitation greater than or equal to one inch in the growing season. The second group grows from October to March and only includes winter wheat. The associated climate variables for winter wheat are monthly mean temperature, total precipitation, number of days with precipitation greater than or equal to one inch, and number of days with minimum temperature less than or equal to 0 ℉ over the growing season. As for the DCV phase specification data by year, they were obtained from Fernandez (2013), and are presented in Table 2-1. These data are yearly dummies and constant across counties in a year.

2.7 Results and Discussions

2.7.1 Model Justification

Before implementing the Bayesian procedures to estimate the model, we first carry out a preliminary examination of the data that we use for estimation. Figure 2-1 shows the levels of the corn yield and summer mean temperature in different counties over time. Figure 2-1(a) suggests an increasing trend for corn yield over time in most counties, but with evident between-county variation. Figure 2-1(b) also shows between-county variation in the climate variable. Figure 2-1 indicates that the between-county heterogeneity needs to be considered in both climate and crop yield equations.[8]

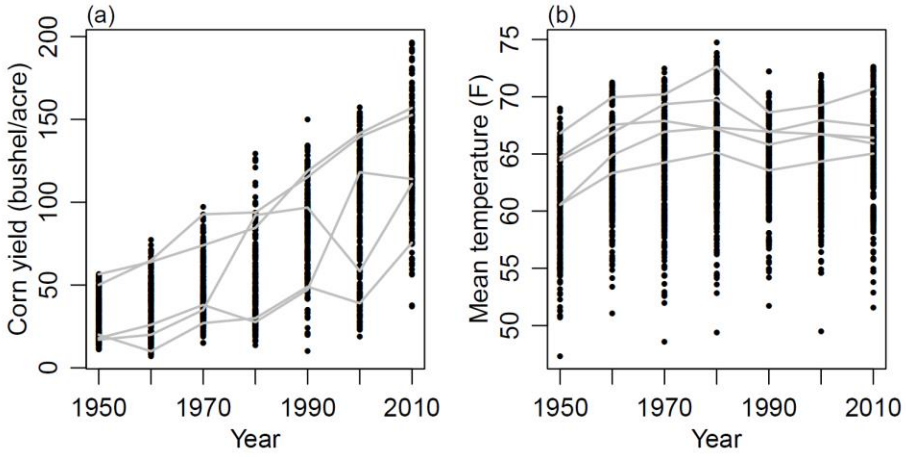

Figure 2-1: Crop yield and climate data in every 10 years. (a) Corn yields for counties that have planted such crop (black), with trajectories (gray) for 5 randomly selected counties. (b) A continuous climate variable (black), mean temperature in growing season, and trajectories (gray) for five random counties

[8] We have generated the same type of figures for other crop yields and climate variables. They all have the same pattern displaying between-county variation.

The distributions for crop yield and parameters in (2.11) are assumed to be skew-normal. Figure 2-2 presents data regarding the applicability of this assumption. Figure 2-2(a) presents a plot of the county-specific skewness index for crop yield data. The gray dots indicate that most skewness indices indicate skewed yield distributions. We also calculate skewness indices for pooled crop yield data across counties and find positive skewness for all crops as shown in black dots.

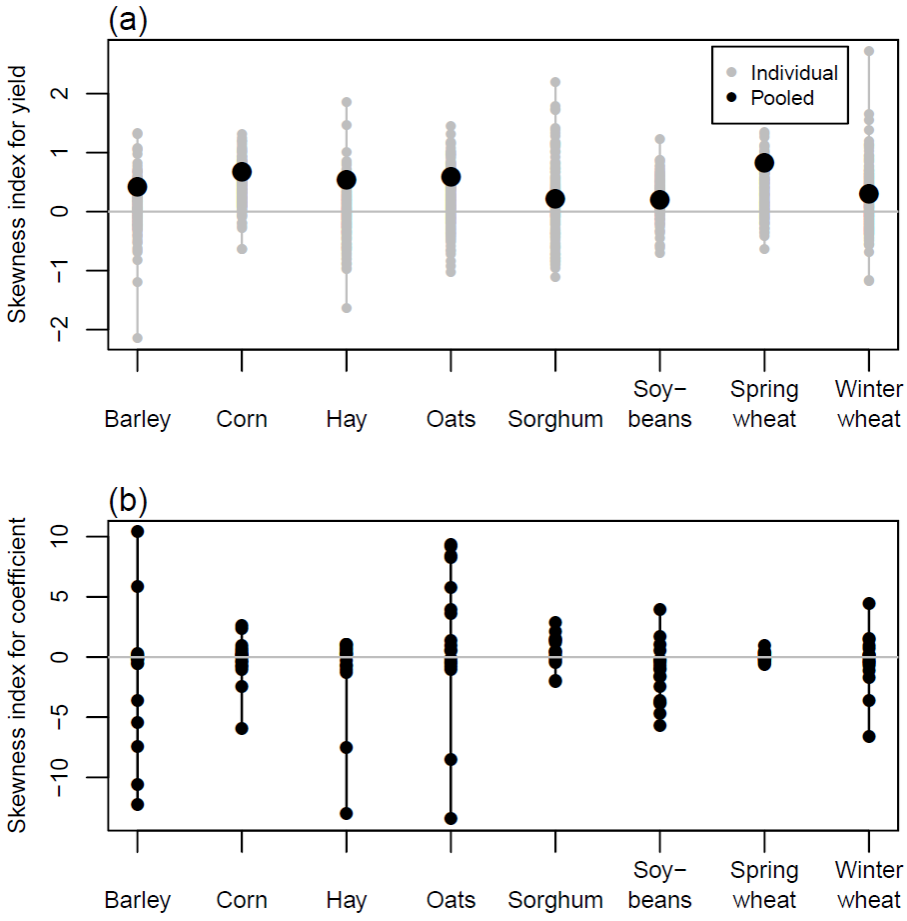

Figure 2-2: Skewness index of crop yields and OLS estimates, with zero representing no skewness. (a) County-specific skewness indices of yields for 8 crops (gray) and skewness index for each crop calculated from pooled yield data (black). (b) Skewness indices for estimated parameters in 8 yield equations from the individual OLS fits

To investigate potential skewness for the parameters in the yield equation, we fit a simple OLS regression model for each county individually, and pool the county-specific parameters to calculate the skewness indices. The results for parameters in 8 crops are plotted in Figure 2-2(b). This suggests that estimated parameters in most crop yield equations have significant skewness indices.

2.7.2 Bayesian Estimates

A type of MCMC algorithm has been implemented for each equation in the model system. The Gibbs sampler with normal distributions is applied to the continuous climate equations as discussed in Appendix A.1. The integrated Gibbs and Metropolis-Hastings algorithm is implemented for the discrete climate equations as elaborated in Appendix A.2. The Gibbs sampler with skew-normal distributions discussed in Appendix A.4 is used for the crop yield equation.

Each MCMC sampler ran 100,000 scans and saved every 100th scan to avoid autocorrelation in the samples. Hence, each equation produces a sequence of 1,000 values for each unknown parameter in the model. We then use the samples to make Bayesian inference. The resulting parameter estimates are the posterior means of the MCMC samples.

A good feature of the Bayesian method is that it shrinks extreme estimates for groups with small sample size towards the population mean, while keeping heterogeneity across groups. Figure 2-3 represents a graph of estimates associated with DCV variables in the corn yield equation under the OLS and Bayesian hierarchical

approaches.[9] The individual OLS results exhibit considerable disparity, as shown in the gray dots. The Bayesian point estimates are shown as the black dots, indicating less disparity across counties.

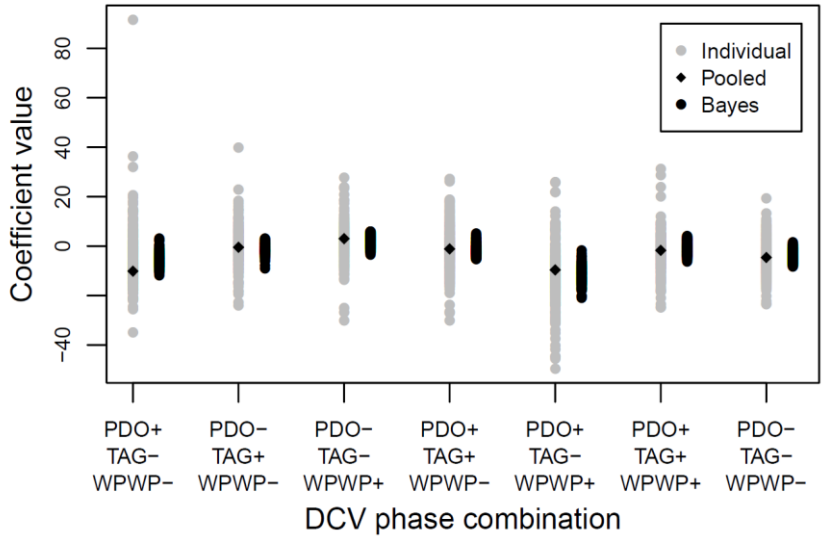

Figure 2-3: The comparison of estimates associated with DCV variables in the corn yield equation between results from the individual OLS fits (gray) and from the Bayesian approach (black)

2.7.3 County-specific Marginal Total Effects of DCV

The marginal total effects for each crop under 8 DCV phase combinations are calculated according to the procedures discussed in Section 2.5.1. Below we discuss the MTE results for 8 major crops in the MRB region.

[9] We have generated the same graphs for rest of the crops. They all display the same pattern.

2.7.3.1 Barley

The county-specific DCV impacts on barley yields are presented in Figure 2-4. We see substantial heterogeneity across DCV phase combinations and counties. Overall, the phase combination PDO+ TAG+ WPWP+ has the most positive effects as shown in the panel (g), while the phase combination PDO+ TAG− WPWP+ has the most negative effects as displayed in the panel (e). Figure 2-4(a) suggests that under the phase combination PDO+ TAG− WPWP−, barley yields in most counties of Montana, Colorado, and Nebraska decrease by up to 25% from the predicted mean yields; while in most counties of North Dakota and South Dakota, barley yields increase by up to more than 10%. Barley yield changes under the DCV phase combinations (b) PDO− TAG+ WPWP−, (c) PDO− TAG− WPWP+, and (f) PDO− TAG+ WPWP+ have similar spatial patterns but with different magnitudes of variation. Figure 2-4(d) implies that the phase combination PDO+ TAG+ WPWP− has small impacts on most counties in northern MRB, but slight negative effects with less than 10% yield loss on counties in the middle part of MRB. It is interesting to note that in response to the DCV phase combination (e) PDO+ TAG− WPWP+, barley yields decrease up to 30% in almost all counties in the MRB. The negative effects of this combination of DCV phenomena are greater in northern counties than in southern counties. Under the phase combination (g) PDO+ TAG+ WPWP+, barley yields in most counties of Montana, Wyoming, Colorado, and North Dakota increase by 10-30%. The phase combination (h) PDO− TAG− WPWP− has positive effects on northern counties by more than 5% but negative effects on some southern counties by 10%.

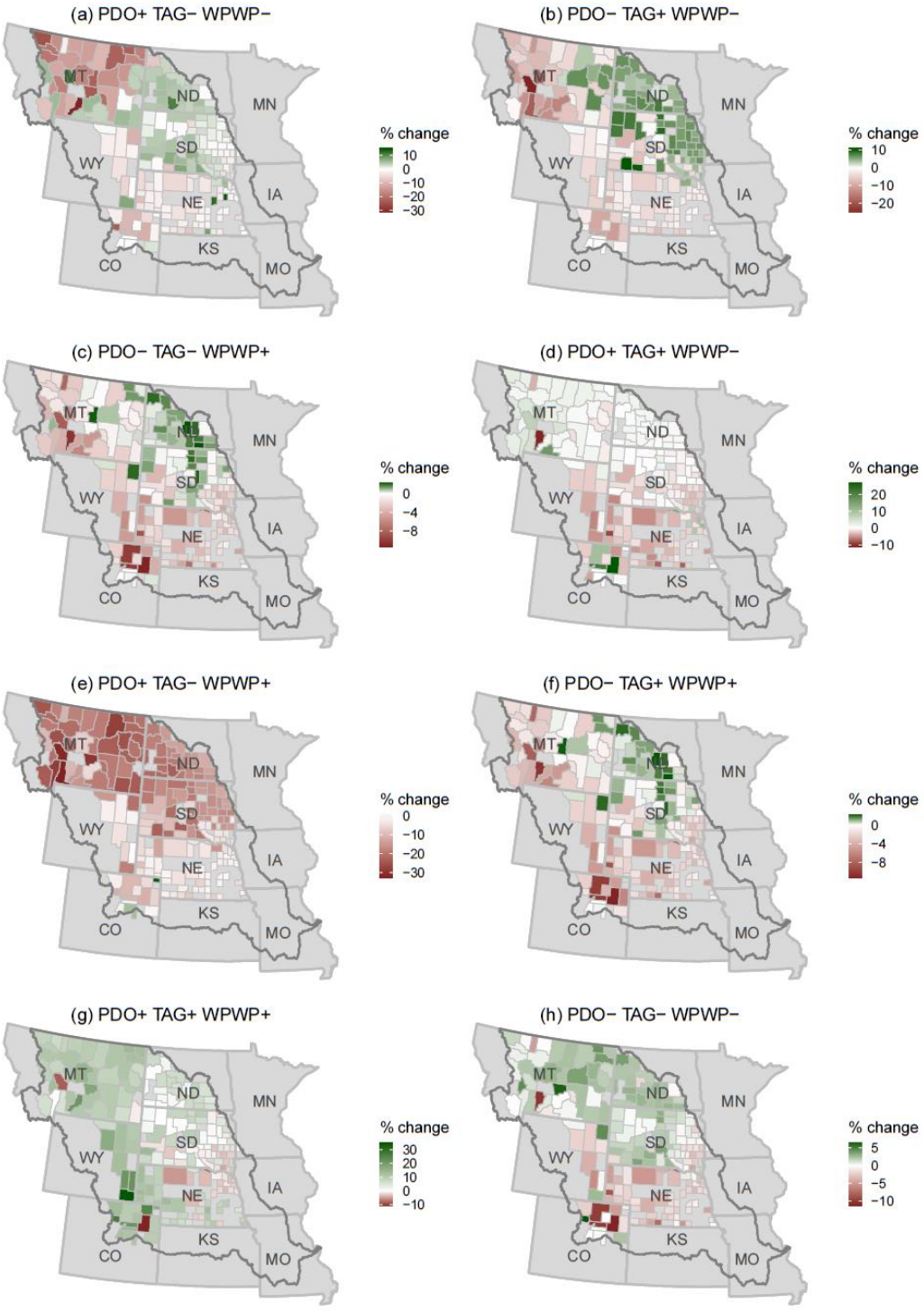

Figure 2-4: County-specific total DCV effects on barley yields (bushel/acre). (a)-(h) represent comparisons between crop yields in 8 DCV phase combinations and the predicted mean yields

2.7.3.2 Corn

The DCV impacts on corn yields are presented in Figure 2-5. In the western MRB, there are no effects showing due to very small corn planting in the area. In general, Figure 2-5 illustrates that most phase combinations have positive effects on corn yields except for the phase combination (e) PDO+ TAG− WPWP+ and (h) PDO− TAG− WPWP−. Particularly for the phase combination (e) PDO+ TAG− WPWP+, the corn yields decrease by 25% in some counties. Figure 2-5(a) and (d) have similar spatial effects but with different magnitudes, where corn yield decreases appear in the eastern part of the MRB, while corn yield increases occur in the middle part of the MRB. This spatial pattern is opposite in the phase combination (g) PDO+ TAG+ WPWP+, where corn yield reductions mainly result in the southwestern part of the MRB. In the phase combination (b) PDO− TAG+ WPWP−, there are negative changes in corn yields, and most severe corn yield losses appear in South Dakota. The phase combinations (c) PDO− TAG− WPWP+ and (f) PDO− TAG+ WPWP+ suggest that corn yields increase in most MRB counties by 4% except for a few decreases.

2.7.3.3 Alfalfa Hay

Figure 2-6 shows yield changes of alfalfa hay under different DCV phase combinations. The DCV phenomena have more significant effects on alfalfa hay yields in the western MRB compared to the southeastern part. In response to the DCV phase combination (a) PDO+ TAG- WPWP−, alfalfa hay yields decrease by 10-30% in most

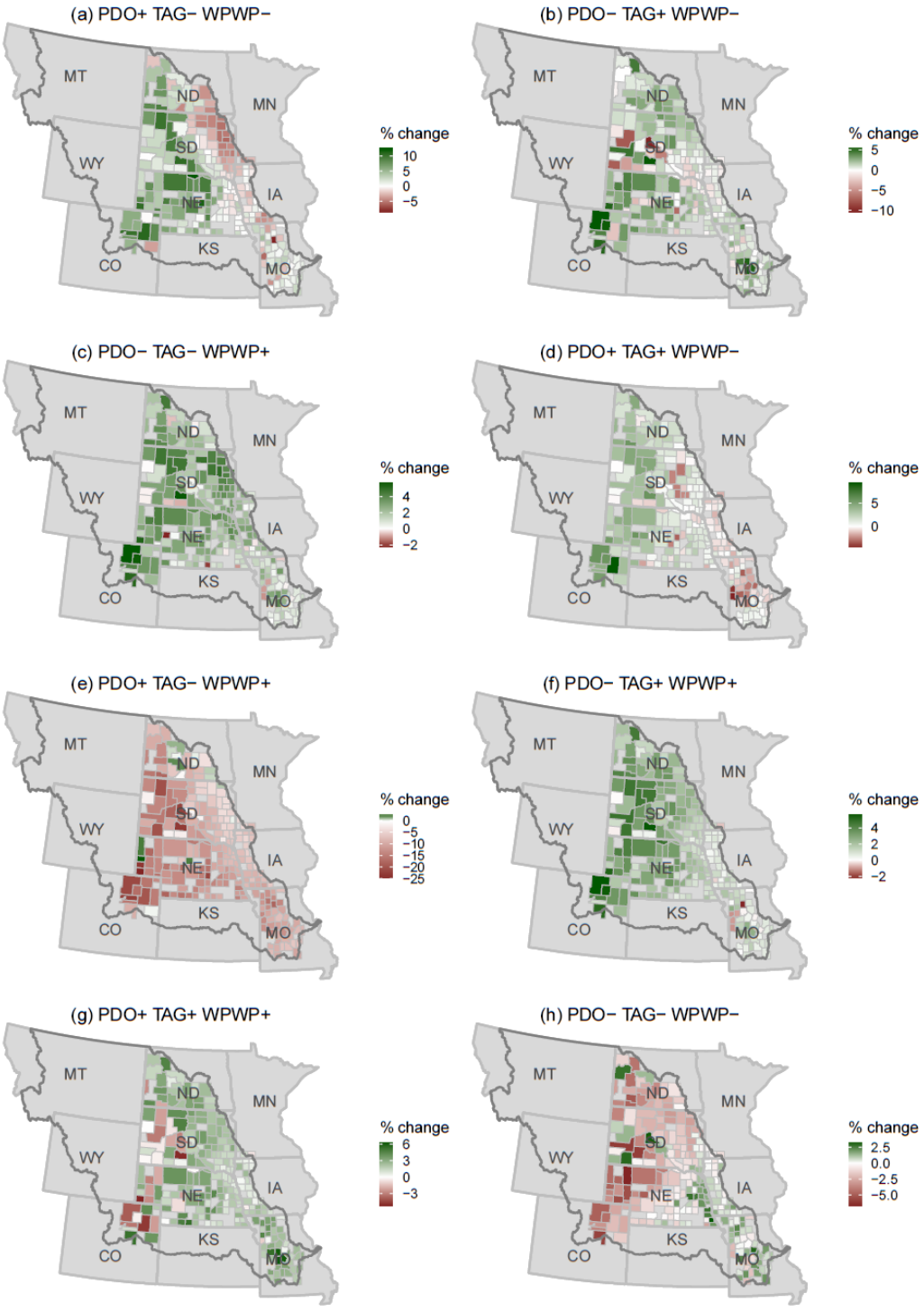

Figure 2-5: County-specific total DCV effects on corn yields (bushel/acre). (a)-(h) represent comparisons between crop yields in 8 DCV phase combinations and the predicted mean yields

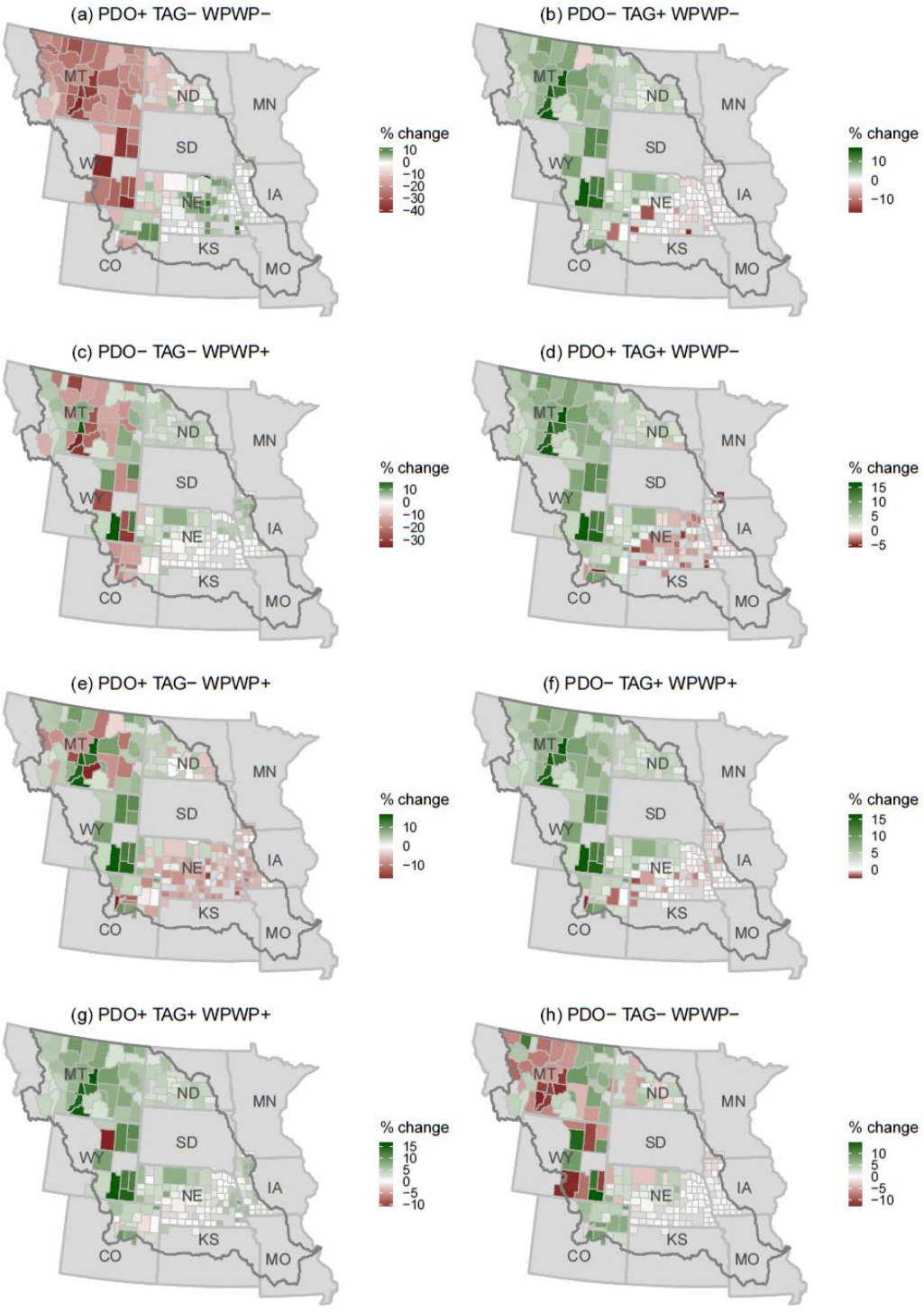

Figure 2-6: County-specific total DCV effects on alfalfa hay yields (tons/acre). (a)-(h) represent comparisons between crop yields in 8 DCV phase combinations and the predicted mean yields

counties of Montana and Wyoming. This combination of DCV phenomena has the most significant and widespread negative effects on alfalfa hay yields. In contrast to the phase combination (a), there are yield increases in Montana and Wyoming under the phase combinations (b) PDO− TAG+ WPWP−, (d) PDO+ TAG+ WPWP−, and (f) PDO− TAG+ WPWP+. It is interesting to note that the impacts of the phase combination (g) PDO+ TAG+ WPWP+ are positive in most counties, but negative in a few counties. There are both positive and negative effects distributing in Montana, Wyoming, and Colorado under (c) PDO− TAG− WPWP+, (e) PDO+ TAG− WPWP+, and (h) PDO− TAG− WPWP−.

2.7.3.4 Oats

Figure 2-7 shows that the oats yield data were available for most MRB counties. The DCV effects exhibit substantial variation both across counties and DCV phase combinations. In the phase combination (a) PDO+ TAG− WPWP−, the positive effects concentrate on the northern part of MRB, while the negative effects appear in the southern MRB. The phase combinations (b) PDO− TAG+ WPWP− and (e) PDO+ TAG− WPWP+ have broad negative impacts on oat yields in the MRB with small positive effects located in a few counties. Figure 2-7 also suggests that positive DCV effects cluster in North Dakota and South Dakota in the phase combinations (a) PDO+ TAG− WPWP−, (c) PDO− TAG− WPWP+, (f) PDO− TAG+ WPWP+, (g) PDO+ TAG+ WPWP+, and (h) PDO− TAG− WPWP−.

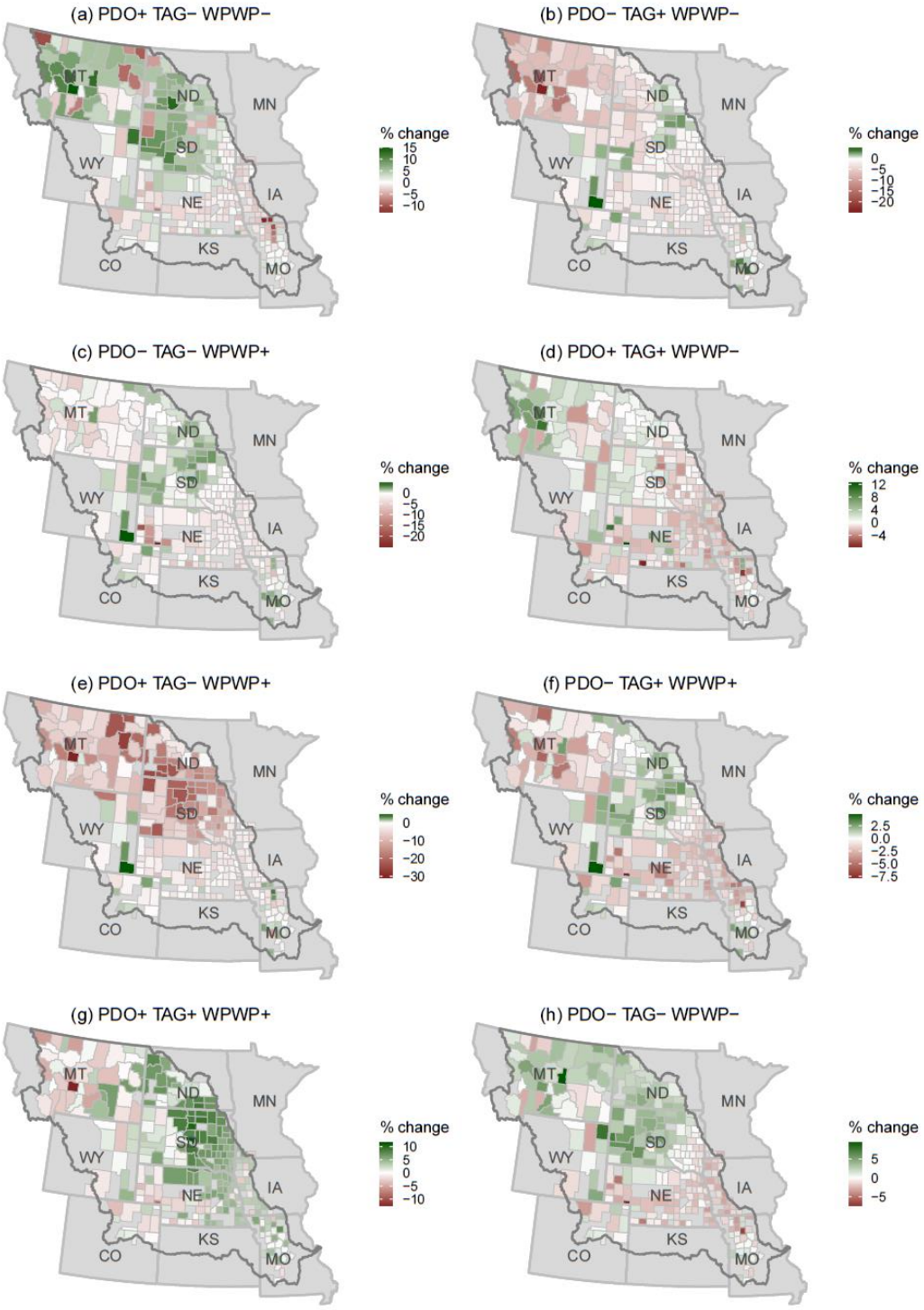

Figure 2-7: County-specific total DCV effects on oat yields (bushel/acre). (a)-(h) represent comparisons between crop yields in 8 DCV phase combinations and the predicted mean yields

2.7.3.5 Sorghum

Figure 2-8 presents the sorghum yield changes under various DCV phase combinations. In the phase combination (a) PDO+ TAG− WPWP−, the positive effects appear in western South Dakota and some counties of Nebraska and Colorado; the negative effects concentrate on eastern South Dakota, most areas of Nebraska and Missouri. The phase combination (b) PDO− TAG+ WPWP−, (c) PDO− TAG− WPWP+, and (f) PDO− TAG+ WPWP+ have widespread positive effects on counties that planted sorghum. In contrast, under the other three phase combinations (e) PDO+ TAG− WPWP+, (g) PDO+ TAG+ WPWP+, and (h) PDO− TAG− WPWP−, the sorghum yields decrease by 10-20% in most counties. Figure 2-8(d) suggests that the DCV phase combination PDO+ TAG+ WPWP− has positive effects in the central part while negative effects in the southeastern part of MRB.

2.7.3.6 Soybeans

The areas where soybean yield data were available are similar to the case of corn, which concentrate on the southern and eastern parts of MRB, as shown in Figure 2-9. The yield effects of DCV phenomena on soybeans are mild compared to other crops except for the phase combination (e) PDO+ TAG− WPWP+ that causes the soybean yields decrease by 10-20% in most MRB counties. In the phase combinations (c) PDO− TAG− WPWP+, (f) PDO− TAG+ WPWP+, and (g) PDO+ TAG+ WPWP+, there are soybean yield increases in most counties. For the other DCV phase combinations (a) PDO+ TAG− WPWP−, (b) PDO− TAG+ WPWP−, (d) PDO+ TAG+ WPWP−, and (h)

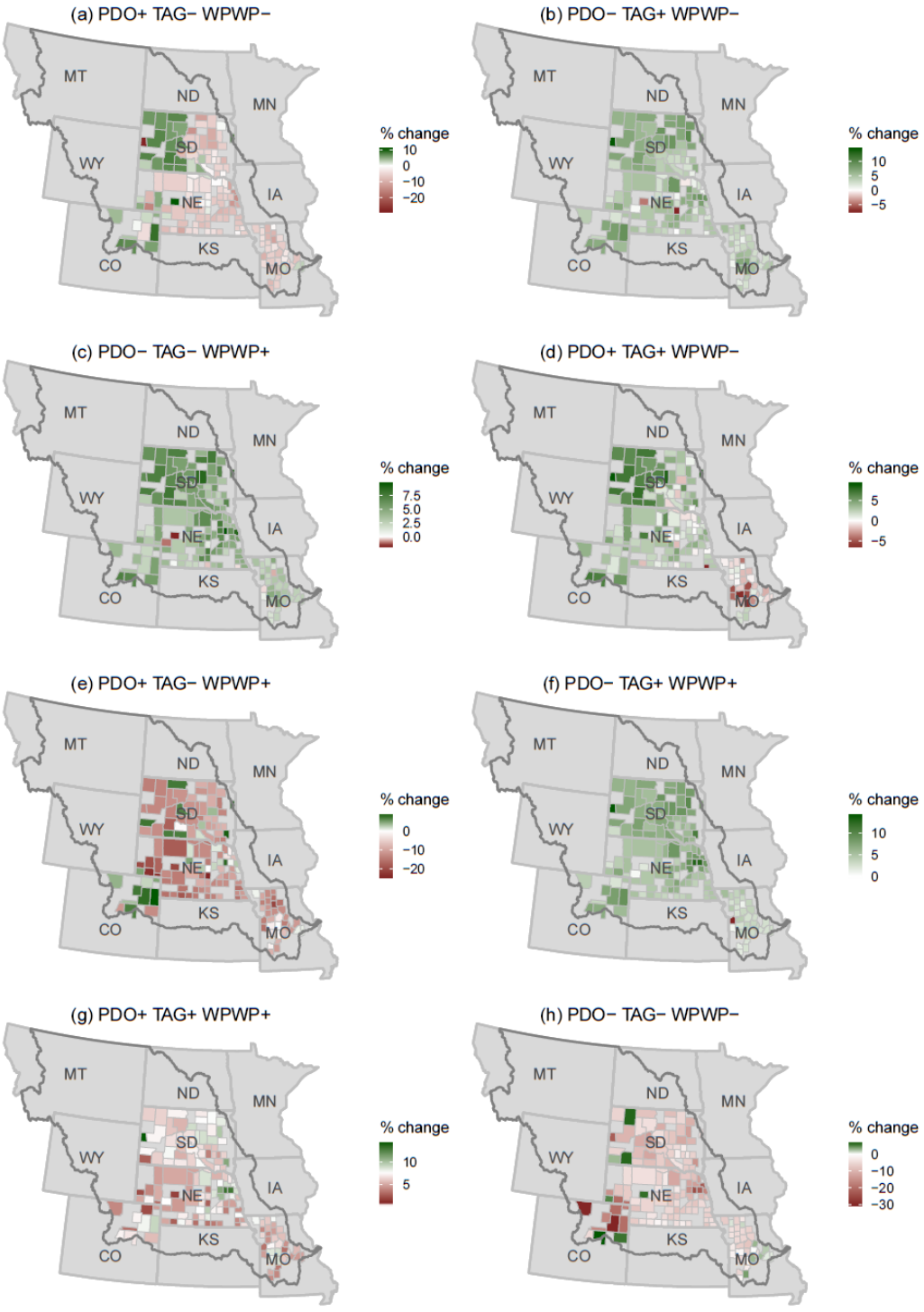

Figure 2-8: County-specific total DCV effects on sorghum yields (bushel/acre). (a)-(h) represent comparisons between crop yields in 8 DCV phase combinations and the predicted mean yields

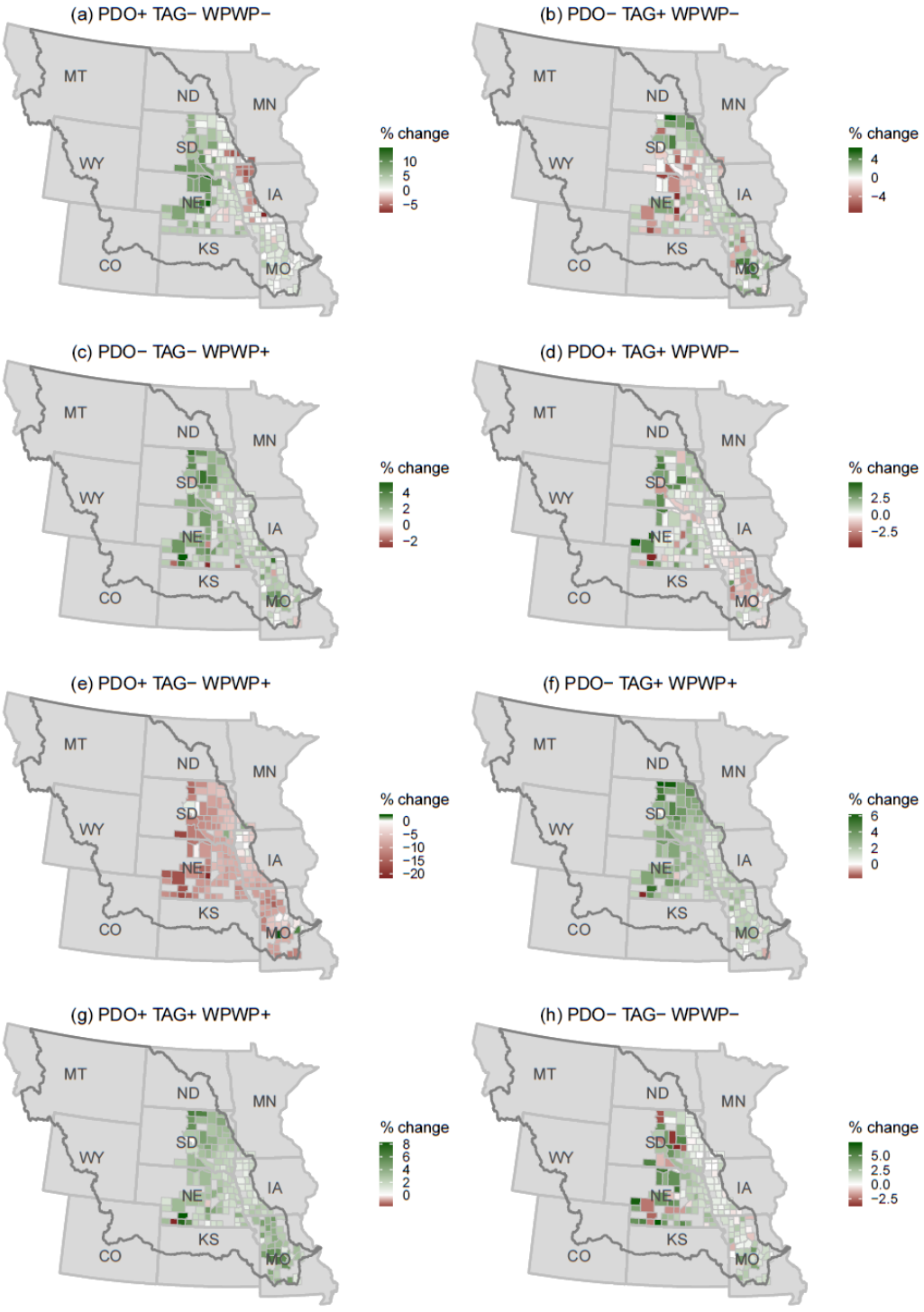

Figure 2-9: County-specific total DCV effects on soybean yields (bushel/acre). (a)-(h) represent comparisons between crop yields in 8 DCV phase combinations and the predicted mean yields

PDO− TAG− WPWP−, both positive and negative effects scatter in the area planting soybeans.

2.7.3.7 Spring Wheat

The impacts of DCV phenomena on spring wheat yields in the MRB are displayed in Figure 2-10. In phase combination (a) PDO+ TAG− WPWP−, the negative effects decrease spring wheat yields up to 20% in Montana, Wyoming, and Colorado; the positive effects scatter in Montana, North Dakota, and South Dakota. Figure 2-10(b) suggests that under the phase combination PDO− TAG+ WPWP−, the significant negative effects widely distribute in Montana, which decrease yields by 20-30% compared to expected mean yields, while the spring wheat increases concentrate in North Dakota and South Dakota. The phase combination (c) PDO− TAG− WPWP+ has a similar pattern with the phase combination (f) PDO− TAG+ WPWP+, in which the spring wheat yields decrease by 5-10% in most MRB counties except for some counties in North Dakota and South Dakota. Under the phase combination (d) PDO+ TAG+ WPWP−, the DCV phenomena combination makes the yields increase by 10-20% in western counties of Montana. It is interesting to note that the phase combination (e) PDO+ TAG− WPWP+ has negative effects on crop yields in all counties that planted spring wheat. In contrast, in the phase combination (g) PDO+ TAG+ WPWP+, yields increase in most counties.

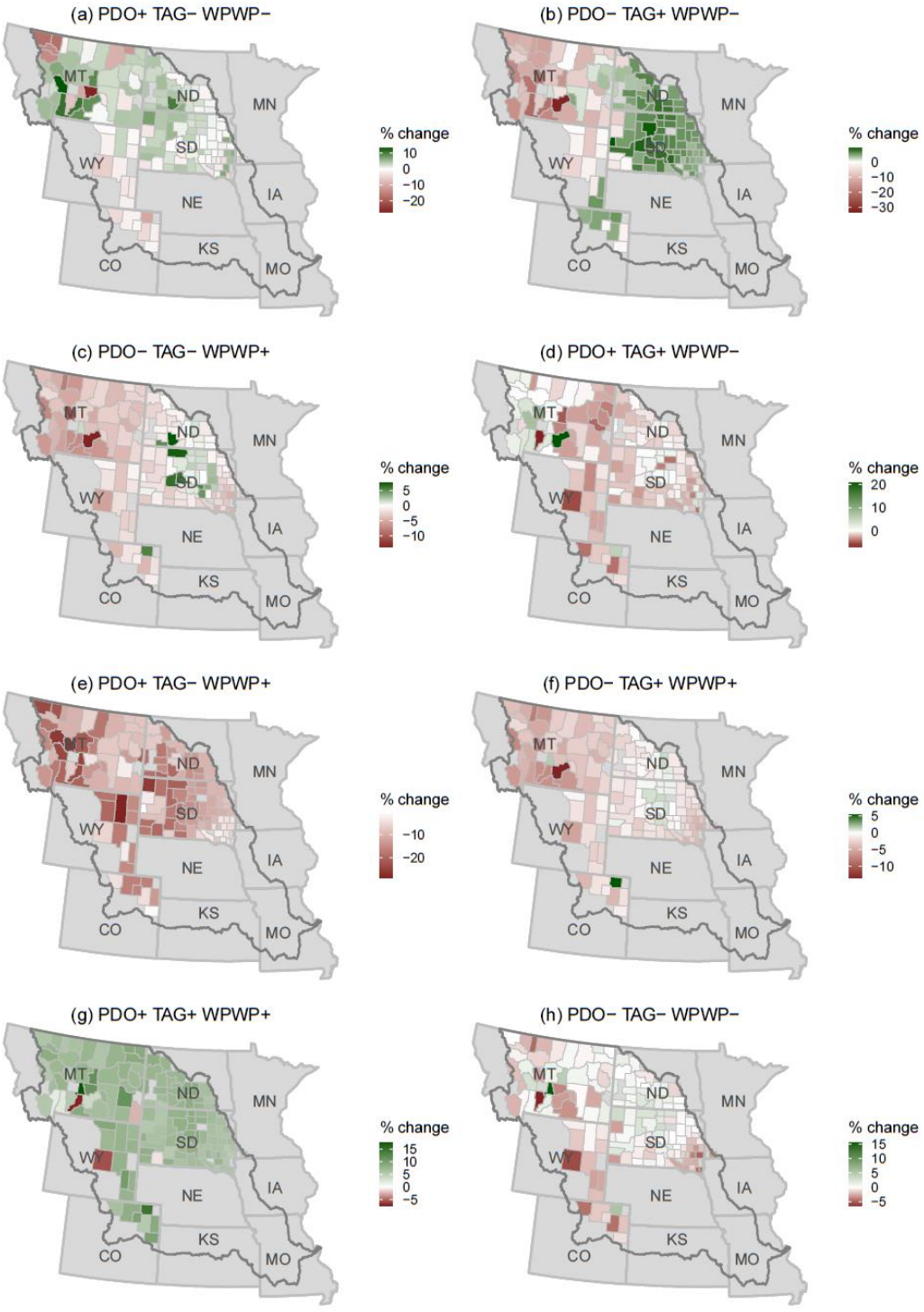

Figure 2-10: County-specific total DCV effects on spring wheat yields (bushel/acre). (a)-(h) represent comparisons between crop yields in 8 DCV phase combinations and the predicted mean yields

2.7.3.8 Winter Wheat

Figure 2-11 represents the estimated DCV effects on winter wheat in the MRB. Winter wheat yields decrease in most counties except for those in the northeastern MRB under the phase combination (a) PDO+ TAG− WPWP−. Figure 2-11(b) shows that under the phase combination PDO− TAG+ WPWP−, the positive effects distribute in the eastern side of MRB, while the positive effects appear in the western and middle MRB. There are also clear clustering DCV effects in the phase combination (c) PDO− TAG− WPWP+, in which positive effects locate in the middle MRB and negative effects concentrate on the southern MRB. In the phase combinations (d) PDO+ TAG+ WPWP−, (f) PDO− TAG+ WPWP+, and (h) PDO− TAG− WPWP−, the negative effects are more wide and significant. As noted in previous crop parts, the phase combination (e) PDO+ TAG− WPWP+ has the most negative effects on winter wheat yields up to 25% decreases. In phase combination (g) PDO+ TAG+ WPWP+, the negative effects locate in the middle MRB, while most negative effects locate along the eastern MRB.

2.7.4 Simulated Yield Distributions

The yield distributions for the 8 crops under specific and uncertain DCV phase combinations are simulated based on the procedures discussed in Section 2.5.2. The results are presented in Figure 2-12.

There are several results from the simulation operations worth highlighting. The distributions associated with the phase combination (e) PDO+ TAG− WPWP+ have the lowest mean for all crops even with the right tail far less than yields under other phase

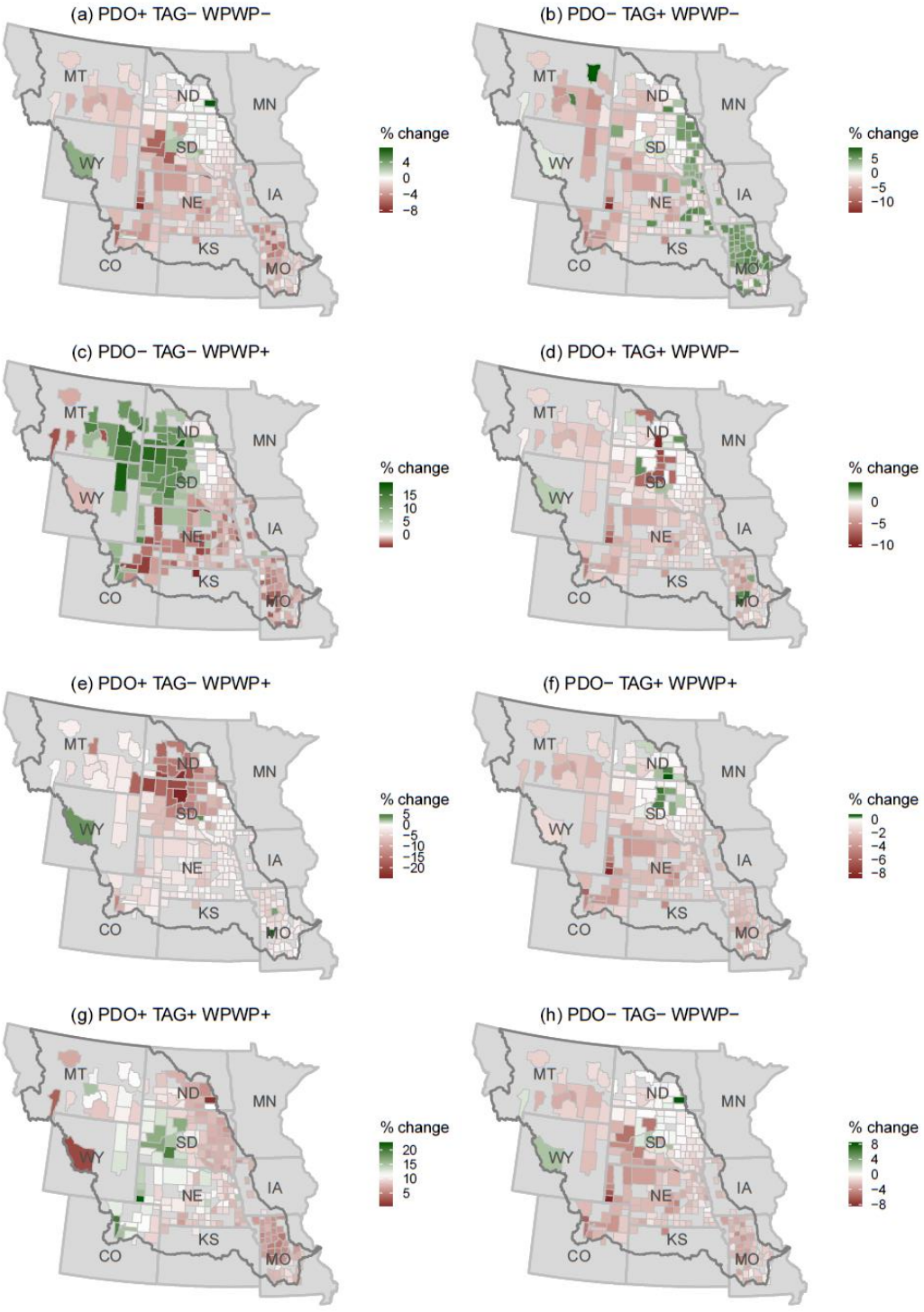

Figure 2-11: County-specific total DCV effects on winter wheat yields (bushel/acre). (a)-(h) represent comparisons between crop yields in 8 DCV phase combinations and the predicted mean yields

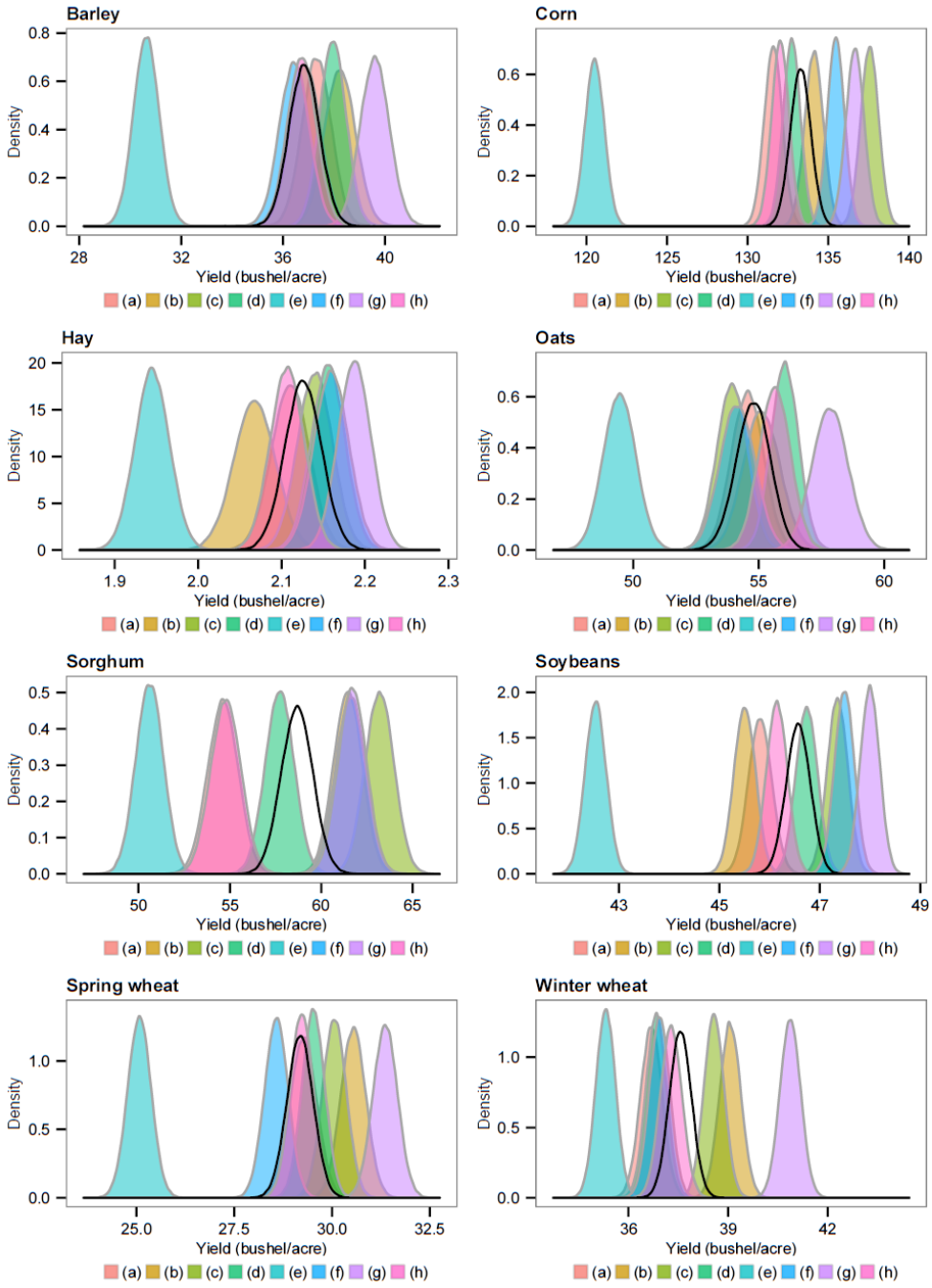

Figure 2-12: The simulated yield distributions under 8 DCV phase combinations (colors) and the expected yield distribution (black) for 8 crops. The DCV phase combinations are: (a) PDO+ TAG− WPWP−, (b) PDO− TAG+ WPWP−, (c) PDO− TAG− WPWP+, (d) PDO+ TAG+ WPWP−, (e) PDO+ TAG− WPWP+, (f) PDO− TAG+ WPWP+, (g) PDO+ TAG+ WPWP+, and (h) PDO− TAG− WPWP−

combinations. This suggests that this phase combination causes lower yields for all 8 crops. Especially for barley, corn, soybeans, and spring wheat, the distributions under the phase combination (e) are completely separated from the ones under other phase combinations. In contrast, the phase combination (g) PDO+ TAG+ WPWP+ results in highest mean yields for all crops but for corn and sorghum.

In addition to mean effects, some combinations generate greater predicted variance for some crops than other DCV phase combinations. For example, for barley, hay, and oats, the variance under the phase combination (b) PDO− TAG+ WPWP− is larger than the variance under other phase combinations. The DCV phase combination (g) PDO+ TAG+ WPWP+ also generates larger variance for the oats yield than other crops.

The yield distributions associated with some DCV phase combinations are overlapped such as the phase combinations (a) and (h), and the phase combinations (b), (f), and (g) for sorghum. Somewhat surprisingly, all simulated distributions presented in Figure 2-12 do not display evident skewness. This may be due to the large sample size that shifts from a skew distribution to a non-skew distribution. The simulated expected yield distributions are presented in black curves. They are located in the middle of each graph, indicating they are the mean combination of distributions under specific DCV phase combinations.

2.7.5 A Glance at Adaptation

The results presented in Section 2.7.3 indicate that DCV impacts show spatial and crop heterogeneity. The yield across crops in a region may respond differently to a

realized DCV phase combination. Thus, given the yield effect information, farmers can adjust their crop mix to adapt to certain DCV phase combinations. Based on the results displayed through Figure 2-4 and Figure 2-11, here we briefly discuss adaptation possibilities under some DCV phase combinations in terms of crop yield effect.

Under the DCV phase combination PDO+ TAG− WPWP−, in most counties located in Montana, the yield effect on barley (Figure 2-4(a)), alfalfa hay (Figure 2-6(a)), and winter wheat (Figure 2-11(a)) is negative, while the effect on oats (Figure 2-7(a)) and spring wheat (Figure 2-10(a)) is positive. This implies that adaptation can decrease the area of planting negatively affected crops and increase that of positively affected crops. Again, under the phase combination PDO+ TAG− WPWP+, crop yield effect in most MRB counties is negative for all crops except for alfalfa hay, allowing more hay to be planted as a way of adaptation.

2.8 Conclusions

This section examines the effects of three decadal climate variability phenomena on crop yields in the Missouri River Basin. The DCV phenomena exert impacts on crop yields through both changes in regional climate conditions and changes in other unobserved factors. In this section, these are labeled as indirect and direct effects, respectively. In the model, both the climate equations and yield equations are integrated to form an estimate of the total DCV effects on the crop yields of 8 major crops in the MRB.

Previous studies indicate that DCV effects vary across locations. Thus, regional heterogeneity is permitted in the models, in which a Bayesian framework is used. The results of the estimation show that DCV effects are spatial heterogeneous across counties and vary with phase combinations. DCV phase combinations have positive effects in some counties, but negative effects in other parts of the MRB.

The estimated posterior distributions for parameters are used to form yield distributions under different DCV phase combinations. These could be useful information for farmers, policy makers, and insurance companies in the area. The results indicate how the distribution of crop yields would be altered when we face a specific DCV phase combination. We also could gain some insights of DCV effects on crop yields from the predicted yield distributions. For example, the phase combination PDO+ TAG− WPWP+ leads to the lowest mean for all crops compared to other phase combinations, while most crops except for corn and sorghum perform better under the phase combination PDO+ TAG+ WPWP+ than under other DCV phase combinations.

3 THE INFORMATION VALUE OF DECADAL CLIMATE VARIABILITY AND ADAPTATION: A CASE IN THE MISSOURI RIVER BASIN

3.1 Introduction

Decadal climate variability (DCV) refers to a number of long term ocean-related phenomena that cause climate fluctuations (Rajagopalan, Kushnir, and Tourre 1998; McCabe, Palecki, and Betancourt 2004; Wang and Mehta 2008). There are multiple DCV phenomena that have been widely studied (Mantua et al. 1997; Mehta 1998; Mantua and Hare 2002; Deser, Phillips, and Hurrell 2004; Sutton and Hodson 2005). In this section, we study the economic value of information (VOI) about three DCV phenomena: the Pacific Decadal Oscillation (PDO), the Tropical Atlantic Gradient (TAG), and the West Pacific Warm Pool (WPWP). Each phenomenon is classified as exhibiting either a positive (+) or a negative (−) phase based on sea surface temperature observations. Collectively, there are 8 total possible combinations of the positive and negative phases across the three DCV phenomena. This analysis will examine the value of information regarding such DCV phenomenon combinations and crop yield effects of these items.

Human activities dependent on climate conditions can be substantially affected by DCV phenomena (McCabe et al. 2008; Mehta, Rosenberg, and Mendoza 2012). The essay in Section 2 found regionally specific physical impacts of DCV on crop yields. This section addresses the value of DCV information due to crop yield fluctuation plus

examines the crop mix and management adaptation strategies given such DCV information.

The basic logic that the DCV information may have value arises from the following: DCV phenomena have systematic effects on regional crop yields that vary across crops and given such information on systematic yield alterations, farmers might modify their possible crop choice, which in turn alters crop supplies, prices, and farm income. The increased value due to adaptation actions in terms of crop mix and management adjustment would be the value of DCV information (Challinor 2009; Fernandez 2013).

In this section, a conceptual stylized model is first specified to illustrate three types of DCV information: the uninformed case based on historical DCV incidences; the conditional information illustrated by a Markov Chain transition matrix; the perfect information knowing the exact DCV phase combination in a year. Each information type is represented by a specific form of probability distribution in the model. Based on the stylized framework, a stochastic mathematical programming model is used to simulate the value of DCV phase information and agricultural adaptation.

The mathematical programming model in this section is based on the model developed by Fernandez (2013), which simulates crop production, water flows, water diversions, agricultural adaptation, and social welfare in the Missouri River Basin (MRB) region. We extend the original model by using more crop yield data impacted by DCV in the MRB region, which were estimated in Section 2; we also alter the modeling methods of crop mix adaptation. The results provide insight into the value of various

types of DCV information plus possible adaptation strategies in terms of switching crop mix and irrigation use.

3.2 Literature Review

A literature review regarding ocean-related climate variability phenomena and their associated impacts on crop yields is discussed in Section 2. This section focuses on literature in the value of climate information and empirical economic studies of certain climate variability phenomena.

Early theoretical frameworks for modeling the economic value of climate information were developed by Nelson and Winter (1964) and Hilton (1981). Many subsequent studies have used that framework (Mjelde and Hill 1999; Chen, McCarl, and Hill 2002; Letson et al. 2005; Meza, Hansen, and Osgood 2008). The evaluation of climate information assumes that agents are rational and making decisions based on available information but that they initially do not have access to improved climate information. This decision making process is ex-ante, that is, the agents make input decisions before they know the climate outcome (Meza, Hansen, and Osgood 2008), but assumes that climate forecasts may influence the expectations about ex-post results and thus might alter ex-ante decisions.

Several studies have addressed economic values obtained from forecasting El Niño-Southern Oscillation (ENSO) phenomenon, a shorter ocean-related climate variability than DCV (Adams et al. 1995; Mjelde et al. 1997; Solow et al. 1998; Hill et al. 2000; Chen and McCarl 2000; Chen, McCarl, and Hill 2002; Adams et al. 2003; Hill et al.

2004). In a number of these studies, the value of ENSO information is estimated from aggregate, sector-wide models that are able to investigate market movements and societal welfare changes (Meza, Hansen, and Osgood 2008). The value of climate information is then interpreted as the difference in welfare between cases where farmers make their decisions with and without knowing the climate information in priori. In general, the value of such ENSO information has been found to be positive with the modeled farmers adjusting their cropping decisions based on the climate information to avoid adverse effects or exploit opportunities.

Solow et al. (1998) conduct an interdisciplinary study integrating models from meteorology, plant science, and economics to examine the economic value of ENSO to agriculture in the U.S. A similar study by Chen and McCarl (2000) measure the value of ENSO phase knowledge from the agriculture sector using a mathematical programming model, in which the full distribution of ENSO phase strength effects are considered rather than average strength effects. Chen, McCal, and Hill (2002) examine the value associated with the release of five ENSO phase information, which allows agricultural producers to adapt their cropping practices and in turn bring about welfare gains in the agricultural sector. The results from their simulation model suggest that more detailed ENSO phase definition almost doubles the value of information.

In addition to measuring the value of climate information, many studies have explored general economic impacts of the short-period climate variability. For example, Brunner (2002) indicates that the ENSO cycle has significant effects on world prices and economic activity. Specifically, ENSO appears to contribute to almost 20% of world

commodity price inflation for the past years. Berry and Okulicz-Kozaryn (2008) find that locally specific effects of ENSO may vanish into the noise surrounding macroeconomic trends, although many studies have addressed the influence of ENSO on particular sectors and regions.

Although the ENSO information has been broadly explored in economic literature, studies of examining DCV information are still rare. Fernandez (2013) assesses crop production and water consumption given DCV impacts on crop yields. The model evaluates welfare changes and cropping adaptations in the Missouri River Basin. The author concludes that a perfect forecast of DCV produces values worth 0.65 billion dollars and a conditional forecast leads to 4.75 billion. The simulated results also indicate that adaptation in the form of land use shifts between crops can be made under different DCV phase combinations. However, the data of DCV impacts on crop yields in the model were limited for both crops and counties and the crop mix adjustment upon reflection had some technical issues in its modeling.

Ding (2014) investigates the economic value of DCV information in another area in the U.S., the Edwards Aquifer region of Texas. The model covers water usage in multiple sectors, cropping and grazing land allocation, and welfare changes under various DCV phase information. The author finds that a perfect DCV forecast leads to 40.25 million dollars in the area and a conditional forecast results in 1.01 million dollars.

3.3 Model Specification

3.3.1 Value of DCV Information

Here we present a conceptual framework to illustrate the economic value of DCV information and adaptation following Katz and Murphy (1997) and Meza, Hansen, and Osgood (2008). In general, we assume that a farmer selects the optimal level of inputs to maximize his/her annual expected utility given obtainable DCV information regarding likely climate outcomes.

Specifically, we consider 8 possible DCV phase combinations with certain probabilities in a discrete setting. Although the exact climate outcomes may be still uncertain under a realized DCV phase combination, due to data limitations and for the sake of simplicity, we assume that the only stochastic component in this model setting is the DCV phase combination and all other components deterministically take mean values. Hence, if the DCV phase combination is known, we assume that the farmer can make choices with no uncertainty.

3.3.1.1 Uninformed DCV Case

We consider three possible information settings. First, without any DCV information, the uninformed case, expectations regarding the likelihood of different DCV phase combinations would be based on the frequency-based probability distribution of historical events. A farmer would in this case maximize his/her expected utility in a stochastic problem taking into account the distribution of historic DCV events, i.e.,

(3.1) $$W^0 = \max_{\mathbf{x}} \sum_{i=1}^{s} p_i U\left(Y_i\left(\mathbf{x}, \varepsilon\right), w\right),$$

where the optimal level of the objective function is denoted as W^0. p_i indicates the frequency-based probability for the DCV phase combination i ($i = 1, \ldots, s$, where $s = 8$) and ε represents the random variable associated with DCV phase combinations. Profit Y_i is a function of decision variables $\mathbf{x}$ and the random variable ε. The optimal solution in this problem is denoted as $\mathbf{x}^*$, which is a set of decision variables that are not contingent on DCV phase combinations.

3.3.1.2 Conditional DCV Information Case

The decision setting under the uninformed case may be improved by providing better information, knowing the specific DCV phase combination in the current year. This, to some extent, reduces climate and yield uncertainty faced by decision makers, since DCV information conditional on the current year narrows down the possible DCV phase combinations in the following year.

One way of portraying the conditional DCV information involves the use of a Markov chain transition probability matrix. The dimension of the matrix is $s \times s$ with entries π_{ij} ($i = 1, \ldots, s$ and $j = 1, \ldots, s$), which represent the probability of transitioning from this year's state i to the following year's state j. These probabilities are defined as:

(3.2) $$\pi_{ij} = \Pr\left(DCV_{t+1} = j \middle| DCV_t = i\right),$$

such that $\sum_j \pi_{ij} = 1$ for each i. The probability π_{ij} is interpreted as the probability of the phase combination j in time $t+1$ given the DCV phase combination i in time t.

Given the conditional DCV information, a farmer is assumed to make input decisions for the next year, which solves the following expected utility problem for each possible DCV phase combination i in the current year:

$$W_i^1 = \max_{\mathbf{x}_i} \sum_{j=1}^{s} \pi_{ij} U\left(Y_j\left(\mathbf{x}_i, \varepsilon\right), w\right), \ \forall i, \tag{3.3}$$

where the optimal expected utility is expressed as W_i^1 for each phase combination i in the current year. The decision variable $\mathbf{x}_i$ is specific for each i. The optimal decision is denoted as $\mathbf{x}_i^{**}$ in this problem setting. Then the total expected utility in the long-run is expressed as:

$$W^1 = \sum_{i=1}^{s} p_i W_i^1, \tag{3.4}$$

where p_i is the long-term probability of DCV phase combination i in the current year, which is based on historical frequency.

3.3.1.3 Perfect DCV Information Case

If the DCV phase combination for the next year can be perfectly predicted, farmers may choose a management strategy under certainty that maximizes the utility associated with this upcoming DCV phase combination. Again, in this problem setting, we assume all other components except for the DCV phase combination are deterministic once the

DCV phase combination is known. Thus, the utility maximization problem with certainty associated with the perfect DCV information is represented as:

$$W_i^2 = \max_{\mathbf{x}_i} U\left(Y_i\left(\mathbf{x}_i\right), w\right), \quad \forall i, \tag{3.5}$$

where the corresponding optimal utility level is denoted as W_i^2 and we denote the optimal level of decision variable as $\mathbf{x}_i^{***}$, which is specific to phase combination i. Then the long-run expected utility is calculated as:

$$W^2 = \sum_{i=1}^{s} p_i W_i^2. \tag{3.6}$$

3.3.1.4 Value of DCV Information and Adaptation

The value of DCV information can be computed for the two information cases discussed above. Under the conditional information case, the value of information is:

$$\text{VOI}_1 = W^1 - W^0, \tag{3.7}$$

while the value of perfect DCV information is calculated as:

$$\text{VOI}_2 = W^2 - W^0. \tag{3.8}$$

The amount of crop mix or management adaptation associated with climate information can be assessed by computing the amount of percentage change in the optimal decision variables in the expected utility maximization problems. We use the

uninformed DCV case as the base. The adaptation under the conditional information compared to the base is:

$$\text{AD}_1 = \frac{\left(\mathbf{x}_i^{**} - \mathbf{x}^*\right)}{\mathbf{x}^*}, \ \forall i; \tag{3.9}$$

the adaptation under perfect information is:

$$\text{AD}_2 = \frac{\left(\mathbf{x}_i^{***} - \mathbf{x}^*\right)}{\mathbf{x}^*}, \ \forall i. \tag{3.10}$$

3.3.2 A Mathematical Programming Model

To implement the above framework, we use a mathematical programming model, which simulates consumers' and producers' surplus. A mathematical programming model will be used to simulate consumers' and producers' surplus and then to investigate VOI and adaptation. The model is stochastic, which simulates perfectly competitive market equilibrium and the associated land allocation under a given probability distribution for DCV phase combinations plus data on the way they affect crop yields. The basic assumption is that a representative risk-neutral "producer" selects the level of inputs that maximizes expected net benefits subject to a set of resource constraints. According to 2nd welfare theorem in economics, the input allocation that clears the market is efficient for the society under certain assumptions. Specifically, the model covers agricultural production for 10 major crops (alfalfa hay, barley, canola,

corn, durum wheat, oats, sorghum, soybeans, spring wheat, and winter wheat) in 427 counties in the MRB region.

In brief, the objective function maximizes consumers' and producers' surplus (McCarl and Spreen 1980). The general form for the objective function is:

$$(3.11)\ \max_{ACRE_{clr}} \sum_{i} prob_i \left(\begin{array}{l} \sum_{c} \int_{0}^{AGQ_{ic}} P_{ic}\left(AGQ_{ic}\right) \mathrm{d}AGQ_{ic} - \\ \sum_{c}\sum_{l}\sum_{r}\sum_{t} unitcost_t \cdot inputq_{clrt} \cdot \left(1+\varepsilon_t\right) \cdot dcvimpact_{icr} \cdot ACRE_{clr} \end{array} \right),$$

where items typed in lower case represent parameters, while those typed in upper case are variables that are solved in the model. In this specification, the probability distribution $prob_i$ represents the probability of DCV phase combination i, which is altered given the three settings for DCV information. P_{ic} in (3.11) is the inverse demand function by crop c and DCV phase combination i such that price is a function of the quantity demanded AGQ_{ic}. Since the inverse demand curve is non-linear, the integration process is approximated into different linear steps following Adams et al. (1996) for the sake of calculation simplicity. The second part in the parenthesis of (3.11) represents the total production cost. Note that the production cost differs by DCV phase combination i. In particular, $unitcost_t$ is the unit cost per acre that is required to produce crops for each input item t. $inputq_{clrt}$ is the baseline quantity of input use for each crop c under a practice l ($l = \{dryland, irrigated\}$) in a county r using management strategy input t. ε_t is the input-quantity elasticity for each input t that illustrates the quantity of input change in response to crop yield change. $dcvimpact_{icr}$ indicates yield variation for crops c in counties r corresponding to each DCV phase combination i. $ACRE_{clr}$ is the crop

acreage variable by crop c, practice l, and county r. The rationale of this supply part is that DCV affects crop yields, which in turn alters production costs and ultimately shifts crop mixes and the resultant supply.

A set of constraints is needed to make the problem setting feasible. First, the constraint specifying the market clearing condition such that the market demand equals the supply is presented as:

$$AGQ_{ic} = \sum_{l}\sum_{r} ACRE_{clr} \times yield_{iclr}, \ \forall i, c, \tag{3.12}$$

where $yield_{iclr}$ is the crop yield contingent on DCV phase combinations i for each crop c, practice l, and county r. In each probability setting, the decision variable $ACRE_{clr}$ is not contingent on DCV phase combinations i.[10] However, the solved $ACRE_{clr}$ could vary across DCV phase combinations under the conditional or perfect information, since the probability settings in the model change.

Since crop land is a limited resource, land constraints are needed to restrain the expected utility maximization problem. The following constraint limits the total dryland and irrigated crop acres plus the acres converted from irrigated land to dryland as a way of adaptation. The irrigated land balance is given as:

$$\sum_{c} ACRE_{cr,irrigated} \leq availirr_{r} - IRRTODRY_{r}, \ \forall r, \tag{3.13}$$

[10] This setup is an alteration from Fernandez (2013), in which the decision variable is dependent on DCV phase combinations in three information cases.

where $availirr_r$ is irrigated land availability by county r; $IRRTODRY_r$ is the acres of irrigated land converted to dryland in each county r. Similarly, the dryland balance is specified as:

$$\sum_c ACRE_{cr,dryland} \le availdry_r + IRRTODRY_r, \ \forall r, \tag{3.14}$$

where $availdry_r$ is the dryland availability in each county r. For land conversion, the total land converted from irrigated cannot be greater than the irrigated land availability. Thus, we need another constraint, that is,

$$IRRTODRY_r \le availirr_r, \ \forall r. \tag{3.15}$$

To avoid extreme crop acre solutions, we follow the method in McCarl (1982) to specify the crop mix constraint such that the crop acre is a convex combination of the historical crop data. This approach guarantees that the aggregate level model is able to generate realistic results without knowing details of resource at the farm level (McCarl 1982). The crop mix constraint is represented as:

$$ACRE_{clr} = \sum_y mixdata_{clry} \times CROPMIX_{lry}, \ \forall c,l,r, \tag{3.16}$$

where $mixdata_{clry}$ represents crop mix data by crop c, practice l, county r, and year y; $CROPMIX_{lry}$ is the crop mix variable for each practice l, county r, and year y, which is interpreted as the contribution factor from historical harvests.

Hence, (3.11)-(3.16) constitute the stochastic programming model for the agricultural market in the MRB, in which the form of probability distribution $prob_i$

represents farmers' belief about future DCV phase combinations when they make cropping decisions.

3.3.3 Model Implementation

The model is run 17 times under different probability settings to generate consumers' and producers' surplus estimates and crop land allocations that can be used to assess the value of DCV information and the corresponding adaptations. First, under the uninformed DCV case, the model is run once and generates a set of decision variables and the expected consumers' and producers' surplus. This yields W^0 from equation (3.1).

In the conditional DCV information case, the model is run 8 times to simulate agricultural production for the following year with the transition probabilities conditional on the DCV phase combination in the current year. This yields W_i^1 from (3.5) for $i = 1,\ldots,8$. Subsequently, the value of information is calculated as the expected value over the 8 realized objective values minus the surplus level under the uninformed case, as shown in (3.7).

Under the perfect DCV information case, the model is solved 8 times with probability one for each perfectly forecasted DCV phase combination and zeros for the rest. This yields W_i^2 from (3.5) for $i = 1,\ldots,8$. The value of information in this case is also the expected value of the 8 objective values minus the surplus level under the uninformed case, as shown in (3.8).

3.4 Data

The data used in the model were obtained from multiple sources. Data associated with input cost and demand integration in (3.11) were adapted from the latest version of the Forestry and Agriculture Sector Model (FASOM) (Beach et al. 2010). The DCV impact data on crop yields were obtained from Soil and Water Assessment Tool (SWAT) model simulations.[11] The crop yield data in (3.12), crop acreage data such as dryland and irrigated land availability in (3.13)-(3.15), and crop mix data in (3.16) were collected from USDA Quickstats.[12] The historical data of DCV phases for constructing frequency-based and Markov chain transition probabilities were attained from Fernandez (2013).

3.5 Results and Discussions

3.5.1 Markov Chain Transition Probability Matrix

The Markov chain transition probability matrix depicting the likelihood of movements between phase combinations is estimated using maximum likelihood

[11] I thank Katherin Mendoza who works on SWAT model for providing the DCV impact data on crop yields.

[12] For those counties having crop mix data but not DCV impact data, we use averages of DCV impacts at the agricultural reporting district level. Also, the number of dryland crops in the model is greater than the number of crops studied for DCV impacts in in the SWAT model. Then we use crop proxy method to match crops with similar growing patterns. Particularly, we use the DCV impact data of spring wheat for durum wheat and corn for canola.

estimation over historical DCV phase data. The probability transitioning from phase combination i to j is estimated as:

$$\hat{\pi}_{ij} = \frac{n_{ij}}{\sum_{j=1}^{s} n_{ij}}, \tag{3.17}$$

where n_{ij} is the number of observations for DCV phase combination transitioning from i to j.

The estimated Markov chain transition matrix is displayed in Table 3-1. Each row indicates the probability distribution of alternative DCV phase combinations in the next year given this year's specific DCV state. For example, if the DCV phase combination in this year is PDO+ TAG− WPWP−, then the probability of DCV phase combination in the next year is 0.400 for PDO+ TAG− WPWP−, 0.400 for PDO− TAG+ WPWP−, and 0.200 for PDO− TAG− WPWP+, as indicated by the first row of Table 3-1. The summation of each row should equal one.

Table 3-1: Markov chain transition probability matrix for DCV phase combinations

	PDO+ TAG− WPWP−	PDO− TAG+ WPWP−	PDO− TAG− WPWP+	PDO+ TAG+ WPWP−	PDO+ TAG− WPWP+	PDO− TAG+ WPWP+	PDO+ TAG+ WPWP+	PDO− TAG− WPWP−
PDO+ TAG− WPWP−	0.400	0.000	0.000	0.400	0.000	0.000	0.000	0.200
PDO− TAG+ WPWP−	0.000	0.333	0.333	0.000	0.000	0.333	0.000	0.000
PDO− TAG− WPWP+	0.000	0.000	0.143	0.000	0.000	0.571	0.143	0.143
PDO+ TAG+ WPWP−	0.300	0.000	0.000	0.300	0.100	0.100	0.200	0.000
PDO+ TAG− WPWP+	0.000	0.000	0.000	0.200	0.400	0.000	0.200	0.200
PDO− TAG+ WPWP+	0.000	0.067	0.067	0.000	0.067	0.400	0.067	0.333
PDO+ TAG+ WPWP+	0.000	0.000	0.286	0.286	0.000	0.143	0.286	0.000
PDO− TAG− WPWP−	0.000	0.091	0.182	0.182	0.091	0.182	0.000	0.273

Note: The rows represent the DCV phase combinations in the current period, while the columns represent those in the following period.

3.5.2 Model Results

3.5.2.1 Value of DCV Information

The stochastic programming model was used to make runs under each of the three information cases. This involves modifying the probability settings $prob_i$ in (3.11). The difference between the uninformed case, the conditional case, and the perfect information case is the value of DCV information. These values are calculated according to (3.7) and (3.8), and the results are presented in Table 3-2. Note that the values presented in the table are annual terms.

Table 3-2: Expected benefits and value of DCV information

DCV information	Expected CS+PS (billion $)	Improvement over uninformed case (%)	VOI (million $)
Uninformed case	35.41	–	–
Conditional case	35.43	0.05	28.83
Perfect case	35.48	0.20	82.29

Note: CS+PS stands for consumers' surplus and producers' surplus.

Table 3-2 shows the total expected consumers' and producers' surplus do not vary substantially, as indicated in the second column. The percentage changes of expected net benefits in the three cases are relatively small (0.05% and 0.20% respectively) compared to the magnitude of the expected values, as shown in the third and fourth column. The results imply that different DCV information slightly changes consumers' and producers' surplus.

Regarding the value of DCV information, we estimate that compared to the uninformed case, the conditional DCV information would be worth $28.83 million annually, while the perfect DCV information would yield $82.29 million. The perfect

information case generates value of information almost three times higher than the conditional information case, although the magnitude of increment is much less than the level of expected welfare measures.

3.5.2.2 Crop Acreage Shifts

Farmers can adjust land allocations of different crops to adapt to upcoming climate conditions based on different DCV information. The crop acreage results from the model provide insight into the potential adaptation strategies in terms of crop adjustment. The total acreage for 10 major crops in the MRB under the historical frequency probability case is presented in Table 3-3. By only knowing the probability distribution for 8 DCV phase combinations, farmers choose a crop mix that maximizes expected net benefit. This part of results serves as a base for investigating crop acreage shifts under the improved DCV information scenarios. As illustrated in Table 3-3, corn, soybeans, and wheat are the most planted crops in the MRB regions.

Table 3-3: Total crop acreage allocations under the uninformed DCV case

Crop	Acreage (acre)
Alfalfa hay	4,926,819
Barley	377,169
Canola	356,059
Corn	25,830,785
Durum wheat	1,072,096
Oats	340,645
Sorghum	229,113
Soybeans	15,948,820
Spring wheat	5,419,238
Winter wheat	4,493,661

Table 3-4 reports the percentage changes of crop acreage under the conditional information case compared to the uninformed case crop mix in Table 3-3. The results show possible adaptations for the next year that could occur under the knowledge of climate and yield consequences given the specific DCV phase combination realized in the current year. For example, if farmers know that the DCV phase combination in the current year is PDO+ TAG− WPWP−, the crop acreage mix would change in a way indicated in the second column of Table 3-4 compared to the uniformed case. The results in Table 3-4 suggest that alfalfa hay, barley, and oats have greater magnitude of percentage changes in most DCV phase combinations than other crops. For example, under the PDO+ TAG− WPWP−, the crop acreage of barley increases by 14.24%. When the DCV phase combination in the current year is PDO+ TAG+ WPWP+, the possible acreage adjustment as adaptation is relatively small for all crops in the next year.

Table 3-4: The percentage changes of crop acreage under the conditional information case compared to the uninformed case

Crop	PDO+ TAG− WPWP−	PDO− TAG+ WPWP−	PDO− TAG− WPWP+	PDO+ TAG+ WPWP−	PDO+ TAG− WPWP+	PDO− TAG+ WPWP+	PDO+ TAG+ WPWP+	PDO− TAG− WPWP−
Alfalfa hay	-6.96	8.93	5.23	-4.84	-4.82	2.34	2.38	1.54
Barley	14.24	-1.10	-2.35	13.55	13.01	-2.19	-0.69	-0.91
Canola	-2.52	2.21	-0.45	-1.50	-1.25	0.35	0.24	0.10
Corn	0.90	-2.80	-2.30	0.61	0.86	-1.95	-0.26	-1.26
Durum wheat	0.93	-2.12	-1.68	1.12	1.03	-1.40	-0.47	-1.45
Oats	9.28	-12.23	-9.83	10.06	8.47	-11.31	-4.77	-7.44
Sorghum	-1.89	-5.18	-4.04	-2.24	-2.44	-1.25	-1.36	0.31
Soybeans	-0.77	0.92	0.54	-0.27	-0.63	0.26	0.29	-0.13
Spring wheat	0.11	-0.55	-0.64	0.37	0.39	-0.30	-0.08	0.02
Winter wheat	0.37	-0.94	-0.76	0.64	0.63	-0.82	-0.77	-0.87

When the DCV phase combinations are perfectly forecasted, the crop acreage is able to be optimally adjusted to suit the forthcoming climate event. The percentage changes of crop acreage under the perfect information case compared to the uninformed case are reported in Table 3-5. Furthermore, compared to the conditional information case in Table 3-4, the results show that the acreage changes for most crops are greater under the perfect information case. The results suggest that barley has the largest acreage change up to 16.29% under the DCV phase combination PDO+ TAG− WPWP−. Under the perfect DCV information, alfalfa hay, barley, canola, and oats have greater acreage shifts than other crops similar to the conditional information case. The results also show that the combination PDO− TAG− WPWP+ has relatively large impacts on crops under the perfect information case.

Table 3-5: The percentage changes of crop acreage under the perfect information case compared to the uninformed case

Crop	PDO+ TAG− WPWP−	PDO− TAG+ WPWP−	PDO− TAG− WPWP+	PDO+ TAG+ WPWP−	PDO+ TAG− WPWP+	PDO− TAG+ WPWP+	PDO+ TAG+ WPWP+	PDO− TAG− WPWP−
Alfalfa hay	-8.56	4.00	12.09	-7.91	-2.94	6.54	-3.23	-8.73
Barley	16.29	-0.64	-1.63	16.09	15.15	-1.31	13.20	-0.34
Canola	-2.56	1.06	5.16	-2.98	-1.58	3.75	-1.19	-1.64
Corn	1.04	-1.23	-2.63	0.62	-0.22	-3.52	0.59	-1.27
Durum wheat	1.55	-1.62	-2.36	1.36	1.08	-3.15	0.89	-1.54
Oats	12.22	-9.71	-14.43	10.66	8.34	-15.23	8.17	-5.34
Sorghum	-0.75	0.86	-10.87	-0.09	-0.32	-3.33	-0.71	-6.54
Soybeans	-1.24	1.04	0.37	-0.53	-1.04	1.65	-0.25	-0.46
Spring wheat	0.40	-0.24	-0.09	0.28	0.43	-1.02	0.39	-0.39
Winter wheat	0.84	-0.73	-1.12	0.81	0.73	-1.04	0.71	-1.19

3.5.2.3 Conversion to Dryland Agriculture

The model also allows the amount of irrigated land to be converted to dryland as a way of adaptation.[13] Since DCV affects crop yields, which in turn impacts the marginal return of dryland and irrigated land, thus a priori DCV information may help farmers decide whether to switch irrigated land.

The acres of converted irrigated land under both the conditional and perfect information cases for 8 DCV phase combinations are displayed in Figure 3-1. The horizontal line in Figure 3-1 indicates that with only knowing the historical frequency of DCV phases, the amount of irrigated land converted to dryland is around five million acres compared to the model baseline. Under the conditional information case, less irrigated land is converted to dryland under the DCV phase combinations PDO+ TAG− WPWP−, PDO− TAG+ WPWP−, PDO− TAG− WPWP+, and PDO− TAG− WPWP−, compared to the uninformed case. If the perfect DCV information is obtainable, more irrigated land is converted in the DCV phase combinations PDO+ TAG+ WPWP− and PDO− TAG+ WPWP+ than the land conversion under the conditional information case.

3.5.3 A Closer Look at the Marias Basin

Section 3.5.2 presents model results for the whole MRB region. In this section, we focus on the Marias basin as a case study to examine the effects of DCV information in a sub-region of MRB. The Marias basin is an upper sub-basin of the whole MRB, which is

[13] In the model, we do not include the possibility of switching from dryland to irrigate land. In the MRB area, the water right is usually predetermined. Switching from dryland to irrigate land requires surface or underground water, which is usually unobtainable due to lack of water rights.

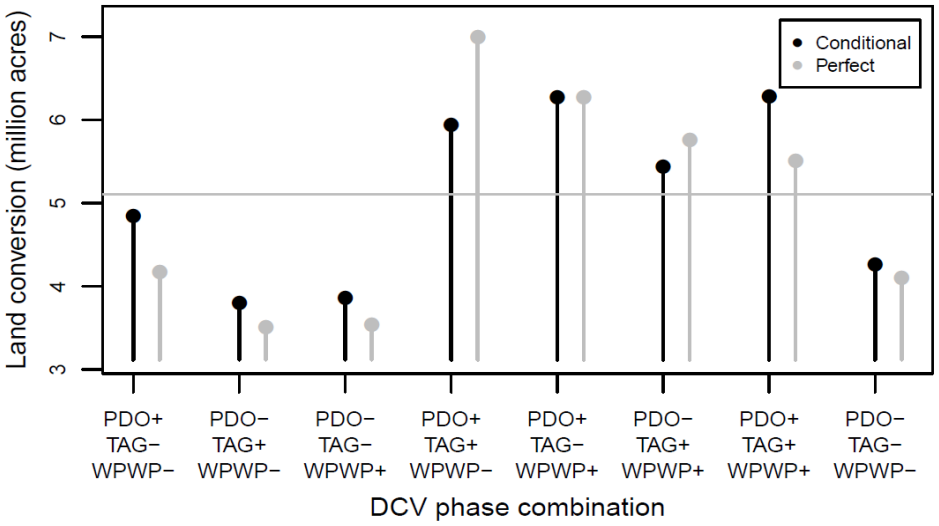

Figure 3-1: Irrigated land converted to dryland under the conditional and perfect information cases

located in the central north Montana. The sub-basin is a major agricultural production area in Montana.[14] The main crops grown in this area are: alfalfa hay, canola, spring wheat, and winter wheat, which are impacted by DCV.

Table 3-6 reports crop acres for four major crops in the Marias basin under the uninformed DCV case. It shows that winter wheat has the largest number of acres, followed by spring wheat and alfalfa hay. It is interesting to note that when the DCV information is improved to the conditional case, crop acreage does not change across all DCV phase combinations. This may be due to the conditional DCV information is still too uncertain for the decision maker to make acreage adjustments.

[14] There are 14 counties in Montana entirely or partially located in the Marias river basin: Broadwater, Cascade, Chouteau, Gallatin, Glacier, Hill, Jefferson, Judith Basin, Lewis and Clark, Liberty, Meagher, Pondera, Teton, and Toole.

Table 3-6: Total crop acreage allocations for the Marias basin under the uninformed case

Crop	Acreage (acre)
Alfalfa hay	52,041
Canola	11,779
Spring wheat	225,827
Winter wheat	1,369,966

Under the perfect DCV information, the percentage changes of crop acreage compared to the uninformed case for major crops are presented in Table 3-7. Most crops do not change under some phase combinations. However, the acreage of alfalfa hay is reduced by 61% when the DCV phase combination is perfectly predicted to be PDO+ TAG− WPWP−. The acreage of spring wheat and winter wheat slightly changes under the PDO− TAG+ WPWP+. In all, the Marias basin seems insensitive to DCV phase information in terms of crop acreage shift, even if crop yields are impacted by DCV.

Table 3-7: The percentage changes of crop acreage in the Marias basin under the perfect information case compared to the uninformed case

Crop	PDO+ TAG− WPWP−	PDO− TAG+ WPWP−	PDO− TAG− WPWP+	PDO+ TAG+ WPWP−	PDO+ TAG− WPWP+	PDO− TAG+ WPWP+	PDO+ TAG+ WPWP+	PDO− TAG− WPWP−
Alfalfa hay	-0.61	0.00	0.00	0.00	0.00	0.00	0.00	0.00
Canola	0.00	0.00	0.00	0.00	0.00	0.00	0.00	0.00
Spring wheat	0.00	0.00	0.00	0.00	0.00	-0.05	0.00	0.00
Winter wheat	0.00	0.00	0.00	0.00	0.00	0.01	0.00	0.00

3.6 Conclusions

The essay in this section reports on an investigation of the economic value of DCV information and corresponding adaptive decisions, given that crop supplies are affected by DCV phase combinations. This is done by specifying a conceptual decision-making

framework that evaluates the value of DCV climate and yield information. A mathematical programming model is used to evaluate potential changes in welfare and in turn the value of DCV information as well as the crop mix and management adaptations in the Missouri River Basin area.

We find that more accurate DCV information slightly improves welfare compared to the magnitude of the welfare measure. This indicates that DCV information has little impact on welfare. Specifically, conditional DCV information, knowing the status of DCV in the current year, generates an annual value of $28.83 million more than the case of only knowing the historical frequency of DCV phase combinations. The perfect information results in an annual value of $82.29 million more than the uninformed DCV case.

In terms of crop acreage adaptation, with the conditional DCV information, alfalfa hay, barley, and oats have greater percentage acreage changes in most DCV phase combinations than other crops. Specifically, under the DCV phase combination PDO+ TAG− WPWP−, the acreage for barley increases by 14.24% compared to the uninformed case. The perfect information leads to greater acreage changes than the conditional DCV information. Also, irrigated land can be converted to dryland as a method of adaptation. The results show that the number of irrigated acres converted to dryland varies across DCV phase combinations under different DCV information cases.

4 MANAGEMENT EVALUATION FOR THE CHESAPEAKE BAY BLUE CRAB FISHERY: AN INTEGRATED BIOECONOMIC APPROACH[*]

4.1 Introduction

The essay in this section develops and applies a framework to evaluate management regulations within the Chesapeake Bay blue crab fishery. The blue crab fishery has experienced overexploitation for decades (Bunnell and Miller 2005; Miller et al. 2011). In response, management bodies in this region have implemented many management policies to jointly regulate the fishery. In general, many fishery management approaches involve a set of components like maximum total allowable catch, gear restrictions, limited seasons, selective season closures, fish size limits, and spatial closures (Smith, Zhang, and Coleman 2008; Anderson and Seijo 2010; Smith 2012). Historical evidence shows that some policy tools that intend to reduce fishing effort have resulted in a recovery in blue crab population (Pala 2010), and many have altered economic outcomes in other fisheries (Smith and Wilen 2003; Smith, Zhang, and Coleman 2008).

The framework developed in this section is designed to simulate sustainable revenue and yield given a management scenario. In turn, we simulate a large number of cases for fishery policies on allowable crab harvest in terms of sex, size limit and season length.

[*] Reprinted with permission from "Management Evaluation for the Chesapeake Bay Blue Crab Fishery: An Integrated Bioeconomic Approach" by P. Huang, R. T. Woodward, M. J. Wilberg, and D. Tomberlin. 2015. *North American Journal of Fisheries Management* 35(2):216-228, Copyright [2015] by Taylor & Francis.

We then use regression to summarize the marginal impacts of the policy settings on sustainable yield and revenue, respectively.

To do this, a model with three components is used. The first component simulates growth, mortality, fecundity, and harvest for a fixed number of crabs by using the life history individual-based model, as developed by Bunnell and Miller (2005) and Bunnell, Lipton, and Miller. (2010). Therein, the fate of population is tracked over time by age, size, and sex instead of being treated as a uniform biomass (Tahvonen 2009; Smith 2012). The individual-based model can be easily used to evaluate potential joint outcomes associated with a set of management policy components and this allows us to assess the effects of each policy component.

The second component simulates the long-term sustainable stock of blue crabs given a management scenario. This uses equations from the Chesapeake Bay blue crab stock assessment model developed by Miller et al. (2011). This model is a statistically-fitted population dynamics model that estimates the crab abundance and sustainable harvest levels of Chesapeake Bay blue crabs based on harvest and abundance survey data.

The third part is an economic inverse demand model that relates Chesapeake Bay blue crab harvest to market prices and then calculates fishery revenue. This is specifically estimated for this study and differs from previous studies such as Bunnell, Lipton, and Miller (2010), as it incorporates cross commodity effects and allows us to investigate market relationships between crab categories in terms of size, sex, and shell status.

The model that integrates the three components is used to simulate long-term sustainable outcomes from a wide range of alternative fishery regulations involving season length, size limit, and sex limit. This work will extend the previous literature in several ways. First, Bunnell, Lipton, and Miller (2010) developed a similar model and applied it to the Chesapeake Bay blue crab fishery. We benefit from adopting the biological part in their model but extend the stock recruitment and economic components plus employ a Monte Carlo approach to investigate a wider variety of policy settings. In particular, we integrate the Miller et al. (2011) stock assessment model instead of using a fixed number of recruits. Also, we develop a multi-commodity demand model that captures between-category seasonal effects where the previous studies only looked at the commodities separately. Finally, we use regression to summarize the results then investigate the marginal effects of changes in each policy component.

4.2 Literature Review

When fisheries managers consider alternative policies, they often want projections of their outcomes. A variety of frameworks have been built to make such projections, including life history modeling (see Deacon 1989; Heppell et al. 2006; Smith, Zhang, and Coleman 2008; Tahvonen 2009; Tahvonen 2009; Diekert et al. 2010; Macher and Boncoeur 2010) and management strategy evaluation approaches (Dichmont et al. 2008; Needle 2008; Bastardie, Nielsen, and Kraus 2010; Jardim, Cerviño, and Azevedo 2010; Ives, Scandol, and Greenville 2013). Most studies of fishery policies focus on a specific

fishery and policy component, such as size limits for the California abalone fishery (Deacon 1989), season closure for the Gulf of Mexico gag fishery (Smith, Zhang, and Coleman 2008), and gear restrictions for the Bay of Biscay Nephrops fishery (Macher and Boncoeur 2010).

Fisheries models simulate individual cohorts and long-term populations. The individual-based cohort modes are standard tools for fisheries management (Smith, Zhang, and Coleman 2008). They are types of life history model that simulate the fate of individual fish with a sequence of probabilistic procedures. The individuals are treated as heterogeneous groups in terms of size, sex, and shell status. This feature is consistent with the recent fisheries economics literature that uses age-structured models (Tahvonen 2009; Smith 2012).

There have been numerous stock assessments for the Chesapeake Bay blue crab fishery (Rugolo et al. 1997; Miller and Houde 1999; Miller 2001; Fogarty and Miller 2004; Miller et al. 2005; Miller et al. 2011). To inform actual fisheries management, a fishery model should be based on the specific biological system (Diekert et al. 2010). Hence, strong bioeconomic models require a solid biological base (Smith, Zhang, and Coleman 2008). A stock assessment model that determines maximum sustainable yield based reference points can provide this foundation (Maravelias et al. 2010; Ives, Scandol, and Greenville 2013).

In addition to analyses of the biological characteristics of the fishery, there is rich literature on examining the economic consequences of fishery regulations. Smith and Wilen (2003) and Smith, Zhang, and Coleman (2008) argue that isolating economic

incentives from fisheries policy making may lead to inadequate and poorly performing policies. Smith, Zhang, and Coleman (2008) conclude that fishers' behavioral response to seasonal closures undermines the effects of biological controls. Homans and Wilen (2005) study the rent dissipation problem associated with fisheries regulations and find that rents are dissipated due to substantial inputs raise costs as well as inferior product types that reduce revenues.

4.3 Background on the Chesapeake Bay Blue Crab Fishery

Blue crab is an iconic species in the Chesapeake Bay and the greater Mid-Atlantic region. The harvest for this species in the Chesapeake Bay is the source of 50% of the nation's blue crab harvest (Miller et al. 2011). Economically, the blue crab fishery in the Chesapeake Bay generates $46-103 million annually, being one of the most profitable regional commercial fisheries (Bunnell, Lipton, and Miller 2010).

The Chesapeake Bay Blue crab stocks have declined in recent decades, to a large extent, due to overexploitation (Lipcius and Stockhausen 2002; Aguilar et al. 2008; Miller et al. 2011). To cope with this overfishing problem, Maryland, Virginia, and the Potomac River Fisheries Commission implemented a set of management policies since 2001 (Miller 2001). The policy components used include a closed winter season to protect crab recruitment, minimum size limits, and a sex-specific fishing season length. In recent years, the management strategy has leaned towards protecting mature female crabs by temporarily closing female fishing activities within a fishing season (Bunnell, Lipton, and Miller 2010).

The blue crab market in Chesapeake Bay has prices for crabs in five categories: #1 males, #2 males, females, mixed, and soft and peeler crabs (SP hereafter). The #1 males are larger than #2 males. Females are not graded by size; usually they are smaller than #1 males but are similar in size to #2 males. Blue crabs that are less marketable and gender unclassified are reported as "mixed" in Maryland, but "unclassified" in Virginia. Crabs in the "mixed" market category are similar in size to females. Soft shell and peelers category is the most valuable category in the market.

4.4 The Integrated Bioeconomic Model

Figure 4-1 displays the overall modeling framework. We treat the Chesapeake Bay blue crab as independent from other populations with harvested crabs only sold in the Chesapeake Bay region. There are three model components. The first is an individual-

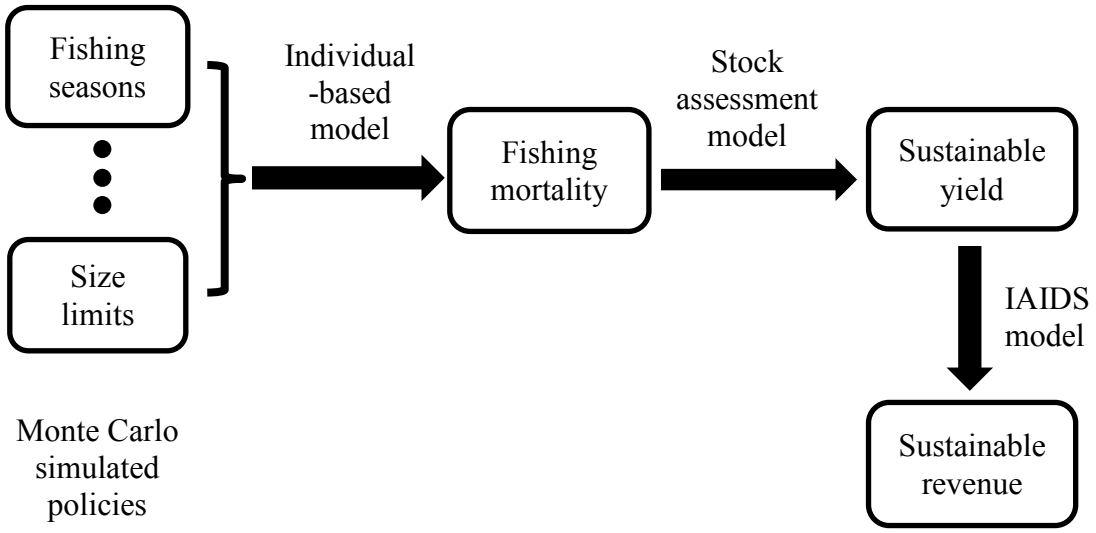

Figure 4-1: Flowchart depicting the key components and paths of the integrated model

based model that simulates the life history of blue crabs and the corresponding annual fishing mortality rate given a set of policies. The second component is a stock assessment model that estimates the long-term sustainable yield given the fishing mortality rate realized in the individual-based model. The third and last component is an economic demand model that predicts commodity prices as well as revenue associated with the resulting sustainable yield. In the next sections, we provide details on each model component and how they are integrated.

4.4.1 Individual-based Model

The first component of the integrated model is an individual-based model developed by Bunnell and Miller (2005) and Bunnell, Lipton, and Miller (2010). The model is a sex-specific, per-recruit model that numerically simulates growth, maturity, natural mortality, and harvest of blue crabs on a daily basis over two years. For each management scenario, the model simulates the fate of a cohort of individuals from January 1st of the first year and ends at December 31st of the second year. Each individual represents a large number of blue crabs. Whether an individual matures and how much it grows are stochastically determined to reflect the life history of such individual. Once blue crabs reach a specific length threshold, they are ready to be harvested.

For each day, the number of blue crabs harvested or that die in a cohort by sex is determined by fishery effort which is influenced by restrictions, crab size, the natural mortality rate, and the nominal fishing mortality rate. The model simulates each

management scenario with a fixed number of recruitment and we assume there is no behavioral response to fishery policies by fishers. Hence, we select a constant nominal fishing catch rate for all management scenarios.[15] This nominal fishing catch rate is the same regardless of management scenarios but realized mortality varies based on the allowable removals under the fishery policies on age, size, sex, and season length.

We run the individual-based model multiple times, altering fishery policies in each run. At the end of each run, realized age- and sex-specific fishing mortality rates are calculated, for later use in the stock assessment model. The rates are calculated using Baranov's catch equation as is done in Quinn II and Deriso (1999) and Bunnell and Miller (2005):

$$F_{st} = \frac{C_{st}\left(\ln\left(N_{st}^{0}\right) - \ln\left(N_{st}^{T}\right)\right)}{2\left(N_{st}^{0} - N_{st}^{T}\right)}, \tag{4.1}$$

where C_{st} equals the total number of crabs harvested for each sex s, $s \in \{m, f\}$, and each age t, $t \in \{0,1\}$. Blue crabs in the first year represent the age-0 class, while crabs in the second year represent the age-1 class. N_{st}^{0} represents the number of sex-specific blue crabs alive at the beginning of each fishing season; N_{st}^{T} indicates the number of blue crabs alive at the end of each year. The realized fishing mortality rate F_{st} is the key

[15] We select a value 2.9 for the nominal fishing mortality, which was also used in Bunnell, Lipton, and Miller (2010). A subsequent sensitivity analysis is conducted for different choices of such nominal fishing mortality rate. We find that the effect of different policies on sustainable revenue is quite robust. However, sustainable yield is more sensitive to specific value of fishing mortality rate, which is generally difficult to know in advance.

parameter out of the individual-based model and is fed into the later stock assessment model.

4.4.2 Stock Assessment Model

The second phase feeds the results from the first step into equations we adapt from the blue crab stock assessment model developed by Miller et al. (2011). Miller et al. (2011) fit a statistically-fitted population dynamics model that estimates the recruitment, total abundance, total fishing mortality rates, and sustainable harvest levels of the Chesapeake Bay blue crabs based on real harvest data and independent stock surveys conducted annually in the Chesapeake Bay. The model predicts the level of equilibrium sustainable harvest given the realized sex- and age- specific fishing mortality rate.

In our framework, we take the parameters estimated from the stock assessment model, together with the realized fishing mortality rates from the individual-based model, to estimate sustainable yield associated with each management scenario. The formulae for calculating sustainable yield are adapted from Miller et al. (2011):

$$(4.2) \qquad SY = \frac{x_s\left(\ln SPR_f + \ln\alpha + \sigma_R^2/2\right)}{\beta\sum_s SPR_s}\sum_s\left(\frac{F_{s1}}{M+F_{s1}}e^{-(M+F_{s0})} + \frac{F_{s0}}{M+F_{s0}}\left(1-e^{-(M+F_{s0})}\right)\right),$$

where SPR_s is sex-specific spawners per recruit:

$$SPR_s = \frac{x_s e^{-\left((1+\kappa)M+F_{s0}+\kappa F_{s1}\right)}}{1-e^{-(M+F_{s1})}}.$$

In the above two equations, the fishing mortality rates are the realized parameters from the first individual-based model component for both sexes and ages, denoted as F_{s0} and F_{s1}, where $s \in \{m, f\}$. Other parameters are directly drawn from Miller et al. (2011). The values and descriptions of the key parameters in (4.2) are presented in Table 4-1.

Table 4-1: Values of key parameters from the blue crab stock assessment model

Parameter	Description	Value
Predetermined		
x_s	Sex ratio (female/male) at recruitment	0.520
κ	Proportion of mortality before spawning	0.370
M	Natural mortality rate	0.900
Estimated		
α	Stock-recruitment parameter	26.673
β	Stock-recruitment parameter	0.052
σ_R	Standard deviation for recruitment	0.339

Source: Miller et al. (2011).

4.4.3 Inverse Demand Model

To add an economic element to our analysis, an inverse demand model that predicts prices for different catch levels is included (Huang 2015). Barten and Bettendorf (1989) indicates that inverse demand systems are appropriate for products that have highly inelastic supply in the short term, such as fish. Hence, we choose the Inverse Almost Ideal Demand (IAIDS) model developed by Eales and Unnevehr (1994) as our demand model.[16] The IAIDS model is derived from economic theory and empirically suitable for exploring the structure of a market that consists of multiple commodities.

[16] The IAIDS is a good fit for our problem for two reasons. First, the IADS model retains most of the desirable theoretical properties held by the AIDS model (Deaton and Muellbauer 1980; Eales and

This demand model, therefore, differs from Bunnell, Lipton, and Miller (2010), which is also an inverse demand model for the Chesapeake Bay blue crab fishery that regresses market prices for four market categories on quantities, seasonal dummies, and disposable income. However, their demand model is constructed with constant slopes and lacks cross-price effects that allow us to investigate market relationships between categories.

Demand for fish usually exhibits seasonality due to variation in consumption and the effects of the species' biological characteristics on supply. Our demand analysis modifies the IAIDS model to include seasonal effects. The estimated system of equations is:

$$w_i = \alpha_i + \sum_m \lambda_{im} D_m + \sum_j \gamma_{ij} \ln q_j + \beta_i \ln Q, \tag{4.3}$$

where w_i is the expenditure share for commodity i;[17] $\ln q_j$ denotes the logarithm of quantity for the j^{th} commodity; D_m is the seasonal dummy for the season m; and the translog term $\ln Q$ is represented as the following equation:

$$\ln Q = \alpha_0 + \sum_j \left(\alpha_j + \sum_m \lambda_{jm} D_m \right) \ln q_j + \frac{1}{2} \sum_i \sum_j \gamma_{ij} \ln q_i \ln q_j . \tag{4.4}$$

Unnevehr 1994). Second, the nonlinear structure provides a way of studying seasonal behavior in the fish market.

[17] Expenditure share for commodity i is calculated as: $w_i = p_i q_i \Big/ \sum_{j=1}^{n} p_j q_j$, where p_i is price and q_i is quantity.

Equation (4.3) and (4.4) together form a nonlinear system of equations.[18] Following Eales and Unnevehr (1994), the estimated parameters ($\alpha, \beta, \gamma, \lambda$) are used to calculate the scale and price flexibilities, the percentage change in price in response to a percentage change in quantity. We extend their results by allowing the flexibilities to differ by season:

$$f_{ijm} = -\delta_{ij} + \frac{\gamma_{ij} + \beta_i \left(\alpha_j + \lambda_{jm} + \sum_k \gamma_{kj} \ln q_{km} \right)}{w_{im}}, \tag{4.5}$$

$$f_{im} = -1 + \frac{\beta_i}{w_{im}}, \tag{4.6}$$

where δ_{ij} is the Kronecker delta ($\delta_{ij} = 1$ if $i = j$; otherwise $\delta_{ij} = 0$); f_{ijm} denotes seasonally price flexibility, while f_{im} denotes seasonal scale flexibility. Note that the flexibilities are dependent on the levels of expenditure share w_{im} and quantity $\ln q_{km}$. Here, we take seasonal averages of w_{im} and $\ln q_{km}$ from the sample data as approximations. These estimated flexibilities are used to predict price changes in response to quantity changes resulting from fishery policy alterations.[19]

---

[18] Accounting and economic restrictions can be imposed and tested in terms of estimated parameters. These restrictions are expressed as: $\sum_i \alpha_i = 1$, $\sum_i \gamma_{ij} = 0$, $\sum_i \beta_i = 0$, $\sum_i \lambda_{im} = 0$ (adding-up); $\sum_j \gamma_{ij} = 0$ (homogeneity); $\gamma_{ij} = \gamma_{ji}$, $\forall i \neq j$ (symmetry). In addition, there is difficulty in estimating the parameter α_0 in the nonlinear model (Deaton and Muellbauer 1980; Moschini, Moro, and Green 1994) . We set α_0 to zero following Moschini, Moro, and Green (1994).

[19] The price of a good is affected by not only own quantity changes but also quantity changes of other commodities in the same market. We assume that the effects of all commodities on the price of a good are multiplicative. In addition, to rule out extreme cases with very large simulated quantities, we also assume

4.4.4 Model Implementation

The integrated model investigates the sustainable revenue and yield outcomes for a large number of size, sex and season length regulations that are randomly generated by the Monte Carlo method. We first generate a large number of management scenarios by randomly varying each policy component within a reasonable range. The sampled management scenarios are evaluated in the integrated model sequentially.

For each management scenario, the integrated model generates the same set of random numbers that are used in the stochastic process for simulating the life history of blue crabs.[20] Thus, the sustainable outcomes out of the integrated model are comparable in levels. The following describes the detail on how we implement the model.

For a single management scenario, the individual-based model simulates the life history of all individual crabs over two years. At the end of simulation, the model predicts age- and sex-specific blue crabs harvests. According to the realized harvest outcomes, we calculate fishing mortality rates for both sexes and ages according to (4.1).

Given the estimated parameters from the stock assessment model and the realized fishing mortality rates from the individual-based model, we estimate the annual sustainable yield according to (4.2). In this step, we decompose the annual sustainable yield into monthly sustainable yield over two years for each category based on the proportion of category harvests from the individual-based model. The final monthly

---

that the prices are predicted within reasonable bounds that are set as 50% up and down of the maximum and minimum monthly prices from the fishery data.

[20] The sensitivity analysis is conducted by using different random seeds in the process of generating random numbers. The results are essentially the same for a specific management scenario.

sustainable yield is the summation of sustainable yield in the same month of first year (age-0 crabs) and second year (age-1 crabs).

The monthly prices for all market categories are predicted by the demand model, given the realized sustainable yield. Since we use the estimated flexibilities to explore how price changes in response to quantity changes, we need to specify a base scenario with prices and quantities. We choose monthly prices in 2007 from the market data as our base prices. For base quantities, we choose a specific simulated scenario that generates monthly sustainable yield. Because the predicted prices are compared to the base, the sustainable revenues are presented in relative terms.

4.4.5 Performance Measures

Two measures are chosen to evaluate the relative performance of different fishery policy components: sustainable yield and sustainable revenue. Sustainable yield is selected because it assesses biological equilibrium outcomes of different fishery management scenarios. Sustainable revenue measures the ability of policy components to achieve economic outcomes while maintaining yield at sustainable levels.

Note that these two measures are not ideal performance measures. First, these measures do not account for dynamic features due to the model structure and a lack of discount rate. Second, sustainable net revenue would be a better criterion for measuring economic outcomes compared to sustainable revenue, since costs to the industry are likely to vary significantly across different policies. For instance, vessel fuel consumption varies across fishing season closures. Unfortunately, we do not have a

suitable dataset to estimate costs associated with the blue crab policies and thus assume costs are constant. This could be a future study if a dataset was available. Finally, for the current analysis, we only focus on the suppliers' side of the benefits evaluation without considering differences in consumers' surplus.

The simulated policies and sustainable yields and revenues are then evaluated with regression methods. The sustainable yield and revenue are separately regressed on a set of policy variables. The performance of each policy component is represented by the resulting coefficients.

4.5 Results and Discussion

4.5.1 Estimation Results from the Demand Component

We estimate the demand for five market categories of blue crab with the nonlinear seemingly unrelated regression method.[21] The demand estimation uses monthly data on harvest from 1994 to 2007. That harvest data obtained from the Maryland Department of

[21] To avoid singularity problem, an equation has to be dropped for estimation. The coefficients of this equation are recovered from the adding-up constraint. The system estimates are not invariant to the deleted equation in the presence of serial correlation when dealing with time series data. To test for serial correlations, the Durbin-Watson (DW) statistics are calculated for four estimated equations. The test statistics range from 1.656 to 2.091, which are all higher than the lower critical value, 1.539, at the 5% significance level. It indicates that there is little evidence showing severe serial correlation in the residuals for our demand model. Moreover, the theoretical restrictions, homogeneity and symmetry are tested by likelihood ratio (LR) test. The LR test results reject both the homogeneity ($\chi^2 = 24.61$) and symmetry ($\chi^2 = 33.74$). Hence, our subsequent flexibilities are calculated based on the results without economic restrictions.

Natural Resources (MDNR) are recorded fishers log books. Monthly price data are obtained from the results of the MDNR monthly survey of seafood dealers.[22]

Since it is not straightforward to interpret parameters directly estimated from (4.3) and (4.4), the coefficient estimates are presented in Table B-1 in Appendix E. The season-varying flexibilities according to (4.5) and (4.6). The flexibility estimates are presented in Table 4-2.

The scale flexibility is interpreted as the percentage change in a normalized price (i.e., price divided by expenditure) due to a scale expansion for all commodities (Park and Thurman 1999). A commodity is classified as a necessity good if its scale flexibility is less than -1, or defined as a luxury good if greater than -1, following Eales and Unnevehr (1994). Blue crabs in the Chesapeake Bay appear to be necessities for all categories, except for soft and peelers.

Demand for a commodity is said to be flexible if the own-price flexibility is negative and greater than one in absolute value (Eales and Unnevehr 1994). The results show that most own-price flexibilities in three seasons are less than one in absolute value and have expected signs, indicating inflexible demand for these market categories. This means that a 1% increase in blue crab quantities results in less than 1% decline in corresponding prices. However, there are some unexpected results for own-price

[22] Since there is no category-specific data for Virginia, we assume the demand structure of blue crab in Maryland is representative for Chesapeake Bay, as in Bunnell, Lipton, and Miller (2010). In the dataset, the prices are converted to the real prices by the consumer price index (CPI) with the base CPI = 100 in 1982. The monthly quantity and price data range from April to November for each year. To account for seasonality, we group April and May as Spring, June to August as Summer, and September to November as Fall.

Table 4-2: Seasonal flexibilities for five categories in the Chesapeake Bay blue crab market

Quantity Change	#1 Male Price Change			#2 Male Price Change			Female Price Change			SP Price Change			Mixed Price Change		
	Spring	Summer	Fall	Spring	Summer	Fall	Spring	Summer	Fall	Spring	Summer	Fall	Spring	Summer	Fall
#1 Male	-0.624***	-0.705***	-0.655***	-1.017***	-0.524***	-0.780***	-0.443***	-0.579***	-0.194***	-1.185***	-0.170	-0.614	-0.571**	-0.451**	-0.537**
	(0.085)	(0.070)	(0.082)	(0.233)	(0.109)	(0.158)	(0.135)	(0.160)	(0.051)	(0.313)	(0.185)	(0.723)	(0.246)	(0.188)	(0.223)
#2 Male	-0.006	-0.014	-0.016	0.147	-0.448***	-0.448***	-0.127*	-0.166**	-0.054**	-0.058	-0.048	-0.218	0.035	0.027	0.033
	(0.034)	(0.028)	(0.033)	(0.108)	(0.052)	(0.052)	(0.067)	(0.082)	(0.027)	(0.054)	(0.070)	(0.258)	(0.117)	(0.092)	(0.110)
Female	-0.167***	-0.155***	-0.227***	-0.067	-0.042	-0.107	-0.041	0.168*	-0.626***	-0.236***	-0.305***	-0.701*	-0.158	-0.125	-0.149
	(0.041)	(0.033)	(0.039)	(0.125)	(0.061)	(0.090)	(0.076)	(0.095)	(0.032)	(0.071)	(0.095)	(0.364)	(0.132)	(0.104)	(0.126)
SP	-0.199***	-0.135***	-0.135***	-0.308***	-0.117***	-0.143***	-0.224***	-0.234***	-0.070***	-0.481***	-0.390***	1.224***	-0.009	-0.006	-0.006
	(0.033)	(0.027)	(0.031)	(0.093)	(0.038)	(0.050)	(0.055)	(0.056)	(0.016)	(0.062)	(0.092)	(0.386)	(0.094)	(0.059)	(0.061)
Mixed	-0.049	-0.042	-0.045	0.092	0.045	0.072	-0.123*	-0.151*	-0.048*	0.061	0.088	0.301	-0.372***	-0.505***	-0.410***
	(0.037)	(0.030)	(0.035)	(0.118)	(0.057)	(0.083)	(0.072)	(0.089)	(0.029)	(0.059)	(0.076)	(0.280)	(0.126)	(0.099)	(0.118)
Scale	-1.136***	-1.118***	-1.141***	-1.216***	-1.105***	-1.155***	-1.104***	-1.128***	-1.042***	-0.674***	-0.521***	1.046***	-1.004***	-1.003***	-1.003***
	(0.015)	(0.013)	(0.016)	(0.056)	(0.027)	(0.040)	(0.035)	(0.044)	(0.014)	(0.018)	(0.027)	(0.113)	(0.062)	(0.049)	(0.058)

Note: *** denotes 1% significance; ** denotes 5% significance; * denotes 10% significance. Standard errors are presented in parentheses.

flexibilities that are greater than zero, such as females in summer (0.168), and soft and peelers in fall (1.224).

For cross-price flexibility, a negative number indicates goods are substitutes, while a positive number denotes complements. The cross-price flexibilities show relationships between products. All significant cross-price flexibilities are negative, which indicates that the five blue crab market categories are substitutes over all three seasons.

4.5.2 Simulation Results from the Integrated Model

For our analysis, we wish to see the effects of alternative settings of the policy limits and wish to run the modeling system across a wide variety of these. This is done by simulating a large number of cases then fitting a summary equation with which we can investigate the effects of policy variations. We do this by running the simulation under a range of random cases for the policy limits on male and female crab size, season start and end dates, a possible mid-season closure for females. The ranges for the random items are reported in Table 4-3 and we used a uniform distribution across the range for each. For example, the fishing start date for males is randomly generated between March 14 and April 14, as shown in the first row of Table 4-3.

The simulated characteristics of the female crab season differ from those for males. Female fishing is allowed to be closed temporarily during a season. This type of policy was implemented by Maryland regulators in 2009. In our simulated scenarios, we allow the female fishing season to be closed never, once, or twice. The Monte Carlo procedure

Table 4-3: The range for randomly generated policies from the Monte Carlo method

Policy	Upper bound	Lower bound	Chance
Start-Date – M	March 14	April 14	–
End-Date – M	September 29	December 15	–
Start-Date – F	March 14	April 14	–
End-Date – F	October 26	December 15	–
No female season closure	–	–	50%
One female season closure	–	–	20%
Two female season closure	–	–	30%
First female season closure days (day)	20	60	–
Second female season closure days (day)	10	30	–
Change male and female min size limit (%)	–	–	50%
Initial Min Size Limit – M & F_0 (mm)	120	130	–
Changed Min Size Limit – M & F_0 (mm)	130	140	–
Change peeler min size limit (%)	–	–	50%
Initial Min Size Limit – Peeler (mm)	75	85	–
Changed Min Size Limit – Peeler (mm)	85	95	–
Min Size Limit – Soft (mm)	80	95	–
Max Size Lim – F_1 (mm)	140	160	–
Min Size Lim – F_1 (mm)	150	170	–

first decides whether and how many times the fishing season is closed, and then randomly generates the length of closures.

For the minimum size limit for males and immature females, it can be either the traditional range - 120mm and 130mm or a larger range 130mm and 140mm after July 15. Peeler crabs minimum limits have the similarly setting. The minimum and maximum size limits for mature females are separately generated within their own ranges.

We consequently generate 4,000 sets of simulation results and in turn estimate a regression that allows us to develop estimates of the marginal importance of each policy component of the management scenario set. Plots of the revenue and sustainable yield from these runs appear in Figure 4-2. It shows that the management scenarios with varying policies generate a wide range of sustainable yield and revenue combinations.

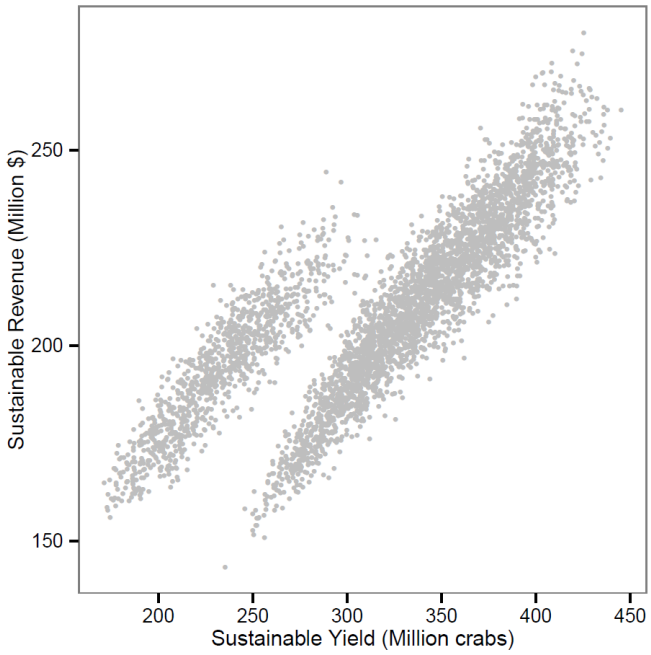

Figure 4-2: Sustainable yield and revenue for 4,000 simulated scenarios

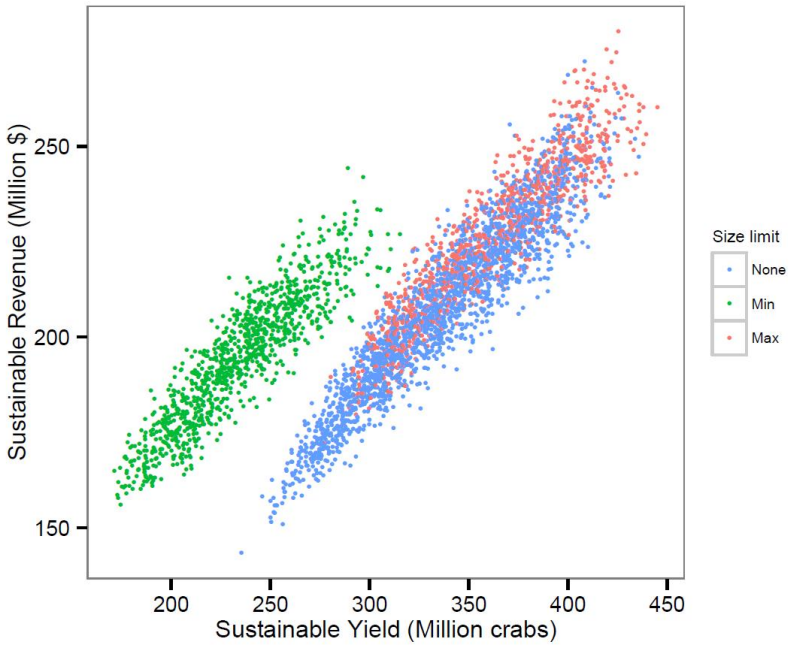

Figure 4-3: Clustered simulated scenarios based on the policy component of mature female size limit

Figure 4-2 clearly shows that the simulated scenarios results fall into two groups. And what divides the two groups basically is whether there is effective minimum size limit for mature females, as presented in Figure 4-3. The scenarios with minimum size limits, i.e., sizes of harvestable female crabs must be greater than the limit, lead to lower levels of sustainable yield, as shown with green dots. The scenarios with maximum size limits, i.e., sizes of harvestable female crabs must be less than the limit, result in higher sustainable revenues on average compared to scenarios without size limits.

The other results are not so apparent. Herein, we summarize them using regression with the dependent variables being sustainable yield and sustainable revenue and the independent variables being the settings of the policy components considered in our model. The regression results are presented in Table 4-4. The estimated coefficients can be interpreted as marginal effects of an alteration in the policy components from the base levels on the outcomes. Since sustainable yield and revenues are relative numbers; the absolute magnitudes of coefficients do not represent real values. The interpretation of Table 4-4 by policy is discussed below.

4.5.2.1 Fishing Season Length

Regulations on fishing season length are widely used for fisheries management. This is implemented in the Chesapeake Bay, where fishing is prohibited during winter. Usually, the fishing season starts around April 1, and ends around December 15. In our model, we take male and female fishing season start-date and fishing season length as fishing season variables.

Table 4-4: Regression results from the simulated management scenarios

Policy Components	Sustainable Revenue	Sustainable Yield
Start-Date – M (day)	0.506***	1.089***
	(0.013)	(0.020)
Season Length – M (day)	0.743***	1.418***
	(0.005)	(0.008)
Start-Date – F (day)	-0.175***	-0.041*
	(0.014)	(0.022)
Season Length – F (day)	-0.317***	-0.248***
	(0.007)	(0.012)
1 Season Closure – F (0 or 1)	0.919	2.339**
	(0.694)	(1.099)
2 Season Closures – F (0 or 1)	2.116***	0.981
	(0.680)	(1.078)
Closure Days – F (day)	-0.204***	-0.012
	(0.018)	(0.028)
Initial Min Size Lim – M & F_0 (mm)	-0.050	-1.641***
	(0.044)	(0.070)
Δ Min Size Lim – M & F_0 (mm)	-0.003	-1.312***
	(0.044)	(0.069)
Δ Min Size Lim – M & F_0 (0 or 1)	0.491	0.248
	(0.505)	(0.800)
Initial Min Size Lim – Peeler (mm)	-1.514***	-0.660***
	(0.047)	(0.074)
Δ Min Size Lim – Peeler (mm)	-1.220***	-0.515***
	(0.043)	(0.068)
Δ Min Size Lim – Peeler (0 or 1)	-0.852*	-1.062
	(0.495)	(0.784)
Min Size Lim – Soft (mm)	-0.532***	-0.252***
	(0.025)	(0.039)
Max Size Lim – F_1 (mm)	-0.847***	-0.731***
	(0.037)	(0.059)
Min Size Lim – F_1 (mm)	-0.794***	-2.465***
	(0.037)	(0.058)
Constant	528.815***	683.887***
	(11.244)	(17.816)
R-square	0.917	0.969

Note: The contents in the parenthesis associated with policy Instruments are units for the explanatory variables. *** denotes 1% significance; ** denotes 5% significance; * denotes 10% significance.

Both the coefficients associated with the male fishing season length are positive, indicating that making the male fishing season longer can result in higher sustainable revenue and sustainable yield, maybe because longer male fishing season allows more males with better quality to be harvested. For breeding purposes, fewer males are needed

for mature females. In addition, positive coefficients associated with male fishing start-date imply that postponing start-date can increase both sustainable revenue and sustainable yield.

Interestingly, the results for the female season are exactly the opposite of those for males. The estimated coefficients associated with female start-date and fishing season length are all negative, indicating a shorter female season would result in greater sustainable yield and revenue. These results likely arise because a shorter female fishing season is more effective in preserving the female stock, which is important for stock recruitment. Further, starting the female season earlier would increase sustainable revenue.

The regression also includes dummy variables indicating whether a closure of the female fishery is used. All of the estimated coefficients are positive and two are significant. This implies that intermittent season closure would be a favorable policy for the Chesapeake Bay blue crab fishery. In addition, the effect of the number of closure days is also examined. The coefficient of this term in the sustainable revenue equation is negative and significant, which indicates that longer intermittent closure can result in lower sustainable revenue.

4.5.2.2 Minimum Size Limits

Minimum size limit for males and females has been implemented for the Chesapeake Bay blue crab fishery. This policy seeks to protect juvenile crabs. Usually, the size limits are the same for both males and females. We follow this rule in our policy simulations. For some management scenarios, the minimum size limit is allowed to

change after July 15 during the fishing season. For example, the regulatory agency in Maryland sets the minimum size limit at 127 mm through July 15 since fishing season starts, and 133 mm thereafter. However, in Virginia, the minimum size limit remains the same throughout the fishing season. In our simulations, the minimum size limit at the beginning of the fishing season is first randomly selected. Then, after July 15, the limit either remains the same, or increases to a higher level.

The coefficients on the minimum size limit are insignificant for sustainable revenue, but negative and significant for sustainable yield except for the dummy variables on whether the minimum size limit is increased during a fishing season. The results indicate that increasing the minimum size limit at the beginning of a fishing season, i.e., making the policy more restrictive leads to lower sustainable yield. Increasing the minimum size limit in the middle of a season appears to bring about a similar effect on sustainable yield. The results suggest that the minimum size limit may be effective on protecting juvenile crabs, but decreases the number of harvested crabs since small crabs are not allowed to be caught. The fishery managers may wish to reconsider this specific policy.

4.5.2.3 Peeler Minimum Size Limits

There is also a minimum size restriction for peelers. The regulations implemented by Maryland in 2007 include the 82.5 mm size limit for peelers before July 15, and 89 mm thereafter (Bunnell, Lipton, and Miller 2010). In the simulated results, first a minimum size limit for peelers is randomly selected. Then the simulation algorithm randomly chooses to upgrade the limit or not on July 15 and, if so, randomly chooses a new size limit. The regression results show that increasing the minimum size limit either

before or during the fishing season tends to decrease both sustainable revenue and sustainable yield. These results are similar to those of minimum size limit for males and immature females. The minimum size limit prevents a number of small peeler crabs being harvested, which have high market prices and thus decreases fishery value.

4.5.2.4 Soft-shell Crabs Minimum Size Limits

A minimum size limit for soft-shell crabs is usually set constant over the season. In 2007 Maryland regulations, for example, the minimum size limit for soft-shell crabs is 89 mm or the entire season (Bunnell, Lipton, and Miller 2010). In our simulations, all simulated scenarios include randomly selected soft-shell minimum size limits. However, the estimated coefficients for sustainable revenue and yield are both negative and significant, suggesting that this policy is of little benefit to the blue crab fishery, since soft crabs generate high market values.

4.5.2.5 Female Size Limits

In actual management scenarios, there are no size restrictions for mature females. To examine the potential effects of this policy tool, some of our simulated scenarios include maximum or minimum size limit for mature females following Bunnell, Lipton, and Miller (2010). The purpose of this policy is to protect adult female crabs that are crucial for spawning.

There are three different scenarios in terms of mature female size limit. A simulated management scenario is determined to impose maximum size limit, minimum size limit, or no size limit. The estimated coefficients are all negative and significant for the size

limit variables, but they have different implications. The use of more restrictive maximum size limit will lead to higher sustainable revenue and yield. It appears that the more restrictive maximum size limit protects adult females from being harvested, yielding benefits in terms of harvests and revenue. In contrast to maximum size limit, increasing the limit reduces sustainable revenue and sustainable yield, suggesting that the minimum size limit should be set at a low level, similar to minimum size limits on males, immature females, and peelers. It should be noted that the magnitude for the coefficient associated with minimum size limit in the sustainable yield equation is much larger than others in absolute value (-2.465). This indicates that increasing minimum size limit will substantially reduce sustainable yield. This result is also shown in Figure 4-3.

4.5.3 Comparison with Previous Studies

Bunnell, Lipton, and Miller (2010) evaluated a similar set of policies, although not with the random variations in the policy settings rather using discrete values. To compare results, we evaluated these 15 management scenarios in our integrated model and compared their results to ours plus the consistency of their conclusions to ours. Descriptions of their scenarios are presented in Table B-2 in Appendix B. The results are combined with ours and graphed as the black dots in Figure 4-4.

The rankings for the 15 management scenarios are different from the Bunnell, Lipton, and Miller (2010) and our model in terms of both yield and revenue, likely due to their lack of the use of the stock assessment and cross commodity demand components. In particular, they conclude that the 165_MaxFemCW results in the highest

revenue, followed by 152_MaxFemCW and 10/1-12/15_FEM. However, we find that 10/1-12/15_FEM generates the highest sustainable revenue. For the specific season closure policy for females, we examine the effects of the length of within-season closure, which was not studied in Bunnell, Lipton, and Miller (2010).

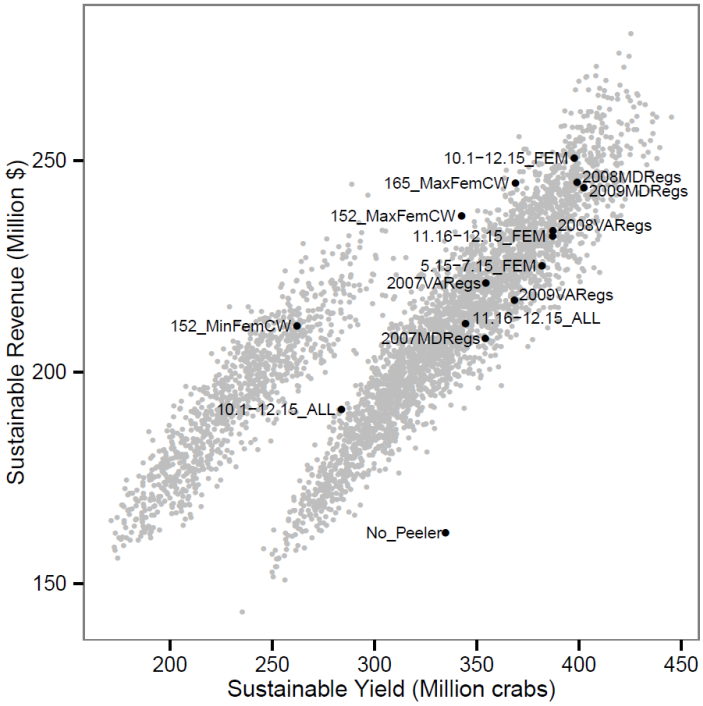

Figure 4-4: Sustainable yield and revenue for fifteen management scenarios (black) in Bunnell, Lipton, and Miller (2010) and 4,000 hypothetical scenarios (gray)

Although there are differences from their result due to model differences, the simulation results from the two models have some similarity. They found that management scenarios with earlier end-date and within-season closures for female crabs lead to higher revenue than those without such policies, which arises in our model as well. In our analysis, the maximum size limit for mature female results in higher

sustainable revenue and yield. Bunnell, Lipton, and Miller (2010) find the same thing but point out that this policy should be viewed with caution because the spawning contributions of different sizes of females are unknown and the life cycle individual-based model may not be doing this accurately.

4.6 Conclusions

The essay in this section examines the blue crab policies in the Chesapeake Bay using an integrated model. Conclusions can be drawn on the potential policies and on the modeling approach. The analysis provides simulation-based information on effects of different fishery policy components for the blue crab fishery. First, the results indicate that sustainable harvest and revenue could be increased if the female crab fishing season is shortened and intermittently closed to protect spawning females plus if maxim female size limits are imposed. We also find minimum size limits for males, immature females, and peelers appear to be ineffective and actually reducing of sustainable revenue and yield. For soft-shell crabs, a minimum size limit appears to be unwise, since they are the most valuable crabs in the market. Whether we should implement both minimum and maximum size limit for mature females is an open question.

In terms of the model, we extend the previous work that largely relied only on individual-based simulation models by connecting one with a stock assessment model and an improved economic demand model. This allows us to better examine the long-run stock implications of policies plus the price effects of interdependency of consumption of different crab types across size, sex, and shell status. We feel that the resulting model

offers potentially valuable insights for blue crab managers and a possible methodology that could be used in other fisheries settings.

The integrated bioeconomic model has some overlap with the model in Bunnell, Lipton, and Miller (2010), but differs in that a large set of management regulations are explored and the results are reported in sustainable levels. In addition, our random simulation and summary function approach make it much easier to explicitly identify the effects of manipulating individual policy components.

5 CONCLUSIONS

This dissertation conducts economic analysis of societal implications in agricultural cropping and fishery harvest within two settings: cropping under decadal climate variability in the Missouri River Basin and Chesapeake Bay blue crab fishery regulation. Specifically, the dissertation contains three main essays.

The first essay in Section 2 examines the physical impacts of decadal climate variability phenomena on crop yields for 8 major crops in the Missouri River Basin. The DCV effects are examined in terms of their indirect and direct effects on crop yields. This is investigated using a Bayesian hierarchical model to capture spatial heterogeneity with a moderate sample size. The model contains both equations for DCV effects on climate and those on yields considering the climate effects. Jointly, these equations allow us to recover an estimate of the total DCV effects on crop yields. The results show that DCV phases alter crop yields on a geographically specific basis and suggest adaptation is possible by altering crop mix.

Following up on the first essay, the second essay in Section 3 investigates the economic value of informing farmers about future DCV phases and their yield implications. Simultaneously, it also examines the possible management adaptations. The study employs a stochastic programming model that simulates crop mix, irrigation use, crop production, prices, and welfare under different DCV information settings of perfect, conditional, and naïve information. The results show that relative to the naïve case, the conditional DCV information generates net benefits of $28.83 million annually

to the region, while the perfect DCV information results in an annual gain of $82.29 million. The results also indicate that adaptations in terms of crop acreage and irrigation use changes are possible given different DCV information.

The third essay in Section 4 turns attention to fisheries policy in the context of the Chesapeake Bay fishery. An analysis tool is built in the form of a bioeconomic simulation model, which integrates two biological models and an economic demand model. The resultant model simulates the long-term outcomes from the imposition of harvest regulations involving sex-specific season length and size limits. The model is run under a wide variety of possible regulation settings and a summary regression function is estimated. The summary results indicate that sustainable harvest and revenue could be increased if the female crab fishing season were shortened and intermittently closed. We also find that minimum size limits appear to be actually reducing sustainable revenue and yield. In addition, increasing the maximum size limit for mature females increases revenue.

Although the dissertation develops environment- and policy-relevant information, each essay has limitations and could be improved for future research. In the first essay, the estimation in the Bayesian framework does not account for spatial correlation among counties, and in particular does not include spatial smoothness parameters for connecting nearby counties. In the future, it would be desirable to introduce such spatial correlation using spatially varying coefficient processes such as those in Gelfand et al. (2003).

For the second essay, the study focused on agricultural cropping in the MRB region and neglected livestock production. In the future, the model could be extended to include

livestock production, which would produce more complete economic value estimate relative to the provision of DCV information. In addition, the study could be extended to study the welfare difference between the value of El Niño Southern Oscillation information and DCV information. ENSO is a well-known climate phenomenon, while DCV is a set of phenomena that have not been as widely considered. It would be of interest to investigate the economic value change associated with information improvement from ENSO to DCV.

In Section 4, the regulation analysis results are based on the validity of the model components – the individual-based model that produces crab mortality and catch plus the stock assessment model that predicts long-term populations. Clearly, if those items have incorrect assumptions, they certainly carry into the unifying bioeconomic model. In this case, the bioeconomic model components could be checked with fisheries scientists. Second, future research could be done on extending the current work to welfare evaluation of blue crab policies including the effects on the consumer side due to altered prices. Third, the model could be extended to include costs, providing that satisfactory data can be found. Fourth, the model only examines long-run static equilibria without considering fishers' behavior alterations in response to fishery policies and extensions could be done to include fisher behavior and their dynamic aspects.

REFERENCES

Adams, D.M., R.J. Alig, J.M. Callaway, B.A. McCarl, and S.M. Winnett. 1996. *The Forest and Agricultural Sector Optimization Model (FASOM): Model Structure and Policy Applications.* Portland, OR: USDA Forest Service.

Adams, R.M., K.J. Bryant, B.A. McCarl, D.M. Legler, J. O'Brien, A. Solow, and R. Weiher. 1995. Value of Improved Long-Range Weather Information. *Contemporary Economic Policy* 13(3):10-9.

Adams, R.M., L.L. Houston, B.A. McCarl, M. Tiscareño L, J. Matus G, and R.F. Weiher. 2003. The Benefits to Mexican Agriculture of an El Niño-Southern Oscillation (ENSO) Early Warning System. *Agricultural and Forest Meteorology* 115(3):183-94.

Aguilar, R., E.G. Johnson, A.H. Hines, M.A. Kramer, and M.R. Goodison. 2008. Importance of Blue Crab Life History for Stock Enhancement and Spatial Management of the Fishery in Chesapeake Bay. *Reviews in Fisheries Science* 16(1-3):117-24.

Anderson, L.G., and J.C. Seijo. 2010. *Bioeconomics of Fisheries Management*. New York: Wiley-Blackwell.

Arellano-Valle, R., H. Bolfarine, and V. Lachos. 2007. Bayesian Inference for Skew-Normal Linear Mixed Models. *Journal of Applied Statistics* 34(6):663-82.

Balcombe, K., M. Burton, and D. Rigby. 2011. Skew and Attribute Non-Attendance within the Bayesian Mixed Logit Model. *Journal of Environmental Economics and Management* 62(3):446-61.

Balcombe, K., A. Chalak, and I. Fraser. 2009. Model Selection for the Mixed Logit with Bayesian Estimation. *Journal of Environmental Economics and Management* 57(2):226-37.

Baron, R.M., and D.A. Kenny. 1986. The Moderator-Mediator Variable Distinction in Social Psychological Research: Conceptual, Strategic, and Statistical Considerations. *Journal of Personality and Social Psychology* 51(6):1173-82.

Barten, A.P., and L.J. Bettendorf. 1989. Price Formation of Fish: An Application of an Inverse Demand System. *European Economic Review* 33(8):1509-25.

Bastardie, F., J.R. Nielsen, and G. Kraus. 2010. The Eastern Baltic Cod Fishery: A Fleet-Based Management Strategy Evaluation Framework to Assess the Cod Recovery Plan of 2008. *ICES Journal of Marine Science: Journal du Conseil* 67(1):71-86.

Beach, R.H., D.M. Adams, R.J. Alig, J.S. Baker, G.S. Latta, B.A. McCarl, B.C. Murray, S.K. Rose, and E.M. White. 2010. *Model Documentation for the Forest and Agricultural Sector Optimization Model with Greenhouse Gases (FASOMGHG).* Research Triangle Park, NC: RTI International.

Berry, B.J., and A. Okulicz-Kozaryn. 2008. Are there ENSO Signals in the Macroeconomy? *Ecological Economics* 64(3):625-33.

Botsford, L.W., J.C. Castilla, and C.H. Peterson. 1997. The Management of Fisheries and Marine Ecosystems. *Science* 277(5325):509-15.

Brunner, A.D. 2002. El Niño and World Primary Commodity Prices: Warm Water Or Hot Air? *Review of Economics and Statistics* 84(1):176-83.

Bunnell, D.B., D.W. Lipton, and T.J. Miller. 2010. The Bioeconomic Impact of Different Management Regulations on the Chesapeake Bay Blue Crab Fishery. *North American Journal of Fisheries Management* 30(6):1505-21.

Bunnell, D.B., and T.J. Miller. 2005. An Individual-Based Modeling Approach to Spawning-Potential Per-Recruit Models: An Application to Blue Crab (Callinectes Sapidus) in Chesapeake Bay. *Canadian Journal of Fisheries and Aquatic Sciences* 62(11):2560-72.

Cayan, D.R., M.D. Dettinger, H.E. Diaz, and N.E. Graham. 1998. Decadal Variability of Precipitation over Western North America. *Journal of Climate* 11(12):3148-66.

Challinor, A. 2009. Towards the Development of Adaptation Options using Climate and Crop Yield Forecasting at Seasonal to Multi-Decadal Timescales. *Environmental Science & Policy* 12(4):453-65.

Chen, C., D. Gillig, B.A. McCarl, and R. Williams. 2005. ENSO Impacts on Regional Water Management: Case Study of the Edwards Aquifer (Texas, USA). *Climate Research* 28(2):175-82.

Chen, C., and B.A. McCarl. 2000. The Value of ENSO Information to Agriculture: Consideration of Event Strength and Trade. *Journal of Agricultural & Resource Economics* 25(2):368-85.

Chen, C., B.A. McCarl, and H.S. Hill. 2002. Agricultural Value of ENSO Information under Alternative Phase Definition. *Climatic Change* 54(3):305-25.

Chen, C., B.A. McCarl, and D.E. Schimmelpfennig. 2004. Yield Variability as Influenced by Climate: A Statistical Investigation. *Climatic Change* 66(1):239-61.

Clark, C.W. 1973. The Economics of Overexploitation. *Science* 181(4100):630-4.

Clarke, A.J., J. Wang, and S. Van Gorder. 2000. A Simple Warm-Pool Displacement ENSO Model. *Journal of Physical Oceanography* 30(7):1679-91.

Deacon, R.T. 1989. An Empirical Model of Fishery Dynamics. *Journal of Environmental Economics and Management* 16(2):167-83.

Deaton, A., and J. Muellbauer. 1980. An almost Ideal Demand System. *The American Economic Review* 70(3):312-26.

Deser, C., A.S. Phillips, and J.W. Hurrell. 2004. Pacific Interdecadal Climate Variability: Linkages between the Tropics and the North Pacific during Boreal Winter since 1900. *Journal of Climate* 17(16):3109-24.

Dichmont, C., A. Deng, A. Punt, N. Ellis, W. Venables, T. Kompas, Y. Ye, S. Zhou, and J. Bishop. 2008. Beyond Biological Performance Measures in Management Strategy Evaluation: Bringing in Economics and the Effects of Trawling on the Benthos. *Fisheries Research* 94(3):238-50.

Diekert, F.K., D.Ø Hjermann, E. Nævdal, and N.C. Stenseth. 2010. Spare the Young Fish: Optimal Harvesting Policies for North-East Arctic Cod. *Environmental and Resource Economics* 47(4):455-75.

Ding, J. 2014. Three Essays on Climate Variability, Water, and Agricultural Production. PhD dissertation, Texas A&M University.

Eales, J.S., and L.J. Unnevehr. 1994. The Inverse almost Ideal Demand System. *European Economic Review* 38(1):101-15.

FAO. 2009. *The State of World Fisheries and Aquaculture 2008*. Rome, Italy: Food and Agriculture Organization of the United Nations.

Fernandez, M.A. 2013. Decadal Climate Variability: Economic Implications in Agriculture and Water in the Missouri River Basin. PhD dissertation, Texas A&M University.

Fogarty, M.J., and T.J. Miller. 2004. Impact of a Change in Reporting Systems in the Maryland Blue Crab Fishery. *Fisheries Research* 68(1):37-43.

Gelfand, A.E., H. Kim, C. Sirmans, and S. Banerjee. 2003. Spatial Modeling with Spatially Varying Coefficient Processes. *Journal of the American Statistical Association* 98(462):387-96.

Ghidey, W., E. Lesaffre, and P. Eilers. 2004. Smooth Random Effects Distribution in a Linear Mixed Model. *Biometrics* 60(4):945-53.

Good, P., J.A. Lowe, and D.P. Rowell. 2009. Understanding Uncertainty in Future Projections for the Tropical Atlantic: Relationships with the Unforced Climate. *Climate Dynamics* 32(2-3):205-18.

Gordon, H.S. 1954. The Economic Theory of a Common-Property Resource: The Fishery. *The Journal of Political Economy* 62(2):124-42.

Hennessy, D.A. 2009. Crop Yield Skewness under Law of the Minimum Technology. *American Journal of Agricultural Economics* 91(1):197-208.

Heppell, S.S., S.A. Heppell, F.C. Coleman, and C.C. Koenig. 2006. Models to Compare Management Options for a Protogynous Fish. *Ecological Applications* 16(1):238-49.

Hill, H.S., J.W. Mjelde, H.A. Love, D.J. Rubas, S.W. Fuller, W. Rosenthal, and G. Hammer. 2004. Implications of Seasonal Climate Forecasts on World Wheat Trade:

A Stochastic, Dynamic Analysis. *Canadian Journal of Agricultural Economics* 52(3):289-312.

Hill, H.S., J. Park, J.W. Mjelde, W. Rosenthal, H.A. Love, and S.W. Fuller. 2000. Comparing the Value of Southern Oscillation Index-Based Climate Forecast Methods for Canadian and US Wheat Producers. *Agricultural and Forest Meteorology* 100(4):261-72.

Hilton, R.W. 1981. The Determinants of Information Value: Synthesizing some General Results. *Management Science* 27(1):57-64.

Hoff, P.D. 2009. *A First Course in Bayesian Statistical Methods*. New York: Springer.

Homans, F.R., and J.E. Wilen. 2005. Markets and Rent Dissipation in Regulated Open Access Fisheries. *Journal of Environmental Economics and Management* 49(2):381-404.

Huang, B., and V.M. Mehta. 2004. Response of the Indo-Pacific Warm Pool to Interannual Variations in Net Atmospheric Freshwater. *Journal of Geophysical Research: Oceans (1978-2012)* 109(C6022).

Huang, P. 2015. An Inverse Demand System for the Differentiated Blue Crab Market in Chesapeake Bay. *Marine Resource Economics* 30(2):139-56.

Ives, M., J. Scandol, and J. Greenville. 2013. A Bio-Economic Management Strategy Evaluation for a Multi-Species, Multi-Fleet Fishery Facing a World of Uncertainty. *Ecological Modelling* 25669-84.

Izaurralde, R.C., N.J. Rosenberg, R.A. Brown, and A.M. Thomson. 2003. Integrated Assessment of Hadley Center (HadCM2) Climate-Change Impacts on Agricultural Productivity and Irrigation Water Supply in the Conterminous United States: Part II. Regional Agricultural Production in 2030 and 2095. *Agricultural and Forest Meteorology* 117(1):97-122.

Jackson, J.B., M.X. Kirby, W.H. Berger, K.A. Bjorndal, L.W. Botsford, B.J. Bourque, R.H. Bradbury, R. Cooke, J. Erlandson, and J.A. Estes. 2001. Historical Overfishing and the Recent Collapse of Coastal Ecosystems. *Science* 293(5530):629-37.

Jara, A., F. Quintana, and E. San Martín. 2008. Linear Mixed Models with Skew-Elliptical Distributions: A Bayesian Approach. *Computational Statistics & Data Analysis* 52(11):5033-45.

Jardim, E., S. Cerviño, and M. Azevedo. 2010. Evaluating Management Strategies to Implement the Recovery Plan for Iberian Hake (Merluccius Merluccius); the Impact of Censored Catch Information. *ICES Journal of Marine Science: Journal du Conseil* 67(2):258-69.

Kass, R.E., and L. Wasserman. 1995. A Reference Bayesian Test for Nested Hypotheses and its Relationship to the Schwarz Criterion. *Journal of the American Statistical Association* 90(431):928-34.

Katz, R.W., and A.H. Murphy. 1997. *Economic Value of Weather and Climate Forecasts*. Cambridge, United Kingdom: Cambridge University Press.

Kim, M., and B.A. McCarl. 2005. The Agricultural Value of Information on the North Atlantic Oscillation: Yield and Economic Effects. *Climatic Change* 71(1-2):117-39.

Knutson, T.R., and S. Manabe. 1995. Time-Mean Response Over the Tropical Pacific to Increased C02 in a Coupled Ocean-Atmosphere Model. *Journal of Climate* 8(9):2181-99.

Lachos, V.H., D.K. Dey, and V.G. Cancho. 2009. Robust Linear Mixed Models with Skew-Normal Independent Distributions from a Bayesian Perspective. *Journal of Statistical Planning and Inference* 139(12):4098-110.

Laird, N.M., and J.H. Ware. 1982. Random-Effects Models for Longitudinal Data. *Biometrics* 38(4):963-74.

Layton, D.F., and R.A. Levine. 2003. How much does the Far Future Matter? A Hierarchical Bayesian Analysis of the Public's Willingness to Mitigate Ecological Impacts of Climate Change. *Journal of the American Statistical Association* 98(463):533-44.

Lee, H.S., T. Yamashita, and T. Mishima. 2012. Multi-Decadal Variations of ENSO, the Pacific Decadal Oscillation and Tropical Cyclones in the Western North Pacific. *Progress in Oceanography* 10567-80.

Leon-Gonzalez, R., and R. Scarpa. 2008. Improving Multi-Site Benefit Functions Via Bayesian Model Averaging: A New Approach to Benefit Transfer. *Journal of Environmental Economics and Management* 56(1):50-68.

Letson, D., G.P. Podestá, C.D. Messina, and R.A. Ferreyra. 2005. The Uncertain Value of Perfect ENSO Phase Forecasts: Stochastic Agricultural Prices and Intra-Phase Climatic Variations. *Climatic Change* 69(2-3):163-96.

Lipcius, R.N., and W.T. Stockhausen. 2002. Concurrent Decline of the Spawning Stock, Recruitment, Larval Abundance, and Size of the Blue Crab Callinectes Sapidus in Chesapeake Bay. *Marine ecology. Progress series* 22645-61.

Lukas, R., and E. Lindstrom. 1991. The Mixed Layer of the Western Equatorial Pacific Ocean. *Journal of Geophysical Research: Oceans (1978–2012)* 96(S01):3343-57.

Macher, C., and J. Boncoeur. 2010. Optimal Selectivity and Effort Cost: A Simple Bioeconomic Model with an Application to the Bay of Biscay Nephrops Fishery. *Marine Resource Economics* 25(2):213-32.

Mantua, N.J., and S.R. Hare. 2002. The Pacific Decadal Oscillation. *Journal of Oceanography* 58(1):35-44.

Mantua, N.J., S.R. Hare, Y. Zhang, J.M. Wallace, and R.C. Francis. 1997. A Pacific Interdecadal Climate Oscillation with Impacts on Salmon Production. *Bulletin of the American Meteorological Society* 78(6):1069-79.

Maravelias, C.D., R. Hillary, J. Haralabous, and E.V. Tsitsika. 2010. Stochastic Bioeconomic Modelling of Alternative Management Measures for Anchovy in the Mediterranean Sea. *ICES Journal of Marine Science: Journal du Conseil* 67(6):1291-300.

McCabe, G.J., M.A. Palecki, and J.L. Betancourt. 2004. Pacific and Atlantic Ocean Influences on Multidecadal Drought Frequency in the United States. *Proceedings of the National Academy of Sciences of the United States of America* 101(12):4136-41.

McCabe, G.J., J.L. Betancourt, S.T. Gray, M.A. Palecki, and H.G. Hidalgo. 2008. Associations of Multi-Decadal Sea-Surface Temperature Variability with US Drought. *Quaternary International* 188(1):31-40.

McCarl, B.A. 1982. Cropping Activities in Agricultural Sector Models: A Methodological Proposal. *American Journal of Agricultural Economics* 64(4):768-72.

McCarl, B.A., and T.H. Spreen. 1980. Price Endogenous Mathematical Programming as a Tool for Sector Analysis. *American Journal of Agricultural Economics* 62(1):87-102.

McCarl, B.A., X. Villavicencio, and X. Wu. 2008. Climate Change and Future Analysis: Is Stationarity Dying? *American Journal of Agricultural Economics* 90(5):1241-7.

Mehta, V.M. 1998. Variability of the Tropical Ocean Surface Temperatures at Decadal-Multidecadal Timescales. Part I: The Atlantic Ocean. *Journal of Climate* 11(9):2351-75.

Mehta, V.M., N.J. Rosenberg, and K. Mendoza. 2012. Simulated Impacts of Three Decadal Climate Variability Phenomena on Dryland Corn and Wheat Yields in the Missouri River Basin. *Agricultural and Forest Meteorology* 152109-24.

———2011. Simulated Impacts of Three Decadal Climate Variability Phenomena on Water Yields in the Missouri River Basin. *JAWRA Journal of the American Water Resources Association* 47(1):126-35.

Mendelsohn, R., W.D. Nordhaus, and D. Shaw. 1994. The Impact of Global Warming on Agriculture: A Ricardian Analysis. *The American Economic Review* 84(4):753-71.

Meza, F.J., J.W. Hansen, and D. Osgood. 2008. Economic Value of Seasonal Climate Forecasts for Agriculture: Review of Ex-Ante Assessments and Recommendations for Future Research. *Journal of Applied Meteorology and Climatology* 47(5):1269-86.

Miller, A.J., and N. Schneider. 2000. Interdecadal Climate Regime Dynamics in the North Pacific Ocean: Theories, Observations and Ecosystem Impacts. *Progress in Oceanography* 47(2):355-79.

Miller, T.J., M.J. Wilberg, A.R. Colton, G.R. Davis, A. Sharov, R.M. Lipcius, G.M. Ralph, E.G. Johnson, and A.G. Kaufman. 2011. *Stock Assessment of Blue Crab in Chesapeake Bay: 2011*. Norfolk, VA: NOAA Chesapeake Bay Office.

Miller, T.J. 2001. *The Precautionary Approach to Managing the Blue Crab in Chesapeake Bay: Establishing Limits and Targets*. Solomons, MD: University of Maryland Chesapeake Biological Laboratory.

Miller, T.J., S.J.D. Martell, D.B. Bunnell, G. Davis, L. Fegley, A. Sharov, C. Bonzek, D. Hewitt, J. Hoenig, and R.N. Lipcius. 2005. *Stock Assessment of Blue Crab in Chesapeake Bay: 2005*. Solomons, MD: University of Maryland Center for Environmental Science Chesapeake Biological Laboratory.

Miller, T.J., and E.D. Houde. 1999. *Blue Crab Target Setting: Final Report*. Solomons, MD: University of Maryland Center for Environmental Science, Chesapeake Biological Laboratory.

Mjelde, J.W., T.N. Thompson, F.M. Hons, J.T. Cothren, and C.G. Coffman. 1997. Using Southern Oscillation Information for Determining Corn and Sorghum Profit-Maximizing Input Levels in East-Central Texas. *Journal of Production Agriculture* 10(1):168-75.

Mjelde, J.W., and H.S.J. Hill. 1999. The Effect of the use of Improved Climate Forecasts on Variable Costs, Input Usage, and Production. *Agricultural Systems* 60(3):213-25.

Moschini, G., D. Moro, and R.D. Green. 1994. Maintaining and Testing Separability in Demand Systems. *American Journal of Agricultural Economics* 76(1):61-73.

Murphy, J., V. Kattsov, N. Keenlyside, M. Kimoto, G. Meehl, V. Mehta, H. Pohlmann, A. Scaife, and D. Smith. 2010. Towards Prediction of Decadal Climate Variability and Change. *Procedia Environmental Sciences* 1(0):287-304.

Needle, C.L. 2008. Management Strategy Evaluation for North Sea Haddock. *Fisheries Research* 94(2):141-50.

Nelson, R.R., and S.G. Winter. 1964. A Case Study in the Economics of Information and Coordination: The Weather Forecasting System. *The Quarterly Journal of Economics* 73(3):420-41.

Nigam, S., B. Guan, and A. Ruiz-Barradas. 2011. Key Role of the Atlantic Multidecadal Oscillation in 20th Century Drought and Wet Periods Over the Great Plains. *Geophysical Research Letters* 38(16).

Pala, C. 2010. Chesapeake Crabs: Engineering a Rebound. *Science* 330(6010):1474.

Park, H., and W.N. Thurman. 1999. On Interpreting Inverse Demand Systems: A Primal Comparison of Scale Flexibilities and Income Elasticities. *American Journal of Agricultural Economics* 81(4):950-8.

Picaut, J., M. Ioualalen, C. Menkes, T. Delcroix, and M.J. McPhaden. 1996. Mechanism of the Zonal Displacements of the Pacific Warm Pool: Implications for ENSO. *Science* 274(5292):1486-9.

Quinn II, T.J., and R.B. Deriso. 1999. *Quantitative Fish Dynamics*. New York: Oxford University Press.

Rajagopalan, B., Y. Kushnir, and Y.M. Tourre. 1998. Observed Decadal Midlatitude and Tropical Atlantic Climate Variability. *Geophysical Research Letters* 25(21):3967-70.

Ramirez, O.A., S. Misra, and J. Field. 2003. Crop-Yield Distributions Revisited. *American Journal of Agricultural Economics* 85(1):108-20.

Rosa, G., C.R. Padovani, and D. Gianola. 2003. Robust Linear Mixed Models with Normal/Independent Distributions and Bayesian MCMC Implementation. *Biometrical Journal* 45(5):573-90.

Rowell, D.P., C.K. Folland, K. Maskell, and M.N. Ward. 1995. Variability of Summer Rainfall Over Tropical North Africa (1906-92): Observations and Modelling. *Quarterly Journal of the Royal Meteorological Society* 121(523):669-704.

Rugolo, L.J., K. Knotts, A. Lange, V. Crecco, M. Terceiro, C.F. Bonzek, C. Stagg, R. O'Reilly, and D.S. Vaughan. 1997. *Stock Assessment of Chesapeake Bay Blue Crab (Callinectes Sapidus)*. Norfolk, VA: NOAA Chesapeake Bay Office.

Sahu, S.K., D.K. Dey, and M.D. Branco. 2003. A New Class of Multivariate Skew Distributions with Applications to Bayesian Regression Models. *Canadian Journal of Statistics* 31(2):129-50.

Schlenker, W., W.M. Hanemann, and A.C. Fisher. 2006. The Impact of Global Warming on US Agriculture: An Econometric Analysis of Optimal Growing Conditions. *Review of Economics and Statistics* 88(1):113-25.

Schlenker, W., and M.J. Roberts. 2009. Nonlinear Temperature Effects Indicate Severe Damages to U.S. Crop Yields Under Climate Change. *Proceedings of the National Academy of Sciences of the United States of America* 106(37):15594-8.

Scott, A. 1955. The Fishery: The Objectives of Sole Ownership. *The Journal of Political Economy* 63(2):116-24.

Sherrick, B.J., F.C. Zanini, G.D. Schnitkey, and S.H. Irwin. 2004. Crop Insurance Valuation under Alternative Yield Distributions. *American Journal of Agricultural Economics* 86(2):406-19.

Smith, M.D. 2012. The New Fisheries Economics: Incentives Across Many Margins. *Annual Review of Resource Economics* 4(1):379-402.

Smith, M.D., and J.E. Wilen. 2003. Economic Impacts of Marine Reserves: The Importance of Spatial Behavior. *Journal of Environmental Economics and Management* 46(2):183-206.

Smith, M.D., J. Zhang, and F.C. Coleman. 2008. Econometric Modeling of Fisheries with Complex Life Histories: Avoiding Biological Management Failures. *Journal of Environmental Economics and Management* 55(3):265-80.

Solomon, A., and F. Jin. 2005. A Study of the Impact of Off-Equatorial Warm Pool SST Anomalies on ENSO Cycles. *Journal of Climate* 18(2):274-86.

Solow, A.R., R.F. Adams, K.J. Bryant, D.M. Legler, J.J. O'Brien, B.A. McCarl, W. Nayda, and R. Weiher. 1998. The Value of Improved ENSO Prediction to US Agriculture. *Climatic Change* 39(1):47-60.

Sutton, R.T., and D.L. Hodson. 2005. Atlantic Ocean Forcing of North American and European Summer Climate. *Science (New York, N.Y.)* 309(5731):115-8.

Tack, J., A. Harri, and K. Coble. 2012. More than Mean Effects: Modeling the Effect of Climate on the Higher Order Moments of Crop Yields. *American Journal of Agricultural Economics* 94(5):1037-54.

Tahvonen, O. 2009. Economics of Harvesting Age-Structured Fish Populations. *Journal of Environmental Economics and Management* 58(3):281-99.

———2009. Optimal Harvesting of Age-Structured Fish Populations. *Marine Resource Economics* 24(2):147.

Torrence, C., and P.J. Webster. 1999. Interdecadal Changes in the ENSO-Monsoon System. *Journal of Climate* 12(8):2679-90.

Verbeke, G., and E. Lesaffre. 1997. The Effect of Misspecifying the Random-Effects Distribution in Linear Mixed Models for Longitudinal Data. *Computational Statistics & Data Analysis* 23(4):541-56.

Wang, H., and V.M. Mehta. 2008. Decadal Variability of the Indo-Pacific Warm Pool and its Association with Atmospheric and Oceanic Variability in the NCEP-NCAR and SODA Reanalyses. *Journal of Climate* 21(21):5545-65.

Webster, P.J., and R. Lukas. 1992. TOGA COARE: The Coupled Ocean-Atmosphere Response Experiment. *Bulletin of the American Meteorological Society* 73(9):1377-416.

Wooldridge, J.M. 2010. *Econometric Analysis of Cross Section and Panel Data*. Boston: MIT press.

Yan, X., C. Ho, Q. Zheng, and V. Klemas. 1992. Temperature and Size Variabilities of the Western Pacific Warm Pool. *Science* 258(5088):1643-5.

Yu, T., and B.A. Babcock. 2010. Are US Corn and Soybeans Becoming More Drought Tolerant? *American Journal of Agricultural Economics* 92(5):1310-23.

Zhang, D., and M. Davidian. 2001. Linear Mixed Models with Flexible Distributions of Random Effects for Longitudinal Data. *Biometrics* 57(3):795-802.

APPENDIX A

APPENDIX FOR SECTION 2

A.1. Bayesian Algorithm for the Normal Hierarchical Model

This appendix section presents the details, via which the Bayesian algorithm is used in estimating the normal hierarchical model, as shown in equations (2.3), (2.5), and (2.6) in the text. The whole procedure describes the steps of deriving and sampling posterior distributions for all unknown parameters in the model.

A.1.1. Joint Posterior Distribution

It is often of interest to examine the joint posterior distribution for all unknown parameters that arise from a Bayesian analysis. The joint posterior distribution for the normal hierarchical model can be derived according to the Bayes' rule, which is proportional to the multiplication of the sampling distributions and prior distributions. The general form of the joint posterior distribution is represented as:

$$
\begin{aligned}
& p\left(\boldsymbol{\theta}_1^C,\ldots,\boldsymbol{\theta}_m^C,\boldsymbol{\beta}^C,\sigma_C^2,\boldsymbol{\Sigma}^C \,\middle|\, \mathbf{w}_1^C,\ldots,\mathbf{w}_m^C,\mathbf{X}^W\right) \\
\propto\ & p\left(\mathbf{w}_1^C,\ldots,\mathbf{w}_m^C \,\middle|\, \boldsymbol{\theta}_1^C,\ldots,\boldsymbol{\theta}_m^C,\sigma_C^2,\mathbf{X}^W\right) \rightarrow \text{Multi-Normal sampling} \\
\times\ & p\left(\boldsymbol{\theta}_1^C,\ldots,\boldsymbol{\theta}_m^C \,\middle|\, \boldsymbol{\beta}^C,\boldsymbol{\Sigma}^C\right) \rightarrow \text{Multi-Normal sampling} \\
\times\ & p\left(\boldsymbol{\beta}^C,\sigma_C^2,\boldsymbol{\Sigma}^C\right). \rightarrow \text{Priors}
\end{aligned}
\tag{A.1}
$$

In (A.1), components associated with $\mathbf{w}_j^C$ and $\boldsymbol{\theta}_j^C$ for all j are specified by their sampling distributions (2.5) and (2.6), respectively. We plug in the sampling

distributions and the prior distributions for $\boldsymbol{\beta}^C$, σ_C^2, and $\boldsymbol{\Sigma}^C$, which will be discussed in Section A.1.2 to generate the specific form of the joint posterior distribution.

A.1.2. Prior Distributions

The unknown parameters in equation (A.1) that require pre-specified priors are $\boldsymbol{\beta}^C$, σ_C^2, and $\boldsymbol{\Sigma}^C$. We assume that the priors are independent in the model such that the joint prior distribution in (A.1) can be expressed as:

$$p\left(\boldsymbol{\beta}^C, \sigma_C^2, \boldsymbol{\Sigma}^C\right) = p\left(\boldsymbol{\beta}^C\right) p\left(\sigma_C^2\right) p\left(\boldsymbol{\Sigma}^C\right).$$

As discussed in Section 2.4.2, conjugate prior distributions are used in order to guarantee a proper closed form posterior distribution (Arellano-Valle, Bolfarine, and Lachos 2007), which are:

$$\begin{aligned}
\boldsymbol{\beta}^C &\sim \text{Multi-Normal}_p\left(\boldsymbol{\mu}_0^C, \boldsymbol{\Lambda}_0^C\right), \\
\sigma_C^2 &\sim \text{Inv-Gamma}\left(\frac{\nu_0^C}{2}, \frac{\nu_0^C \sigma_{C0}^2}{2}\right), \\
\boldsymbol{\Sigma}^C &\sim \text{Inv-Wishart}\left(\eta_0^C, \mathbf{S}_{C0}^{-1}\right).
\end{aligned}$$

We need to assign values for a large set of parameters in the prior distributions. As noted before, if we do not have correct information regarding the priors, it is appropriate to use non-informative priors that lead to objective results. This prior choice represents that how much information we gain after we observe the data if we do not have information in priori.

The prior for $\boldsymbol{\beta}^C$ is selected to be a multivariate normal distribution. The parameters in the prior are specified following the general approach in Kass and Wasserman (1995). We take $\boldsymbol{\mu}_0^C$, the prior expectation of $\boldsymbol{\beta}^C$, to be equal to the average of the OLS estimates of (2.3) over counties and $\boldsymbol{\Lambda}_0^C$ to be the sample covariance of these estimates. Such a choice of prior for $\boldsymbol{\beta}^C$ represents unbiased but weak information (Hoff 2009).

In the inverse Gamma prior distribution for σ_C^2, we choose σ_{C0}^2 to be equal to the average of residual sum of squares (RSS) from the OLS estimations of (2.3) across counties and we set ν_0^C be one, which guarantees that the inverse Gamma distribution is diffuse and is non-informative.

The prior distribution for $\boldsymbol{\Sigma}^C$ is an inverse Wishart distribution. The parameter $\mathbf{S}_{C0}$ is equal to the covariance of the OLS estimates, similar to $\boldsymbol{\Lambda}_0^C$. The degree of freedom parameter η_0^C is set to be $q+2$, where q is the number of covariates in the regression equation, so that the prior distribution for $\boldsymbol{\Sigma}^C$ is somewhat diffuse as well.

A.1.3. Full Conditional Distributions

Since it is quite difficult to directly sample from the joint posterior distribution, we need to derive the full conditional distributions for all unknown parameters, and sample from those. Following Hoff (2009), the full conditional distributions for the normal hierarchical model are:

$$\boldsymbol{\theta}_j^C \left| \boldsymbol{\beta}^C, \sigma_C^2, \boldsymbol{\Sigma}^C \right. \sim \text{Multi-Normal}_p\left(\boldsymbol{\mu}_j^C, \boldsymbol{\Lambda}_j^C\right), \quad j = 1, \ldots m, \text{ where}$$

(A.2)
$$\boldsymbol{\Lambda}_j^C = \left(\left(\boldsymbol{\Sigma}^C\right)^{-1} + \frac{\left(\mathbf{X}^W\right)^T \mathbf{X}^W}{\sigma_C^2} \right)^{-1},$$

$$\boldsymbol{\mu}_j^C = \boldsymbol{\Lambda}_{\theta_j}^c \left(\left(\boldsymbol{\Sigma}^C\right)^{-1} \boldsymbol{\beta}^C + \frac{\left(\mathbf{X}^W\right)^T \mathbf{w}_j^c}{\sigma_C^2} \right);$$

$$\boldsymbol{\beta}^C \left| \boldsymbol{\theta}_1^C, \ldots, \boldsymbol{\theta}_m^C, \boldsymbol{\Sigma}^C \right. \sim \text{Multi-Normal}_p\left(\boldsymbol{\mu}_\beta^C, \boldsymbol{\Lambda}_\beta^C\right), \text{ where}$$

(A.3)
$$\boldsymbol{\Lambda}_\beta^C = \left(\left(\boldsymbol{\Lambda}_0^C\right)^{-1} + m\left(\boldsymbol{\Sigma}^C\right)^{-1} \right)^{-1},$$

$$\boldsymbol{\mu}_\beta^C = \boldsymbol{\Lambda}_\beta^c \left(\left(\boldsymbol{\Lambda}_0^C\right)^{-1} \boldsymbol{\mu}_0^C + \left(\boldsymbol{\Sigma}^C\right)^{-1} \sum_{j=1}^m \boldsymbol{\theta}_j^C \right);$$

(A.4)
$$\sigma_C^2 \left| \boldsymbol{\theta}_1^C, \ldots, \boldsymbol{\theta}_m^C \right. \sim \text{Inv-Gamma}\left(\frac{\nu_0^C + \sum_{j=1}^m n_j}{2}, \frac{\nu_0^C \sigma_{C0}^2 + \text{SSR}^C}{2} \right), \text{ where}$$

$$\text{SSR}^C = \sum_{j=1}^m \left(\mathbf{w}_j^C - \mathbf{X}^W \boldsymbol{\theta}_j^C\right)^T \left(\mathbf{w}_j^C - \mathbf{X}^W \boldsymbol{\theta}_j^C\right);$$

(A.5)
$$\boldsymbol{\Sigma}^C \left| \boldsymbol{\theta}_1^C, \ldots, \boldsymbol{\theta}_m^C, \boldsymbol{\beta}^C \right. \sim \text{Inv-Wishart}\left(\eta_0^C + m, \left(\mathbf{S}_{C0} + \mathbf{S}_{Cm}\right)^{-1}\right), \text{ where}$$

$$\mathbf{S}_{Cm} = \sum_{j=1}^m \left(\boldsymbol{\theta}_j^C - \boldsymbol{\beta}^C\right)\left(\boldsymbol{\theta}_j^C - \boldsymbol{\beta}^C\right)^T.$$

A.1.4. Gibbs Sampler

Once we obtain the full conditional distributions, we can construct a Gibbs sampler to approximate the joint posterior distribution. The Gibbs sampler is a type of MCMC algorithm that iteratively samples each parameter from its full conditional distribution

given the most current state of other parameters. The order of generating a new set of parameters does not affect the approximation.

Given current values of all parameters $\boldsymbol{\Theta}^{C(s)} = \left\{\boldsymbol{\theta}_1^{C(s)},\ldots,\boldsymbol{\theta}_m^{C(s)},\boldsymbol{\beta}^{C(s)},\sigma_C^{2(s)},\boldsymbol{\Sigma}^{C(s)}\right\}$ at scan s, new values are generated at scan $s+1$ using the following steps:

1. For each $j=1,\ldots,m$, sample of values for $\boldsymbol{\theta}_j^{C(s+1)} \sim p\left(\boldsymbol{\theta}_j^C \middle| \boldsymbol{\beta}^{C(s)},\sigma_C^{2(s)},\boldsymbol{\Sigma}^{C(s)}\right)$ according to the posterior distributions in (A.2).
2. Generate a sample for $\boldsymbol{\beta}^{C(s+1)} \sim p\left(\boldsymbol{\beta}^C \middle| \boldsymbol{\theta}_1^{C(s+1)},\ldots,\boldsymbol{\theta}_m^{C(s+1)},\boldsymbol{\Sigma}^{C(s)}\right)$ according to the posterior distribution shown in (A.3).
3. Generate a sample for $\sigma_C^{2(s+1)} \sim p\left(\sigma_C^2 \middle| \boldsymbol{\theta}_1^{C(s+1)},\ldots,\boldsymbol{\theta}_m^{C(s+1)}\right)$ according to the posterior distribution represented in (A.4).
4. Generate a sample for $\boldsymbol{\Sigma}^{C(s+1)} \sim p\left(\boldsymbol{\Sigma}^C \middle| \boldsymbol{\theta}_1^{C(s+1)},\ldots,\boldsymbol{\theta}_m^{C(s+1)},\boldsymbol{\beta}^{C(s+1)}\right)$ based on the distribution in (A.5).

Through the above steps, a new scan of the parameters is generated. Repeating the steps multiple times produces a sample for the elements of the parameter set. As $s \to \infty$, the sampling distribution of $\boldsymbol{\Theta}^C$ converges to the target joint posterior distribution, and the sampling distribution for each component in the parameter set $\boldsymbol{\Theta}^C$ converge to its marginal posterior distribution. We then can make inferences for the parameters based on the sampling distributions.

A.2. Bayesian Algorithm for the Generalized Normal Hierarchical Model

This appendix section presents the procedures used in implementing the Bayesian algorithm for the generalized normal hierarchical model, as shown in (2.7), (2.9), and

(2.10) in the text. In Section A.1, procedures were discussed that generated full conditional distributions for each parameter in standard form. In turn, a Gibbs sampling algorithm can be implemented to sample parameters from the full conditional distributions. However, for the generalized normal hierarchical model (2.7), Hoff (2009) indicates that standard full conditional distributions only exist for $\boldsymbol{\beta}^D$ and $\boldsymbol{\Sigma}^D$. For other parameters such as $\boldsymbol{\theta}_j^D$, a Metropolis-Hastings algorithm can be used for sampling.

The full conditional distributions for $\boldsymbol{\beta}^D$ and $\boldsymbol{\Sigma}^D$ have the same form as that given in (A.3) and (A.5), respectively. The prior distributions for $\boldsymbol{\beta}^D$ and $\boldsymbol{\Sigma}^D$ are specified as non-informative with same strategy as for $\boldsymbol{\beta}^C$ and $\boldsymbol{\Sigma}^C$ discussed in Section A.1.

The update of $\boldsymbol{\theta}_j^D$ can be formed with a Metropolis-Hastings algorithm (Hoff 2009). A new value $\boldsymbol{\theta}_j^{D*}$ is sampled from a proposal distribution $J\left(\boldsymbol{\theta}_j^{D*} \middle| \boldsymbol{\theta}_j^{D(s)}\right)$ nearby the current value $\boldsymbol{\theta}_j^{D(s)}$, and then it is accepted or rejected based on an acceptance criterion. A common choice of the proposal distribution for $\boldsymbol{\theta}_j^D$ would be a multivariate normal distribution such that the mean equals the current value $\boldsymbol{\theta}_j^{D(s)}$ and the covariance matrix is set to be equal to $r\boldsymbol{\Sigma}^{D(s)}$, where r is a scale parameter and $\boldsymbol{\Sigma}^{D(s)}$ is the current value of $\boldsymbol{\Sigma}^D$ updated from the Gibbs sampling steps. Here, we set $r = 0.4$, which generates a well-mixing Markov chain that moves around the parameter space.

Following Hoff (2009), we use an integrated algorithm including both the Gibbs and Metropolis-Hastings samplers to approximate the joint posterior distribution. Given current values of parameters at scan s, $\boldsymbol{\Theta}^{D(s)} = \left\{\boldsymbol{\theta}_1^{D(s)}, \ldots, \boldsymbol{\theta}_m^{D(s)}, \boldsymbol{\beta}^{D(s)}, \boldsymbol{\Sigma}^{D(s)}\right\}$, the new values are generated as follows:

1. Generate a sample $\boldsymbol{\beta}^{D(s+1)}$ from its full conditional distribution that has the same structure with the **Error! Reference source not found.**, that is, $\boldsymbol{\beta}^{D(s+1)} \sim p\left(\boldsymbol{\beta}^{D} \left| \boldsymbol{\theta}_1^{D(s)}, \ldots, \boldsymbol{\theta}_m^{D(s)}, \boldsymbol{\Sigma}^{D(s)} \right.\right)$.
2. Generate a sample $\boldsymbol{\Sigma}^{D(s+1)}$ from its full conditional distribution that is similar to **Error! Reference source not found.**, i.e., $\boldsymbol{\Sigma}^{D(s+1)} \sim p\left(\boldsymbol{\Sigma}^{D} \left| \boldsymbol{\theta}_1^{D(s)}, \ldots, \boldsymbol{\theta}_M^{D(s)}, \boldsymbol{\beta}^{D(s+1)} \right.\right)$.
3. For each $j = 1, \ldots, m$,
    a. Propose a new value $\boldsymbol{\theta}_j^{D*} \sim \text{Multi-Normal}\left(\boldsymbol{\theta}_j^{D(s)}, r\boldsymbol{\Sigma}^{D(s+1)}\right)$;
    b. Compute the acceptance ratio by comparing the posterior probability densities between the proposed value $\boldsymbol{\theta}_j^{D*}$ and the current value $\boldsymbol{\theta}_j^{D(s)}$:

$$\rho = \frac{p\left(\mathbf{w}_j^D \left| \boldsymbol{\theta}_j^{D*}, \mathbf{X}^W \right.\right) p\left(\boldsymbol{\theta}_j^{D*} \left| \boldsymbol{\beta}^{D(s+1)}, \boldsymbol{\Sigma}^{D(s+1)} \right.\right)}{p\left(\mathbf{w}_j^D \left| \boldsymbol{\theta}_j^{D(s)}, \mathbf{X}^W \right.\right) p\left(\boldsymbol{\theta}_j^{D(s)} \left| \boldsymbol{\beta}^{D(s+1)}, \boldsymbol{\Sigma}^{D(s+1)} \right.\right)},$$

    where $p\left(\mathbf{w}_j^D \left| \boldsymbol{\theta}_j^{D*}, \mathbf{X}^W \right.\right)$ and $p\left(\mathbf{w}_j^D \left| \boldsymbol{\theta}_j^{D(s)}, \mathbf{X}^W \right.\right)$ are the Poisson density functions evaluated at $\boldsymbol{\theta}_j^{D*}$ and $\boldsymbol{\theta}_j^{D(s)}$, respectively, while $p\left(\boldsymbol{\theta}_j^{D*} \left| \boldsymbol{\beta}^{D(s+1)}, \boldsymbol{\Sigma}^{D(s+1)} \right.\right)$ and $p\left(\boldsymbol{\theta}_j^{D(s)} \left| \boldsymbol{\beta}^{D(s+1)}, \boldsymbol{\Sigma}^{D(s+1)} \right.\right)$ are the multivariate normal density functions;
    c. Generate a sample a value $u \sim \text{uniform}(0,1)$. Update $\boldsymbol{\theta}_j^{D(s+1)}$ to $\boldsymbol{\theta}_j^{D*}$ if $u < \rho$, and keep $\boldsymbol{\theta}_j^{D(s+1)}$ to $\boldsymbol{\theta}_j^{D(s)}$ if $u > \rho$.

The above steps generate a new set of parameters. Repeating the procedures multiple times produces a sequence of parameters. As $s \to \infty$, the sampling distribution of the generated parameters converges to the target joint posterior distribution.

A.3. Multivariate Skew-normal Distribution

This appendix section presents background material on multivariate skew-normal distribution probability density function and the associated stochastic form. Details on how the distribution is incorporated in the Bayesian analysis appear in Section A.4.

Arellano-Valle, Bolfarine, and Lachos (2007) show that the density function for a random vector $\mathbf{y}$ that has a multivariate skew-normal distribution is:

$$p\left(\mathbf{y}\middle|\boldsymbol{\mu},\boldsymbol{\Sigma},\boldsymbol{\Delta}\right)=2^{n}\phi_{n}\left(\mathbf{y}\middle|\boldsymbol{\mu},\boldsymbol{\Sigma}+\boldsymbol{\Delta}\boldsymbol{\Delta}^{T}\right)\Phi_{n}\left(\boldsymbol{\Delta}^{T}\left(\boldsymbol{\Sigma}+\boldsymbol{\Delta}\boldsymbol{\Delta}^{T}\right)^{-1}\left(\mathbf{y}-\boldsymbol{\mu}\right)\middle|\mathbf{0},\left(\mathbf{I}+\boldsymbol{\Delta}^{T}\boldsymbol{\Sigma}^{-1}\boldsymbol{\Delta}\right)^{-1}\right),$$

where ϕ_n and Φ_n are the probability density function and the cumulative density function of a multivariate normal distribution with dimension n; $\boldsymbol{\mu}$ is a $n\times 1$ location vector; $\boldsymbol{\Sigma}$ is a $n\times n$ positive definite scale matrix; $\boldsymbol{\Delta}$ is a $n\times n$ diagonal skewness matrix with elements $\boldsymbol{\delta}=\left(\delta_1,\ldots,\delta_n\right)$. We denote the skew-normal distribution for a random vector by $\mathbf{y}\left|\boldsymbol{\mu},\boldsymbol{\Sigma},\boldsymbol{\Delta}\right.\sim\text{Skew-Normal}_n\left(\boldsymbol{\mu},\boldsymbol{\Sigma},\boldsymbol{\Delta}\right)$. Compared to the normal distribution, the skew-normal has one more component of parameters, the skewness matrix. It can be shown that the multivariate skew-normal distribution becomes a multivariate normal distribution when $\boldsymbol{\Delta}=\mathbf{0}$.

Following Proposition 1 in Arellano-Valle, Bolfarine, and Lachos (2007), the multivariate skew-normal distribution for $\mathbf{y}$ can be represented by a stochastic form:

$$\mathbf{y}=\boldsymbol{\Delta}\left|\mathbf{U}_1\right|+\mathbf{U}_2,$$

where $\left|\mathbf{U}_1\right|\sim\text{Trunc-Normal}_n\left(\mathbf{0},\mathbf{I}_n\right)\left\{\mathbf{u}_1>\mathbf{0}\right\}$, which is a truncated normal distribution with positive values $\mathbf{u}_1$; $\mathbf{U}_2\sim\text{Multi-Normal}_n\left(\boldsymbol{\mu},\boldsymbol{\Sigma}\right)$. The skew-normal random variable

is the combination of two random variables with different normal distributions. The stochastic form of the skew-normal distribution is convenient for Bayesian analysis.

A.4. Bayesian Algorithm for the Skew-normal Hierarchical Model

This appendix section covers the steps followed in the Bayesian estimation with the skew-normal distribution assumption, as displayed in (2.11), (2.13), and (2.14) in the text. First, the skew-normal sampling distributions of (2.13) and (2.14) in the text are decomposed into two distributions, respectively, as discussed in Section A.3. Then, the joint posterior distribution for all unknown parameters is derived based on Bayes' rule. The assumptions used for the prior distributions and the derived full conditional distributions are presented. Then, the method for employing the Gibbs sampler that approximates the joint posterior distribution is discussed.

A.4.1. Decomposed Skew-normal Sampling Models

Since a skew-normal distribution can be represented in a stochastic form, as shown in Section A.3, the sampling distribution for $\mathbf{y}_j$ in (2.13) can be decomposed into two parts following Arellano-Valle, Bolfarine, and Lachos (2007):

$$\begin{aligned} \mathbf{y}_j \left| \mathbf{X}_j^Y, \boldsymbol{\theta}_j^Y, \sigma_Y^2, \delta, \mathbf{z}_j \right. &\sim \text{ind. Multi-Normal}_{n_j}\left(\mathbf{X}_j^Y \boldsymbol{\theta}_j^Y + \delta \mathbf{z}_j, \sigma_Y^2 \mathbf{I}_{n_j}\right), \\ \mathbf{Z}_j &\sim \text{i.i.d. Trunc-Normal}_{n_j}\left(\mathbf{0}, \mathbf{I}_{n_j}\right)\mathbf{1}\{\mathbf{z}_j > \mathbf{0}\}, \end{aligned} \tag{A.6}$$

and the sampling distribution for $\boldsymbol{\theta}_j^Y$ in (2.14) is similarly represented as:

$$\text{(A.7)}\qquad \begin{aligned} \boldsymbol{\theta}_j^Y \left| \boldsymbol{\beta}^Y, \boldsymbol{\Sigma}^Y, \boldsymbol{\Pi}, \mathbf{v}_j \right. &\sim \text{i.i.d. Multi-Normal}_p \left(\boldsymbol{\beta}^Y + \boldsymbol{\Pi}\mathbf{v}_j, \boldsymbol{\Sigma}^Y \right), \\ \mathbf{V}_j &\sim \text{i.i.d. Trunc-Normal}_p \left(\mathbf{0}, \mathbf{I}_p \right) \mathbf{1}\left\{ \mathbf{v}_j > \mathbf{0} \right\}, \end{aligned}$$

where $\mathbf{Z}_j$ and $\mathbf{V}_j$ are latent parameters that illustrate the skewness of a distribution.

A.4.2. Joint Posterior Distribution

The joint posterior distribution for all unknown parameters in the skew-normal hierarchical model is derived according to the Bayes' rule:

$$\text{(A.8)}\qquad \begin{aligned} & p\left(\boldsymbol{\theta}_1^Y, \ldots, \boldsymbol{\theta}_m^Y, \boldsymbol{\beta}^Y, \sigma_Y^2, \boldsymbol{\Sigma}^Y, \delta, \boldsymbol{\pi}, \mathbf{z}_1, \ldots, \mathbf{z}_m, \mathbf{v}_1, \ldots \mathbf{v}_m \left| \mathbf{y}_1, \ldots, \mathbf{y}_m, \mathbf{X}_1^Y, \ldots \mathbf{X}_m^Y \right. \right) \\ \propto\ & p\left(\mathbf{y}_1, \ldots, \mathbf{y}_m \left| \boldsymbol{\theta}_1^Y, \ldots, \boldsymbol{\theta}_m^Y, \sigma_Y^2, \delta, \mathbf{z}_1, \ldots, \mathbf{z}_m, \mathbf{X}_1^Y, \ldots \mathbf{X}_m^Y \right. \right) \rightarrow \text{Multi-Normal sampling} \\ \times\ & p\left(\boldsymbol{\theta}_1^Y, \ldots, \boldsymbol{\theta}_m^Y \left| \boldsymbol{\beta}^Y, \boldsymbol{\Sigma}^Y, \boldsymbol{\pi}, \mathbf{v}_1, \ldots \mathbf{v}_m, \mathbf{X}_1^Y, \ldots \mathbf{X}_m^Y \right. \right) \rightarrow \text{Multi-Normal sampling} \\ \times\ & p\left(\mathbf{z}_1, \ldots, \mathbf{z}_m \right) \rightarrow \text{Trunc-Normal sampling} \\ \times\ & p\left(\mathbf{v}_1, \ldots \mathbf{v}_m \right) \rightarrow \text{Trunc-Normal sampling} \\ \times\ & p\left(\boldsymbol{\beta}^Y, \sigma_Y^2, \boldsymbol{\Sigma}^Y, \delta, \boldsymbol{\pi} \right). \rightarrow \text{Priors} \end{aligned}$$

In (A.8), components associated with $\mathbf{y}_j$, $\mathbf{z}_j$, $\boldsymbol{\theta}_j^Y$, and $\mathbf{v}_j$ for all j are specified by their sampling distributions (A.6) and (A.7). The priors for $\boldsymbol{\beta}^Y$, σ_Y^2, $\boldsymbol{\Sigma}^Y$, δ, and $\boldsymbol{\pi}$ are discussed in Section A.4.3.

A.4.3. Prior Distributions

Similar to the normal hierarchical model, we use non-informative conjugate priors for the skew-normal hierarchical model, and assume that the priors are independent such that

$$p\left(\boldsymbol{\beta}^Y, \sigma_Y^2, \boldsymbol{\Sigma}^Y, \delta, \boldsymbol{\pi} \right) = p\left(\boldsymbol{\beta}^Y \right) p\left(\sigma_Y^2 \right) p\left(\boldsymbol{\Sigma}^Y \right) p\left(\delta \right) p\left(\boldsymbol{\pi} \right).$$

Following Arellano-Valle, Bolfarine, and Lachos (2007), the functional forms of the conjugate priors are:

$$\begin{aligned}
\boldsymbol{\beta}^Y &\sim \text{Multi-Normal}_p\left(\boldsymbol{\mu}_0^Y, \boldsymbol{\Lambda}_0^Y\right), \\
\sigma_Y^2 &\sim \text{Inv-Gamma}\left(\frac{\nu_0^Y}{2}, \frac{\nu_0^Y \sigma_{Y0}^2}{2}\right), \\
\boldsymbol{\Sigma}^Y &\sim \text{Inv-Wishart}\left(\eta_0^Y, \mathbf{S}_{Y0}^{-1}\right), \\
\delta &\sim \text{Normal}\left(\gamma_0, \lambda_0^2\right), \\
\boldsymbol{\pi} &\sim \text{Multi-Normal}_p\left(\boldsymbol{\xi}_0, \boldsymbol{\Gamma}_0\right).
\end{aligned}$$

The prior distributions plus the sampling distributions together generate the specific form for the joint posterior distribution (A.8).

We need to specify the parameters in the prior distributions, which guarantees that the priors are weakly informative. For the prior of $\boldsymbol{\beta}^Y$, we set $\boldsymbol{\mu}_0^Y$ to be equal to the average of the individual OLS estimates across counties and $\boldsymbol{\Lambda}_0^Y$ to be the sample covariance of the OLS estimates. For the prior for σ_Y^2, we take $\nu_0^Y = 1$ and σ_{Y0}^2 to be the average of RSS from the OLS estimations, which guarantees that the prior distribution is somewhat diffuse. We set $\eta_0^Y = p + 2$ and $\mathbf{S}_{Y0}$ to be equal to the covariance of the OLS estimates. In this setting, the prior distribution for $\boldsymbol{\Sigma}^Y$ is quite diffuse but has an expectation equal to $\mathbf{S}_{Y0}$. Finally, for the skewness parameters, δ and $\boldsymbol{\pi}$, the priors are assumed to be both normal distribution. We set $\gamma_0 = 0$, $\lambda_0^2 = 100$, $\boldsymbol{\xi}_0 = \mathbf{0}$, and $\boldsymbol{\Gamma}_0 = \text{diag}(100)$. Both prior distributions have large variances such that they are diffuse.

A.4.4. Full Conditional Distributions

The full conditional distributions consist of the distribution of each parameter conditional on all other parameters. Following the Proposition 2 in Arellano-Valle, Bolfarine, and Lachos (2007), we derive the full posterior conditional distributions for the skew-normal hierarchical model:

$$\boldsymbol{\theta}_j^Y \left| \boldsymbol{\beta}^Y, \sigma_Y^2, \boldsymbol{\Sigma}^Y, \delta, \boldsymbol{\pi}, \mathbf{z}_j, \mathbf{v}_j \right. \sim \text{Multi-Normal}_p\left(\boldsymbol{\mu}_j^Y, \boldsymbol{\Lambda}_j^Y\right), \quad j = 1, \ldots m, \text{ where}$$

(A.9)
$$\boldsymbol{\Lambda}_j^Y = \left(\left(\boldsymbol{\Sigma}^Y\right)^{-1} + \frac{\left(\mathbf{X}_j^Y\right)^T \mathbf{X}_j^Y}{\sigma_Y^2} \right)^{-1},$$

$$\boldsymbol{\mu}_j^Y = \boldsymbol{\Lambda}_j^Y \left(\left(\boldsymbol{\Sigma}^Y\right)^{-1} \left(\boldsymbol{\beta}^Y + \boldsymbol{\Pi}\mathbf{v}_j\right) + \frac{\left(\mathbf{X}_j^Y\right)^T \left(\mathbf{y}_j - \delta \mathbf{z}_j\right)}{\sigma_Y^2} \right);$$

$$\boldsymbol{\beta}^Y \left| \boldsymbol{\theta}_1^Y, \ldots, \boldsymbol{\theta}_m^Y, \boldsymbol{\Sigma}^Y, \boldsymbol{\pi}, \mathbf{v}_1, \ldots \mathbf{v}_m \right. \sim \text{Multi-Normal}_p\left(\boldsymbol{\mu}_\beta^Y, \boldsymbol{\Lambda}_\beta^Y\right), \text{ where}$$

(A.10)
$$\boldsymbol{\Lambda}_\beta^Y = \left(\left(\boldsymbol{\Lambda}_0^Y\right)^{-1} + m\left(\boldsymbol{\Sigma}^Y\right)^{-1} \right)^{-1},$$

$$\boldsymbol{\mu}_\beta^Y = \boldsymbol{\Lambda}_\beta^Y \left(\left(\boldsymbol{\Lambda}_0^Y\right)^{-1} \boldsymbol{\mu}_0^Y + \left(\boldsymbol{\Sigma}^Y\right)^{-1} \sum_{j=1}^m \left(\boldsymbol{\theta}_j^Y - \boldsymbol{\Pi}\mathbf{v}_j\right) \right);$$

$$\sigma_Y^2 \left| \boldsymbol{\theta}_1^Y, \ldots, \boldsymbol{\theta}_m^Y, \delta, \mathbf{z}_1, \ldots, \mathbf{z}_m \right. \sim \text{Inv-Gamma}\left(\frac{\nu_0^Y + \sum_{j=1}^m n_j}{2}, \frac{\nu_0^Y \sigma_{Y0}^2 + \text{SSR}^Y}{2} \right), \text{ where}$$

(A.11)
$$\text{SSR}^Y = \sum_{j=1}^m \left(\mathbf{y}_j - \mathbf{X}_j^Y \boldsymbol{\theta}_j^Y - \delta \mathbf{z}_j\right)^T \left(\mathbf{y}_j - \mathbf{X}_j^Y \boldsymbol{\theta}_j^Y - \delta \mathbf{z}_j\right);$$

$$\boldsymbol{\Sigma}^Y \left| \boldsymbol{\theta}_1^Y, \ldots, \boldsymbol{\theta}_m^Y, \boldsymbol{\beta}^Y, \boldsymbol{\pi}, \mathbf{v}_1, \ldots \mathbf{v}_m \sim \text{Inv-Wishart}\left(\eta_0^Y + m,\ \left(\mathbf{S}_{Y0} + \mathbf{S}_{Ym} \right)^{-1} \right), \text{ where} \right.$$

(A.12)
$$\mathbf{S}_{Ym} = \sum_{j=1}^{m} \left(\boldsymbol{\theta}_j^Y - \boldsymbol{\beta}^Y - \boldsymbol{\Pi}\mathbf{v}_j \right) \left(\boldsymbol{\theta}_j^Y - \boldsymbol{\beta}^Y - \boldsymbol{\Pi}\mathbf{v}_j \right)^T ;$$

$$\delta \left| \boldsymbol{\theta}_1^Y, \ldots, \boldsymbol{\theta}_m^Y, \sigma_Y^2, \mathbf{z}_1, \ldots \mathbf{z}_m \sim \text{Normal}\left(\gamma_m, \lambda_m^2 \right), \text{ where} \right.$$

(A.13)
$$\lambda_m^2 = \left(\frac{1}{\lambda_0^2} + \frac{\sum_{j=1}^{m} \mathbf{z}_j^T \mathbf{z}_j}{\sigma_Y^2} \right)^{-1},$$

$$\gamma_m = \lambda_m^2 \left(\frac{\gamma_0}{\lambda_0^2} + \frac{\sum_{j=1}^{m} \mathbf{z}_j^T \left(\mathbf{y}_j - \mathbf{X}_j^Y \boldsymbol{\theta}_j^Y \right)}{\sigma_Y^2} \right);$$

$$\boldsymbol{\pi} \left| \boldsymbol{\theta}_1^Y, \ldots, \boldsymbol{\theta}_m^Y, \boldsymbol{\beta}^Y, \boldsymbol{\Sigma}^Y, \mathbf{v}_1, \ldots \mathbf{v}_m \sim \text{Multi-Normal}_p \left(\boldsymbol{\xi}_\beta, \boldsymbol{\Gamma}_\beta \right), \text{ where} \right.$$

(A.14)
$$\boldsymbol{\Gamma}_\beta = \left(\boldsymbol{\Gamma}_0 + \sum_{j=1}^{m} \text{diag}\left(\mathbf{v}_j \right) \left(\boldsymbol{\Sigma}^Y \right)^{-1} \text{diag}\left(\mathbf{v}_j \right) \right)^{-1},$$

$$\boldsymbol{\xi}_\beta = \boldsymbol{\Gamma}_\beta \left(\boldsymbol{\Gamma}_0^{-1} \boldsymbol{\xi}_0 + \sum_{j=1}^{m} \text{diag}\left(\mathbf{v}_j \right) \left(\boldsymbol{\Sigma}^Y \right)^{-1} \left(\boldsymbol{\theta}_j^Y - \boldsymbol{\beta}^Y \right) \right);$$

$$\mathbf{Z}_j \left| \boldsymbol{\theta}_1^Y, \ldots, \boldsymbol{\theta}_m^Y, \sigma_Y^2, \delta \sim \text{Trunc-Normal}_{n_j} \left(\boldsymbol{\varphi}_{zj}, \boldsymbol{\Omega}_{zj} \right) \mathbf{1}\left\{ \mathbf{z}_j > \mathbf{0} \right\},\ j = 1, \ldots m, \text{ where} \right.$$

(A.15)
$$\boldsymbol{\Omega}_{zj} = \left(1 + \frac{\delta_e}{\sigma_e^{Y2}} \right) \mathbf{I}_{N_j}^{-1},$$

$$\boldsymbol{\varphi}_{zj} = \boldsymbol{\Omega}_{zj} \left(\frac{\delta \left(\mathbf{y}_j - \mathbf{X}_j^Y \boldsymbol{\theta}_j^Y \right)}{\sigma_Y^2} \right);$$

$$\mathbf{V}_j \left| \boldsymbol{\theta}_1^Y, \ldots, \boldsymbol{\theta}_m^Y, \boldsymbol{\beta}^Y, \boldsymbol{\Sigma}^Y, \boldsymbol{\pi} \sim \text{Trunc-Normal}_{n_j} \left(\boldsymbol{\varphi}_{vj}, \boldsymbol{\Omega}_{vj} \right) \mathbf{1}\left\{ \mathbf{v}_j > \mathbf{0} \right\},\ j = 1, \ldots m, \text{ where} \right.$$

(A.16)
$$\boldsymbol{\Omega}_{vj} = \left(\mathbf{I}_p + \boldsymbol{\Pi} \left(\boldsymbol{\Sigma}^Y \right)^{-1} \boldsymbol{\Pi} \right),$$

$$\boldsymbol{\varphi}_{vj} = \boldsymbol{\Omega}_{vj} \left(\boldsymbol{\Pi} \left(\boldsymbol{\Sigma}^Y \right)^{-1} \left(\boldsymbol{\theta}_j^Y - \boldsymbol{\beta}^Y \right) \right).$$

A.4.5. Gibbs Sampler

Since the full conditional distributions are obtainable, we can implement Gibbs sampling algorithm to approximate the joint posterior distribution. The algorithm is similar to the one in Section A.1 but with more steps.

Given current values of the set of all parameters $\boldsymbol{\Theta}^{Y(s)}$ at scan s, new values are iteratively generated through the following steps:

1. For each $j = 1,\ldots,m$, sample $\boldsymbol{\theta}_j^{Y(s+1)} \sim p\left(\boldsymbol{\theta}_j^Y \middle| \boldsymbol{\beta}^{Y(s)}, \sigma_Y^{2(s)}, \boldsymbol{\Sigma}^{Y(s)}, \delta^{(s)}, \boldsymbol{\pi}^{(s)}, \mathbf{z}_j^{(s)}, \mathbf{v}_j^{(s)}\right)$ according to the posterior distributions in (A.9).
2. Sample $\boldsymbol{\beta}^{Y(s+1)} \sim p\left(\boldsymbol{\beta}^Y \middle| \boldsymbol{\theta}_1^{Y(s+1)},\ldots,\boldsymbol{\theta}_m^{Y(s+1)}, \boldsymbol{\Sigma}^{Y(s)}, \boldsymbol{\pi}^{(s)}, \mathbf{v}_1^{(s)},\ldots \mathbf{v}_m^{(s)}\right)$ according to the posterior distribution in (A.10).
3. Generate a sample $\sigma_Y^{2(s+1)} \sim p\left(\sigma_Y^2 \middle| \boldsymbol{\theta}_1^{Y(s+1)},\ldots,\boldsymbol{\theta}_m^{Y(s+1)}, \delta^{(s)}, \mathbf{z}_1^{(s)},\ldots,\mathbf{z}_j^{(s)}\right)$ according to (A.11).
4. Generate a sample $\boldsymbol{\Sigma}^{Y(s+1)} \sim p\left(\boldsymbol{\Sigma}^Y \middle| \boldsymbol{\theta}_1^{Y(s+1)},\ldots,\boldsymbol{\theta}_M^{Y(s+1)}, \boldsymbol{\beta}^{Y(s+1)}, \boldsymbol{\pi}^{(s)}, \mathbf{v}_1^{(s)},\ldots \mathbf{v}_m^{(s)}\right)$ based on the posterior distribution (A.12).
5. Generate a sample $\delta^{(s+1)} \sim p\left(\delta \middle| \boldsymbol{\theta}_1^{Y(s+1)},\ldots,\boldsymbol{\theta}_m^{Y(s+1)}, \sigma_Y^{2(s+1)}, \mathbf{z}_1^{(s)},\ldots,\mathbf{z}_m^{(s)}\right)$ in accordance with (A.13).
6. Generate a sample $\boldsymbol{\pi}^{(s+1)} \sim p\left(\boldsymbol{\pi} \middle| \boldsymbol{\theta}_1^{Y(s+1)},\ldots,\boldsymbol{\theta}_m^{Y(s+1)}, \boldsymbol{\beta}^{Y(s+1)}, \boldsymbol{\Sigma}^{Y(s+1)}, \mathbf{v}_1^{(s)},\ldots \mathbf{v}_m^{(s)}\right)$ based on the distribution shown in (A.14).
7. For each $j = 1,\ldots,m$, sample $\mathbf{Z}_j^{(s+1)} \sim p\left(\mathbf{Z}_j \middle| \boldsymbol{\theta}_1^{Y(s+1)},\ldots,\boldsymbol{\theta}_m^{Y(s+1)}, \sigma_Y^{2(s+1)}, \delta^{(s+1)}\right)$ based on the posterior distributions in (A.15).
8. For each $j = 1,\ldots,m$, sample $\mathbf{V}_j^{(s+1)} \sim p\left(\mathbf{V}_j \middle| \boldsymbol{\theta}_1^{Y(s+1)},\ldots,\boldsymbol{\theta}_m^{Y(s+1)}, \boldsymbol{\beta}^{Y(s+1)}, \boldsymbol{\Sigma}^{Y(s+1)}, \boldsymbol{\pi}^{(s+1)}\right)$ according to (A.16).

Iterating the previous steps for a large number generates a sequence of parameters that approximates the joint posterior distribution and marginal posterior distributions for all parameters. Inference of the parameters can be made based on the sampling values.

APPENDIX B

APPENDIX FOR SECTION 4

Table B-1: The estimated parameters from the IAIDS model

Parameters	#1 male	#2 male	Female	SP	Mixed
γ_{i1} (#1 male)	0.233***	-0.029***	-0.059**	-0.124***	-0.022**
	(0.036)	(0.008)	(0.025)	(0.032)	(0.010)
γ_{i2} (#2 male)	0.005	0.039***	-0.018*	-0.027*	0.001
	(0.017)	(0.004)	(0.011)	(0.016)	(0.004)
γ_{i3} (Female)	-0.083***	-0.002	0.155***	-0.064***	-0.006
	(0.021)	(0.004)	(0.012)	(0.020)	(0.005)
γ_{i4} (Soft and peelers)	-0.090***	-0.010***	-0.034***	0.134***	-0.000
	(0.012)	(0.003)	(0.008)	(0.009)	(0.003)
γ_{i5} (Mixed)	-0.019	0.004	-0.019	0.010	0.024***
	(0.019)	(0.004)	(0.012)	(0.017)	(0.005)
β_i (Translog)	-0.066***	-0.007***	-0.017***	0.090***	-0.000
	(0.007)	(0.002)	(0.006)	(0.005)	(0.002)
λ_{i1} (Spring)	-0.060	-0.001	-0.014	0.083**	-0.008
	(0.044)	(0.009)	(0.026)	(0.040)	(0.011)
λ_{i2} (Summer)	0.043	0.013**	-0.021	-0.033	-0.002
	(0.029)	(0.006)	(0.017)	(0.027)	(0.007)
α_i (Intercept)	0.601**	0.171***	0.033	0.073	0.122**
	(0.238)	(0.049)	(0.143)	(0.218)	(0.059)
R-square	0.987	0.948	0.980	0.947	-

Note: *** denotes 1% significance; ** denotes 5% significance; * denotes 10% significance. Standard errors are presented in parentheses.

Table B-2: Management scenarios implemented by regulators or hypothetically proposed

Scenario	Male fishing season	Female fishing season	Min size limit for males & immature females (mm)		Min size limit for peelers (mm)		Size limit for soft-shell crabs (mm)	Size limit for mature females (mm)	
			Before 7/15	After 7/15	Before 7/15	After 7/15		Min	Max
2007VARegs	17 Mar – 30 Nov	17 Mar – 30 Nov	>127	>127	>76	>76	>89	-	-
2008VARegs	17 Mar – 30 Nov	17 Mar – 26 Oct	>127	>127	>82.5	>89	>89	-	-
2009VARegs	17 Mar – 30 Nov	17 Mar – 20 Nov	>127	>127	>82.5	>89	>89	-	-
2007MDRegs	1 Apr – 15 Dec	1 Apr – 15 Dec	>127	>133	>82.5	>89	>89	-	-
2008MDRegs	1 Apr – 15 Dec	1 Apr – 23 Oct	>127	>133	>82.5	>89	>89	-	-
2009MDRegs	1 Apr – 15 Dec	1 Apr – 31 May, 16 Jun – 25 Sep, 5 Oct – 10 Nov	>127	>133	>82.5	>89	>89	-	-
5/15-7/15_FEM	1 Apr – 15 Dec	1 Apr – 14 May, 16 Jul – 15 Dec	>127	>133	>82.5	>89	>89	-	-
10/1-12/15_FEM	1 Apr – 15 Dec	1 Apr – 30 Sep	>127	>133	>82.5	>89	>89	-	-
11/16-12/15_FEM	1 Apr – 15 Dec	1 Apr – 15 Nov	>127	>133	>82.5	>89	>89	-	-
10/1-12/15_ALL	1 Apr – 30 Sep	1Apr – 30 Sep	>127	>133	>82.5	>89	>89	-	-
11/16-12/15_ALL	1 Apr – 15 Nov	1 Apr – 15 Nov	>127	>133	>82.5	>89	>89	-	-
152_MinFemCw	1 Apr – 15 Dec	1 Apr – 15 Dec	>127	>133	>82.5	>89	>89	>152	-
152_MaxFemCW	1 Apr – 15 Dec	1 Apr – 15 Dec	>127	>133	>82.5	>89	>89	-	<152
165_MaxFemCW	1 Apr – 15 Dec	1 Apr – 15 Dec	>127	>133	>82.5	>89	>89	-	<165
No_Peeler	1 Apr – 15 Dec	1 Apr – 15 Dec	>127	>133	Forbidden	Forbidden	>89	-	-

Note: this table is adapted from the Table 1 in Bunnell, Lipton, and Miller (2010).